8-9-2014

BIOPOLYMERIC HYDROGELS FUNCTIONALIZED WITH TOBACCO MOSAIC VIRUS FOR IN VITRO THREE DIMENSIONAL CULTURE AND DIFFERENTIATION OF STEM CELLS AND IN VIVO TISSUE REGENERATION

Jittima Amie Luckanagul
University of South Carolina - Columbia

BIOPOLYMERIC HYDROGELS FUNCTIONALIZED WITH TOBACCO MOSAIC VIRUS FOR IN VITRO THREE DIMENSIONAL CULTURE AND DIFFERENTIATION OF STEM CELLS AND IN VIVO TISSUE REGENERATION

by

Jittima Amie Luckanagul

Bachelor of Science
Chulalongkorn University, 2008

Submitted in Partial Fulfillment of the Requirements

For the Degree of Doctor of Philosophy in

Chemistry

College of Arts and Sciences

University of South Carolina

2014

Accepted by:

Qian Wang, Major Professor

Mythreye Karthikeyan, Committee Member

Chuanbing Tang, Committee Member

Ehsan Jabbarzadeh, Committee Member

F. Wayne Outten, Committee Member

Lacy Ford, Vice Provost and Dean of Graduate Studies

ACKNOWLEDGEMENTS

Immeasurable appreciation and deepest gratitude for the help and support are extended to the following persons who have contributed in making this dissertation possible.

Dr. Qian Wang, my advisor, his guidance and provision essentially benefit the completion of this dissertation. I am deeply indebted for the opportunities he has given me and many other Thai students to pursue their higher education. His caring and support are not only limited to my research, but also extended to my life and my future.

Dr. Andrew Lim Lee, I am thankful for his patience and untiring effort in teaching me, for his advices, and his valuable comments on my research. He has taught me how to approach a project, a thought process, and many laboratory techniques.

My fellow lab members, who have contributed valuable comments and suggestions, I am grateful for their willing help in many ways during my graduate study. Drs. Pongkwan Sitasuwan, Sharmista Saha, and Xinrui Duan have shared their expertise in biochemistry and cell biology techniques, as well as their constructive discussion and comments in my research. I would like to thank Kamolrat Metavarayuth and Sheng Feng for their contribution in the rat cranial bone defect study, Panita Maturavongsadit for her contribution in the injectable hydrogel project.

Dr. Yuan Lin, Dr. Zhaohui Su and their groups in Changchun Institute of Applied Chemistry, Dr. Peng Bo, and Dr. Jun Hu, I am deeply grateful for their help in living and in the research during my four-month visit in China.

Dr. Tarek Shazly, his help in the analysis of hydrogel mechanical property in Chapter 1 and manuscript revision is greatly appreciated. I would like to extend my gratitude to Dr. Soumitra Ghoshroy and The Electron Microscopy Center at the University of South Carolina for teaching me all electron microscopy techniques and for their meaningful advices. I would like to thank Dr. Xiaoming Yang for his kind help in the *in vivo* study. His insightful instruction and guidance involving all *in vivo* study in this dissertation provided me invaluable experience and expanded my knowledge. I appreciated the advices and help in histological analysis in Chapter 2 and 3 from Dr. Shaojin You. I also owe thanks to Dr. Andres Garcia and his graduate student, Amy Cheng, for their collaboration in microCT analysis.

I wish to express my sincere gratitude to Dr. Mythreye Karthikeyan, Dr. F. Wayne Outten, Dr. Chuanbing Tang, Dr. Ehsan Jabbarzadeh, the committee members, for reviewing this dissertation, as well as their suggestion and kind help throughout my graduate study.

To my family and friends, their endless support had helped me through all the hardship. Kamolrat Metavarayuth, Greysi Irdam, and Trisha Sittisuntorn, my US family who have made my life in the US not as difficult as I imagined. Kornkamol Chaiwatanamethin, Teratorn Rukwijidkun, Praewpan Chala-aim, and Manita Thanasanti, my beloved friends who always send their love and encouragement from distance. Apissadaporn Thumbandit, Matsepo Ramaboli and Vitaya Methavarayuth, their assistance in language review of this dissertation and their friendship are meaningful to me. My big family, grandmothers, aunts, uncles, cousins, nieces, and nephews, their caring and support are invaluable. My little brother, Kreetha Luckanagul, his faith and his

pure soul give me confidence and positive energy. My sister and my friend, Lalita Luckanagul whose loving is unconditional, her help and love have been essential to me. I am thankful since the days they were born. Lastly, my mother and father, my source of strength, wisdom, and inspiration, for their dedication, their hard working, and their unconditional love, I am forever grateful being their daughter.

ABSTRACT

Plant viruses have been highlighted among material research due to their well-defined structures in nanoscale, mono-dispersity, stability, and chemical functionalities. Each of the thousands coated protein subunits on a viral nanoparticle can be homogenously modified, chemically, and genetically with a functional ligand leading to a high-density and spatial distribution of ligands on each particle (multivalency). Many reports from our group have clearly shown that virus coated substrates induced the acceleration of bone marrow stromal cells differentiation into bone cells. We hypothesized that this phenomenon could rely on the multivalency that the viral nanoparticle has to offer. Moving to a more clinical relevant application, we fabricated three-dimensional (3D) biopolymeric scaffolds with functionalized rod-like Tobacco mosaic virus (TMV) for tissue engineering. The virus-functionalized hydrogel materials were developed and characterized. The first three chapters present *in vitro* and *in vivo* data based on the sponge-like preformed hydrogel functionalized with the cellular recognition peptide, arginine-glycine-aspartic acid (RGD), through an incorporation of RGD mutant of TMV (TMV-RGD1). Chapter 6 describes the development of an *in situ* crosslinking injectable hydrogel using cysteine-addition mutant of TMV (TMV-1Cys).

First chapter includes the fabrication method for TMV-incorporated porous alginate hydrogel, *in vitro* stem cell culture in 3D, and *in vitro* bone differentiation of stem cell in the hydrogel. TMV-RGD1 was non-covalently incorporated to introduce the

biofunctionality into the hydrogel. This hydrogel was a preformed scaffold in which stem cells were seeded after the gel was fabricated. Cell attachment, viability were then characterized to assure the presence and accessibility of the RGD peptide on the virus scaffold. Osteogenic differentiation of bone marrow stromal cells was assessed in the composite hydrogels. The virus and its mutant modification with bio-adhesive peptide (RGD) significantly improved cell attachments and afforded a higher level of calcium depositions in comparison to the unmodified hydrogel. The TMV-functionalized hydrogel scaffolds were also used to study cartilage differentiation of bone marrow stromal cells in chapter 5. In chapter 2, *in vivo* biocompatibility studies of the hydrogel scaffolds, functionalized with wild-type and RGD-mutant TMV, showed no systemic toxicity and insignificant immune response against virus-modified hydrogel implants in the BALB/c mice. Chapter 3 confirms the *in vivo* biocompatibility of the hydrogel scaffolds with TMV and its RGD-mutant when bone marrow stromal cells were incorporated in the implants. Moreover, the implanted hydrogels guided the bone regeneration and could consequently repaired cranial defects in laboratory rats, as presented in chapter 4.

In chapter 6, cys-mutant of TMV was used to covalently link the virus particles with methacrylated polymer backbone through Michael addition reaction in the injectable hydrogel. In this system, physical properties of the hydrogel; for example, gelation time and gel moduli could be finely tuned via the degree of methacrylation and/or the addition of the virus. This *in situ* crosslinking method and the resulting hydrogel was cytocompatible for encapsulation and cultivation of bone marrow stromal cells.

Taken together, this dissertation articulates the application of using virus nanoparticles in functionalization and development of hydrogels as biomaterials for 3D cell culture and differentiation, as well as bone substitute matrix. These findings demonstrated that the virus-functionalized hydrogels can be promising materials for tissue engineering.

TABLE OF CONTENTS

LIST OF TABLES

LIST OF FIGURES

CHAPTER 1

POROUS ALGINATE HYDROGEL FUNCTIONALIZED WITH TOBACCO MOSAIC VIRUS AS THREE-DIMENSIONAL SCAFFOLDS FOR BONE DIFFERENTIATION[1]

1.1 INTRODUCTION

1.1.1 Hydrogels as biomaterials for tissue engineering

The key challenges in making off-the-shelf tissue-engineered organs include providing sufficient oxygen and nutrient exchange to engineered tissue constructs with pore size larger than 100 μm, selecting a suitable cell type, and creating advance architecture of matrix to support the tissue.[1-3] Hydrogels, as three dimensional (3D) scaffolds mimicking the natural extracellular environment of cells, have great potential for tissue engineering applications. A carefully designed hydrogel system can offer the ideal support[4] for microvasculature and tissues, as well as the possible equilibration to high, tissue-like water content.[5] The presence of water and the porous structure allows for the influx of low molecular weight solutes and nutrients crucial for cell viability, as well as the transport of cellular waste out of the hydrogel.[6, 7] In addition, different functional groups can be attached to the hydrogel skeleton to impart desirable physical, chemical, and cell responsive properties to serve different biomedical applications.[8-10]

[1] The content in this chapter was modified from Luckanagul J, Lee LA, Nguyen QL, Sitasuwan P, Yang X, Shazly T, Wang Q. Biomacromolecules 2012;13:3949-58 with permission of publisher (Appendix A). Copyright (2012) American Chemical Society.

1.1.2 Roles of virus particles in extracellular matrix designed to control cell behavior

Despite extensive work with peptide conjugates in hydrogels, there are limited studies showing the functionalization of hydrogels with multivalent (multipoint contact) materials. Past studies have shown that complex toxins (e.g., heptavalent protective antigen from anthrax), immune complexes, and surface receptor clusters that reflect the multivalent interactions between the host cell surface receptors and the binding agents are important for cell dynamics.[11-13] To modulate the cellular responses, ligands specific to cell surface receptors are crucial, but studies also suggest that ligand density, the spatial presentation of ligands, and the physical and mechanical properties of the hydrogels all play critical roles.[8-10, 14, 15] Based on previous studies, coating 2D substrates with TMV demonstrated enhanced osteogenic differentiation potentials.[16] The results from these earlier studies indicated that the surface coating with viral particles was essential to accelerate differentiation from 21 to 14 days and supplementing the media with virus particles failed to induce a similar enhanced differentiation.[17] While the interaction between TMV, substrate, and mesenchymal stem cells on 2D substrates appears critical for such an accelerated differentiation process, it is not known whether these similar events can be translated to 3D scaffolds. Tobacco mosaic virus (TMV) is a rod-like plant virus consisting of 2130 identical protein subunits arranged helically around a genomic single-RNA strand. A TMV particle is roughly 300 nm long and 18 nm in diameter, with a 4 nm cylindrical cavity along the central core.[18, 19] TMV particles are multifaceted nanosized building blocks, given its well-defined structure, genetic and chemical modalities, and relative simplicity in its purification process. It has been used as a primary building block to generate a programmable scaffold by chemical or genetic

modification to decorate polyvalent functional motifs or peptide ligands with defined density and distance between ligands.[20-23] For example, TMV can be modified to display certain functional units that promote cell adhesion, proliferation, and differentiation. In a previous study the classical RGD (arginine−glycine−aspartic acid) peptide sequences with different flanking sequencing were genetically engineered on the surface of the TMV coat proteins to bind to the integrin receptors with differential adhesion strengths.[24] A chemical modification approach can also be used to display phosphates or similar RGD ligands via sequential modification of the tyrosine residue with a diazonium salt followed by Cu(I)-catalyzed azide−alkyne cycloaddition reaction.[23, 25] Here, we generated a 3D scaffold that incorporates the virus particles without affecting the virus's quaternary structures in the porous hydrogels. The assembly of the porous hydrogel with the viral particles required no covalent linkages between the alginate and TMV particles. A genetically modified TMV particle was also used to enhance the cell loading capacity within the hydrogels, and as a proof-of-concept, mesenchymal stem cells were seeded and induced to osteogenic lineage.

1.1.3 Alginate as a hydrogel forming biopolymer

Alginate is a linear polysaccharide copolymer of (1−4)-linked β-D-mannuronic acid (M) and α-L-guluronic acid (G) monomers that has been widely used in a variety of medical applications. The choice for alginate hydrogel was due to its ability to form highly porous hydrogels under mild conditions as well as its low toxicity and biodegradability.[26-28] Alginate gels are formed when divalent cations (i.e., Ca^{2+}) cooperatively interact with blocks of G monomers to form ionic bridges between polymers.[27-29] Unfortunately,

alginate has limited bioactivity, meaning that the saccharide units do not specifically interact with cell surface receptors.[9] Covalent modifications of alginates to circumvent this limitation have been well established via carbodiimide-mediated peptide coupling at the carboxylic groups of which the activation step is nonselective to both G and M residues. However, the covalent modification of G content reduces cross-linking sites, thereby interfering with gelation.[30] The modification of alginates could be realized by incorporating large biomacromolecules, such as the virus particles, to generate embedded functionalities without forming covalent modifications to the sugar backbone. In this study, we prepared 3D porous hydrogels that can be functionalized by incorporating the viral nanoparticles to enhance mesenchymal stem cell attachment, proliferation, and differentiation. Given the mild synthetic conditions, we envision a range of functional groups could be incorporated using virus libraries or other macromolecular assemblies in these porous hydrogels.

1.2 Results and Discussion

From the previous work, we have observed a significant shift in utilization of virus as bionanoparticle scaffold to direct stem cell response.[31] We have previously demonstrated that TMV coated surfaces strikingly accelerated BMSCs bone differentiation in comparison to conventional tissue culture polystyrene.[32] Moreover, when a phosphate group was chemically introduced to the TMV coat protein, the osteogenic differentiation of BMSCs was more evident, as indicated by greater increase in osteocalcin mRNA expression level.[25] We proposed that the structural features of TMV played a role in the improvement of stem cell differentiation. Continued efforts by Sitasuwan *et al*. indicated

that an enhanced BMP2 expression at both mRNA and protein levels within 8 h of osteoinduction was only for BMSCs cultured on TMV-coated surfaces and not when TMV was supplemented in media.[17] These findings have suggested the potential of applying TMV as a scaffold to modulate the BMP2 regulation during early osteogenic differentiation and potential osteogenic inducer for stem cells. In this regard, the development of 3D matrices was deemed essential to determine similar enhanced differentiation events observed with BMSCs on 2D scaffolds. In this study, we present an economical, convenient, and versatile method of producing a fuctional 3D culture system by incorporating the TMV particles. Our work is considered a pilot study and the first reported method of noncovalent incorporation of TMV particles in 3D porous hydrogels.

1.2.1 Synthesis and characterization of porous alginate hydrogels

TMV was introduced into the hydrogel by adding the noninfectious virus particles during the formation of gas templated, porous alginate hydrogels (PAH; Figure 1.1). The porous alginate hydrogel was fabricated following the report by Barbetta *et al*., which provided physical and mechanical parameters for potential use as 3D culture system.[28] This process did not require covalent modification or further purification, which reduced concerns for protein deformation during covalent chemical conjugations and eliminated the need to engineer reactive sites to incorporate the biological molecules in the hydrogels. The initial homogeneous mixture of alginate in bicarbonate solution with low concentration of surfactant (Pluronic F-108) is reacted with a mild acid (citric acid) to generate CO_2 *in situ* (Figure 1.1A). After the formation of the initial gas templated foamy material, the virus is added as a solution to the mixture and the entire foamy material is

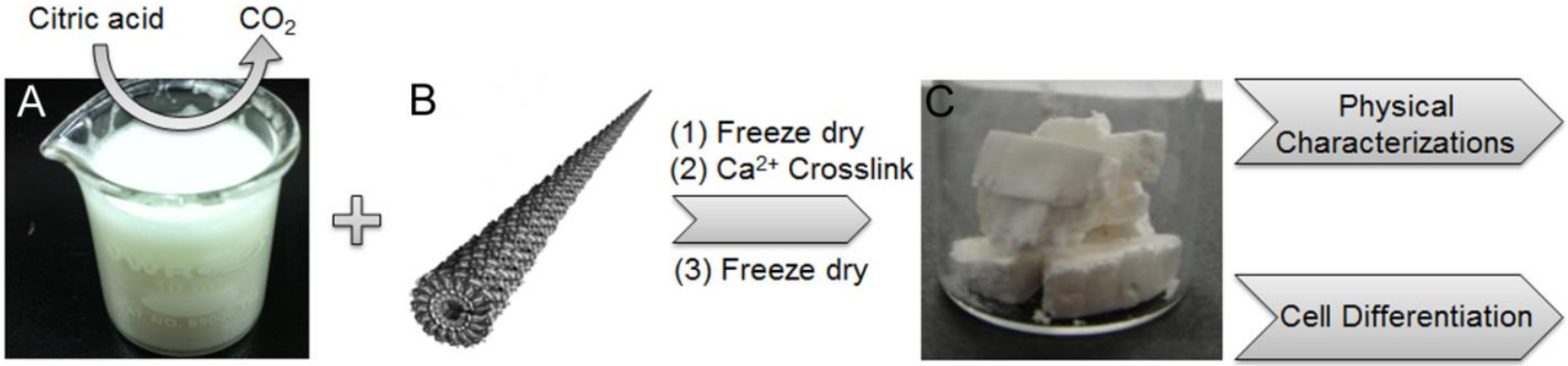

Figure 1.1. Synthetic procedure of generating virus functionalized porous composite hydrogels. Functionalization of composite hydrogels for use in stem cell cultures can be achieved through direct mixing of virus solution to the foamy mixture of alginate. (A) Alginate mixture comprised of low viscosity alginate, Pluronic F108, and sodium bicarbonate with an equivalent amount of citric acid to generate gas template foamy mixture. (B) TMV was added 5 min before the foamy mixture was frozen and lyophilized. The lyophilized sample was crosslinked with $CaCl_2$. (C) Porous composite hydrogel was obtained after dialysis against 0.1 M $CaCl_2$ and lyophilization.

flash frozen then cross-linked. Additional dialysis and lyophilization steps provided the final PAH functionalized with the virus particles. Developing 3D scaffolds for tissue engineering, such materials need to have a range of macropores and proper size of interconnecting channels that allow penetration of gas, nutrient and cellular infiltration.[33, 34] Previous studies revealed that a pore size and an interconnecting channel of 100−300 and 40 μm, respectively, are essential for the cell survival and proliferation.[28, 35] In this porous alginate hydrogel, macropores were generated by *in situ* gas (CO_2) generating system composed of $NaHCO_3$ and citric acid, suspended and stabilized by surfactant (pluronic F108) with the help of high viscosity from 5% alginate until the mixture was freeze-dried and cross-linked. PAH has provided a coarse structure for 3D cell housing but lack the biofunctionalities in general. We fine-tuned the PAH by physically mixing TMV particles during PAH synthesis. As a proof of concept, genetically engineered TMV that precisely display integrin binding ligands, which we called TMV-RGD1,[36, 37] was incorporated into the hydrogel mixture in the same way as TMV. The resulting modified-PAH hydrogel successfully displayed RGD peptide sequences as indicated by enhance cell attachment and cell viability. Similar to wild-type TMV, this RGD mutant could be manufactured by the infected tobacco plants and easily purified in a very similar procedure as wild-type TMV with high yields.[24, 37, 38] The economical production of the mutant TMV particles and the potential virus-based combinatorial functionalization of 3D material may prove to be useful for expanded material development.

The incorporation of the virus particle, its structural integrity, and its effects upon the overall PAH formation (pore deformations, swelling property, and mechanical property) was initially assessed by ESEM. The low magnification images obtained by

ESEM revealed similar macropores and interconnecting channels ranging between 10 and 500 μm for both PAH (Figure 1.2A) and TMV-PAH (Figure 1.2C). These similarities suggest that the addition of the virus did not hinder pore formation. The overall architecture of the pores for PAH (Figure 1.2A) appeared to be more compact when compared to the pores observed for TMV-PAH (Figure 1.2C). At a higher magnification, PAH indeed shows smaller pores and denser networks (Figure 1.2B) than TMV-PAH, whereas larger spherical pores (100−500 μm) were visible in TMV-PAH (Figure 1.2D). These images indicate that the overall hydrogel formation (macropores and interconnecting channels) is not hindered by the incorporation of the virus, which, instead, can further facilitate the formation of large, well-defined pores. It is possible that the addition of TMV stabilizes the interface between gas/liquid phase.[39] TMV particles could help trapping larger hydrophobic gas pockets upon the generation of CO_2 to better mediate the interfacial tension between aqueous and gas phases.

To verify this simple incorporation method and to confirm that the incorporated virus still maintains its original rod-like structure, the existence of TMV intact particles in the hydrogels after the entire synthesis process was observed under TEM. Addition of a chelator, EDTA, was sufficient to de-crosslink the PAH and subsequently release the viral particles to the solution. This de-crosslinking step was used to determine whether the same amount of virus could be recovered from PAH, and whether the viral particles were still structurally intact. The recycled TMV particles (Figure 1.2E) is similar in size and shape under TEM in comparison to the TMV particles prior to incorporation (Figure 1.2F). UV−vis absorbance at 260 nm of the de-crosslinked TMV-PAH solution indicated that nearly all virus particles could be retrieved after treating the hydrogel with EDTA

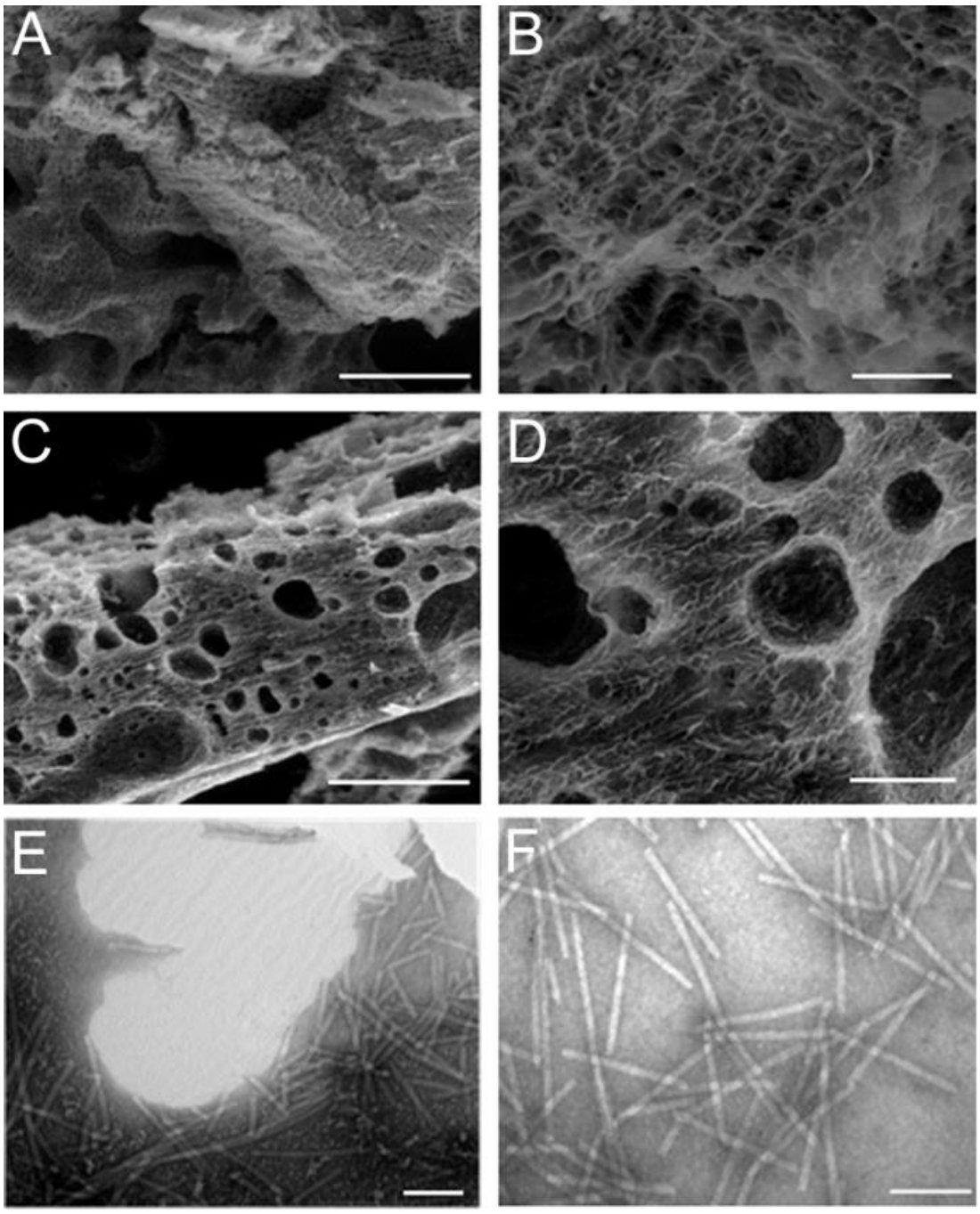

Figure 1.2. (A-D) Scanning electron micrographs of hydrogels and TMV particles: (A) and (B) PAH at different magnifications; (C) and (D) TMV-PAH at different magnifications. The images of TMV-PAH reveal larger macropores and interconnecting channels than PAH. Transmission electron micrographs of (E) intact TMV particles released from TMV-PAH after decrosslinking with EDTA, and (F) purified native TMV particles in buffer. Scale bars are 500 microns for (A) and (C), 100 microns for (B) and (D) and 200 nm for (E) and (F).

(based on 0.1% TMV solution having an absorbance of 3 at 260 nm). A defining physical characteristic of hydrogels is their swelling property that provides an aqueous environment comparable to soft tissue. Both PAH and TMV-PAH hydrated 6−7 times their original dry weight and was fully hydrated within 2 min (Figure 1.3A, B). A slight increase in swelling ratio was observed during the 4-week incubation, which could indicate a possible onset of the degradation of the scaffold, although such an observation was not accompanied by a significant change in macroscopic dimension of the scaffold (Figure 1.3C). Despite the lack of covalent conjugation of TMV to the alginate hydrogel, the virus was stably integrated into the hydrogel. The amount of TMV released from TMV-PAH into the aqueous solution was measured and it confirmed that most TMV particles were entrapped in the hydrogel matrices even upon long-term incubation in solution. The release profile derived from fluorescein-modified virus particles suggests that dye modified TMV is slowly released from the hydrogel to a maximum 13% of its original concentration after 24 h in solution and plateaued thereafter (Figure 1.3D). This release profile may be reflective of any residual small dye molecules, broken particles, or weakly embedded particles on the outer surface that are released to the solution. Future studies probing this initial release profile with long-term release kinetics would be of interest for time-controlled drug or biologics delivery platforms.

The mechanical properties of stem cell microenvironments are well-recognized as essential determinants of differentiation fate. The mechanical factors that promote certain stem cell fates can vary dramatically, with as much as 300-fold difference in elastic modulus between matrices that favor soft brain tissue (0.1 kPa) and decalcifying bone (>30 kPa).[40] In our study, the impact of TMV nanoparticle inclusion on the mechanical

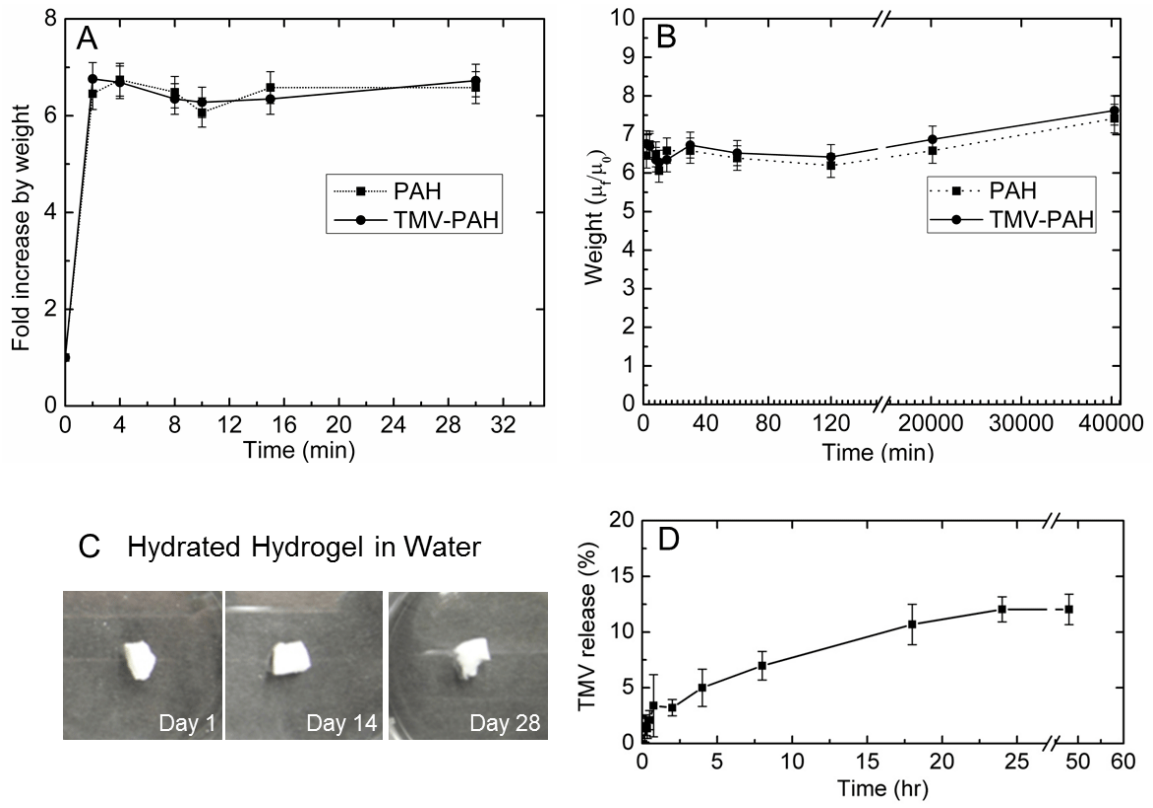

Figure 1.3. Swelling property and stability of porous alginate hydrogels. (A) Both PAH and TMV-PAH can absorb water and swell to the maximum within 2 min. (B) Total masses of hydrogels soaked in water over time (fold increase of initial dry weight) are constant and similar of both PAH (without TMV) and TMV-PAH (with TMV). (C) Photographs of PAH soaked in water for 1 day, 14 days, and 28 days. (D) TMV releasing profile shows the capability of TMV-PAH to maintain majority of the TMV nanoparticles within the hydrogel.

properties of PAH was assessed through unconfined compression testing. Regardless of the irreversible water loss from the hydrated specimens during compression, stress versus strain curves demonstrated that incorporation of virus in PAH induce a shift from a linear to nonlinear mechanical response (Figure 1.4). The incremental elastic moduli extracted from average stress−strain curves indicate that virus-modified materials are stiffer in the lower strain regions (0−0.05), but more compliant at the higher strains (0.1−0.15; Table 1.1). These observations in mechanical properties may be explained by corresponding effects on material pore architecture (Figure 1.2A−D), in which TMV inclusion caused an increase in pore size. It is plausible that the alginate bulk is mechanically reinforced by the inclusion of TMV particles (resulting in increased stiffness at low strains), but the macroporous architecture begins to collapse at higher strains causing a reduction in material stiffness.

In thermal analysis, while modulated differential scanning calorimetry (MDSC) data supported the incorporation of virus particles into PAH, we showed that TMV did not significantly impact the thermostability of original PAH, as indicated by thermogravimetric analysis (TGA). As there were no covalent modifications on the polymer chain structure, alginate still maintained their own properties and dominates as a bulk material. The results showed similar decomposition profiles from TGA as well as heat flow profiles obtained from MDSC in all three types of hydrogels (Figure 1.5). The initial weight loss from TGA appeared to be water loss since the hydrogels are highly hygroscopic. However, the major decomposition point started at 235−240 °C referring to the decomposition of alginate, which is consistent with previous report.[41] There were slight variations in weight loss profiles that could possibly be caused by intrinsic water in

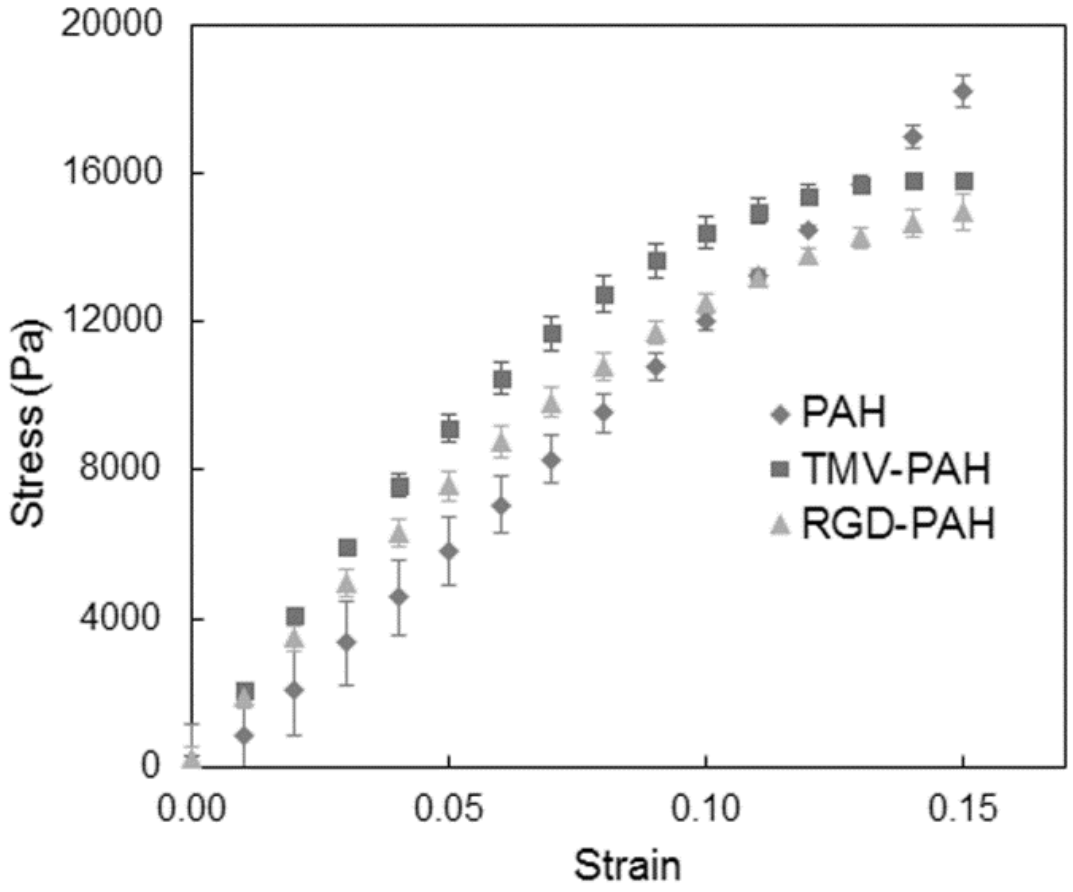

Figure 1.4. The mechanical response of PAH, TMV-PAH, and RGD-PAH to unconfined compression. PAH exhibited linear behavior, while both forms of virus modified PAHs (TMV-PAH and RGD-PAH) induced nonlinearity at high strains (>0.1). Values expressed are means (n=3) ± S.D.

Table 1.1. Incremental elastic moduli of PAH, TMV-PAH, and RGD-PAH in two compressive strain ranges (0-0.05 and 0.1-0.15). Values expressed are means (n=3) ± S.D.

Strain range	Incremental Modulus (kPa)		
	PAH	TMV-PAH	RGD-PAH
0-0.05	103.92±23.10	183.01±13.09	146.56±7.49
0.1-0.15	123.71±13.15	31.17±6.03	49.47±13.15

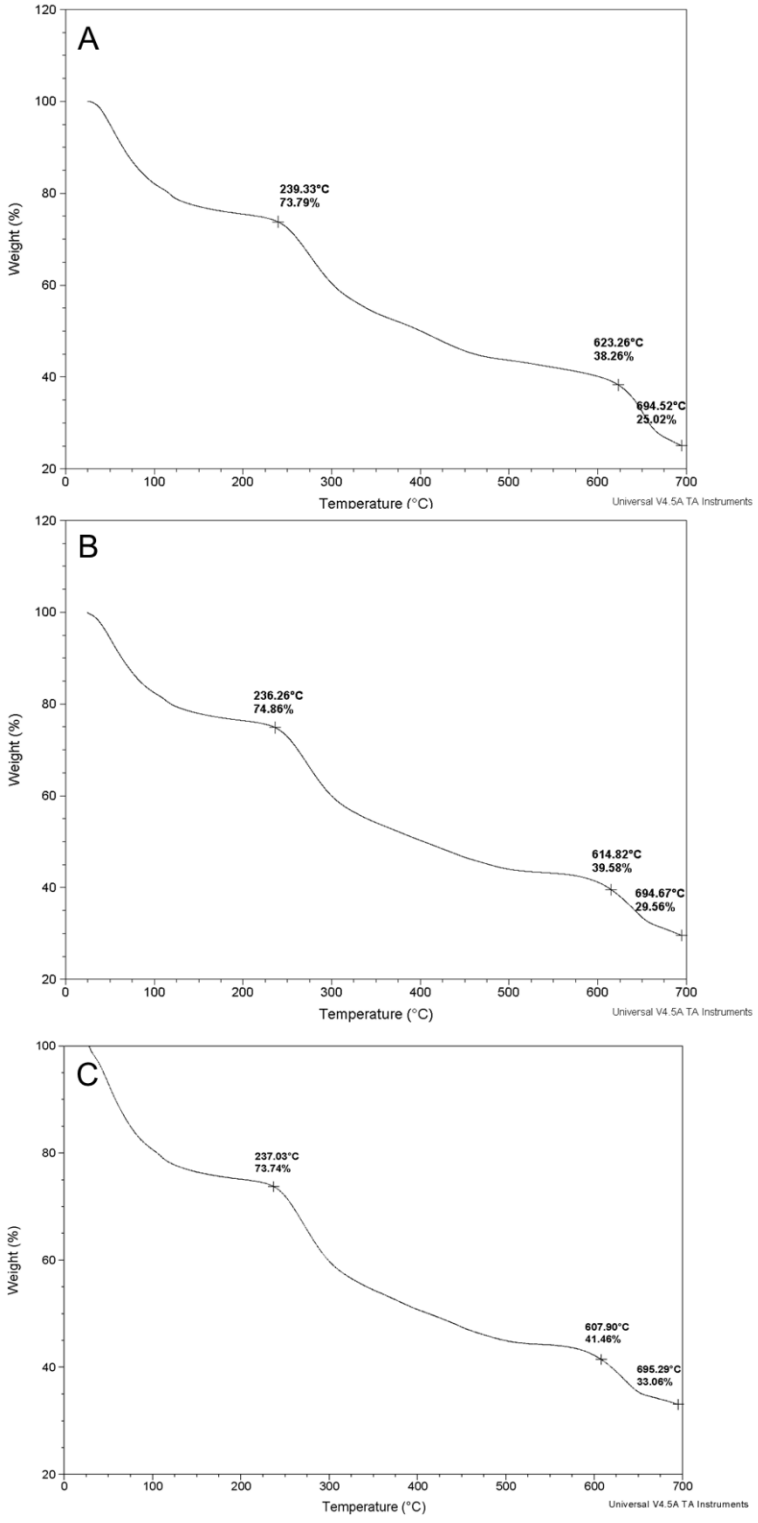

Figure 1.5. TGA (Termogravimetric analysis) characterization of porous composite hydrogels. The porous composite hydrogels (A) PAH, (B) TMV-PAH, and (C) RGD-PAH have similar weight-loss decomposition profiles

hydrogels. The thermal decomposition of TMV could not be observed from this experiment, which is possible that the virus were decomposed in the same temperature range as alginate. MDSC showed very broad endothermic peaks of the overall heat flow profiles from all three types of hydrogels due to the dominance of amorphous characteristic of hydrogels. The peak shift showing a combination of heat profiles from PAH and TMV alone was observed on TMV-PAH, which was similar to the profile of RGD-PAH. This could indicate some interaction occurring between virus particles and PAH (Figure 1.6).

1.2.2 Cell attachment and cell viability in 3D virus-incorporated hydrogels

A number of studies have been done on modifying hydrogel scaffolds with peptide sequence by peptide-polymer conjugation in order to probe substantial cell recognitions. As the concept of multivalency effect in which intracellular cell machinery is believed to be under integrative control of cell microenvironment by means of ligand density and ligand orientation through oligomerized cell-surface receptors, the major threat of peptide modifications is the lack of control over the spatial distribution of ligands displayed on modified polymer in 3D system.[42] Distinctively, we suggested the opportunity of using virus nanoparticle to introduce the multivalency of ligands in 3D system. Our previous experiment showed that the cell binding ligands on TMV-RGD1 mutant were exposed and accessible for the cells.[37] To demonstrate the potential use in cell cultures, cell attachment, and viabilities were determined for the three types of hydrogels. Despite the arrest in metabolic activity from a slow differentiation that might occur without the specific induction in serum-rich condition, the hydrogels were shown to be safe for

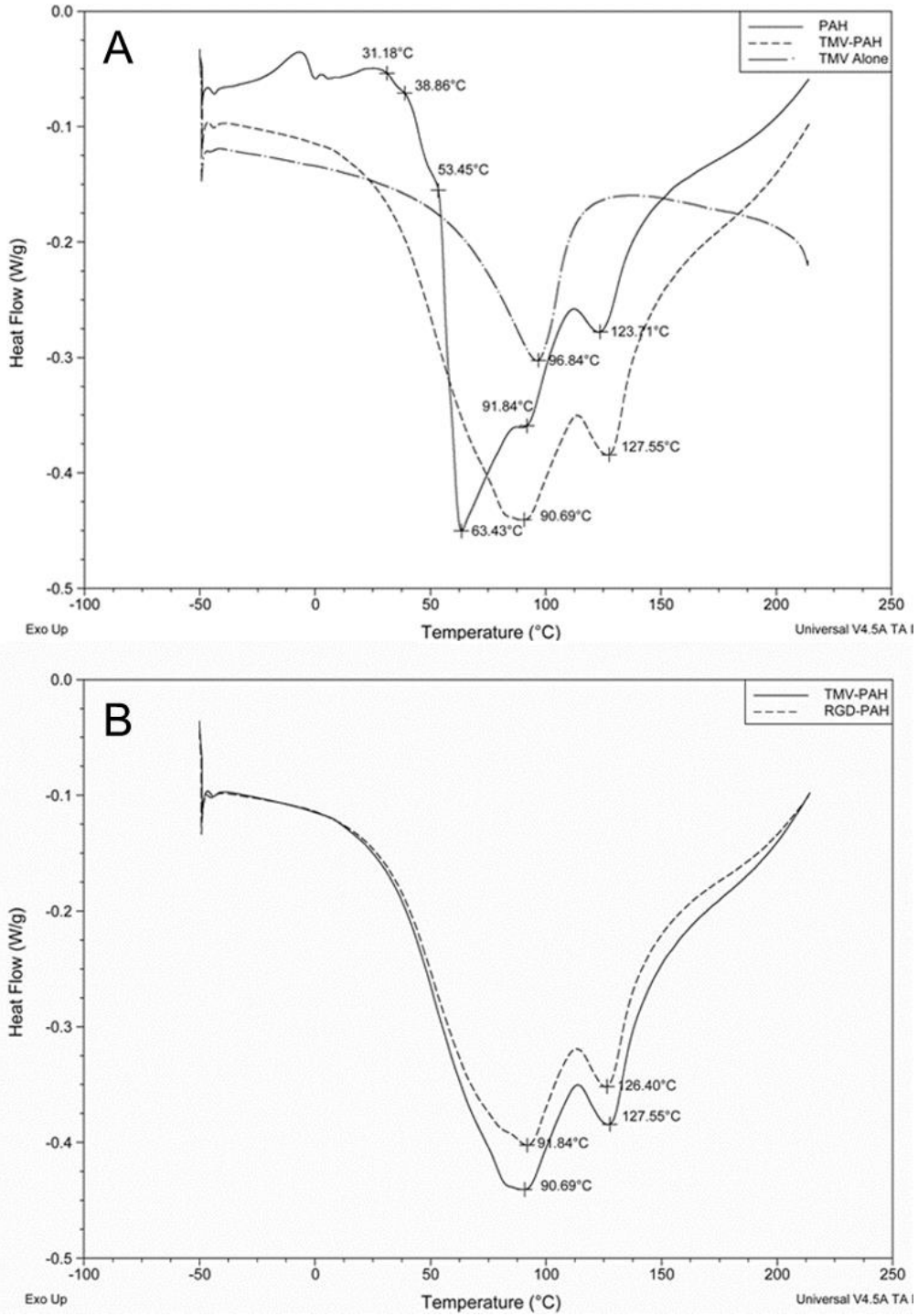

Figure 1.6. MDSC (Modulated Differential Scanning Calorimetry) characterization of porous composite hydrogels. (A) An overlay total heat flow profile of PAH, TMV-PAH and TMV alone showed the temperature shift on TMV-PAH as a combination of PAH and TMV alone. (B) RGD-PAH showed similar total heat flow profiles with TMV-PAH.

BMSCs culture because they survived and were able to grow in the PAH either with or without the viral particles. In cell attachment assay, RGD-PAH (96 ± 1%) had significantly higher cell attachment after 8 h of incubation than PAH (85 ± 3%). The incorporation of TMV did not provide any significant improvement to cell attachment when compared to the control (85 ± 1%; Figure 1.7A). Based on the metabolic assay with CTB reagent, the cell viabilities in all three different types of hydrogels were determined for days 8 and 14 cultures and normalized to metabolic rates of cells in PAH (Figure 1.7B). The results indicate that BMSCs survived in both virus modified PAHs (TMV- and RGD-PAH) and the cells cultured on RGD-PAH continued to have the highest metabolic activity (Figure 1.7B). However, there was no further increase in metabolically active viable cells from day 8 to day 14. One possible explanation is that the change in metabolic activity of cells due to the differentiation also occurred slowly without osteogenic induction supplements in TMV-PAH and RGD-PAH. This explanation was supported by the previous report from our group, which tested on a TMV-coated substrate.[17] Despite the lower attachment numbers and cell numbers for PAH and TMV-PAH samples, the cells could penetrate deeply into the hydrogel, as indicated by ESEM analysis (Figure 1.8). The morphology of the cells was visualized by ESEM in which the BMSCs adhered and spread out for both PAH (Figure 1.8A) and TMV-PAH (Figure 1.8B). The same morphology and spreading of adherent cells is observed for cells cultured in RGD-PAH.

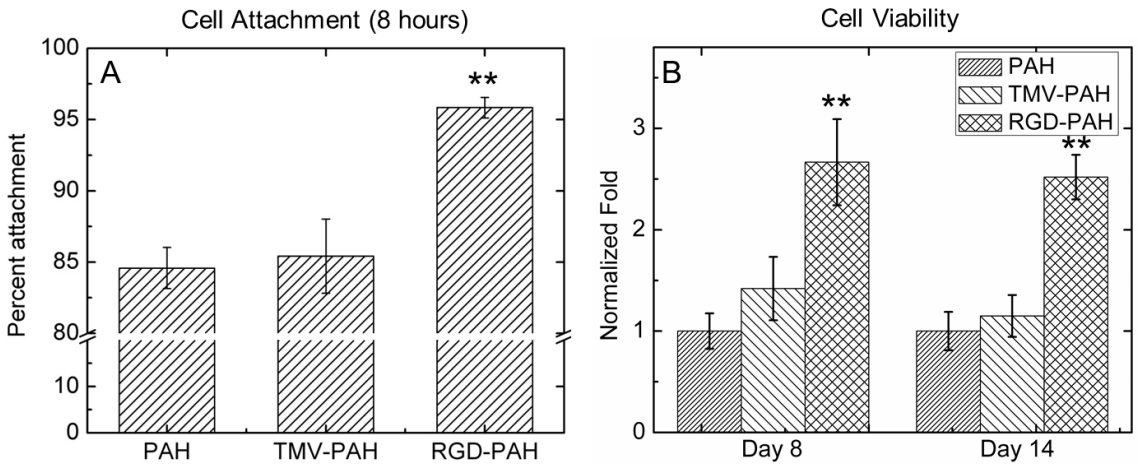

Figure 1.7. Cell attachment and viability in different types of porous composite hydrogels. Cell attachment was observed from counting the floating cells in the media after initial cell seeding for 8 h. (A) Percent attachment of BMSCs in each type of hydrogels. Values expressed are mean (n = 3) ± S.D. (B) CellTiter Blue® metabolic activity assay of BMSCs culture in different types of hydrogels at different time points. Values expressed are mean (n=3) ± S.D. of RFU that were normalized against PAH for each time point. Samples were compared using paired equal variance student t-test, **$p < 0.005$.

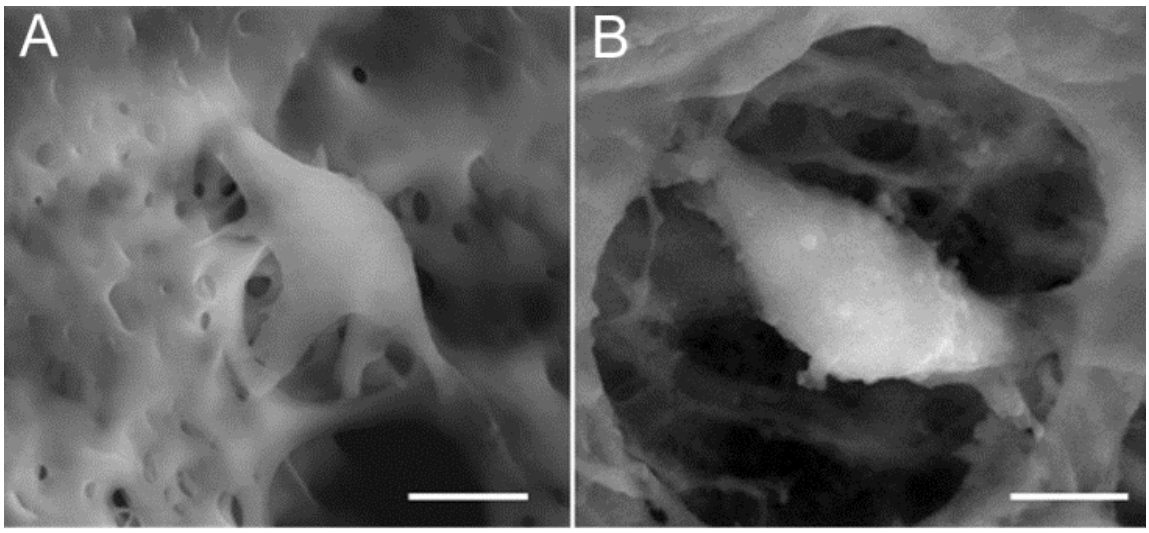

Figure 1.8. Scanning electronic micrographs of cell inside the hydrogels, showing the cell morphology in porous composite hydrogel (A) PAH and (B) TMV-PAH. Scale bar = 10 microns.

1.2.3 Osteogenic differentiation of BMSCs in 3D virus-incorporated hydrogels

For the application point of view, our previous works provided a solid background of bone tissue development improved by TMV and other plant viruses. The 2D studies demonstrated that substrates coated with plant viruses supported BMSCs growth and accelerated cell differentiation.[32] TMV decorated with phosphates caused an increased calcium sequestration and higher expression levels of genes related to osteogenesis.[16] Plus, the concept of diversity in differentiation ability of BMSCs has been well established in the past years. In particular, their osteogenic differentiation potential has become one of the most widely studied topics in bone regeneration. Large extent of research has shown promising results when using osteoblasts differentiated from BMSCs in bone regenerative processes.[43, 44] The differentiation studies in our 3D devices were directed to the osteogenic lineage of BMSCs in osteogenic supplemented media. The differentiation of seeded BMSCs toward the osteogenic lineage was explored by analyzing several cell differentiation markers.

First, the activity of alkaline phosphatase (ALP), an early osteoblastic marker that reflects not only the stage of cell differentiation but also represents the percentage of committed osteoprogenitor cells, was evaluated. The activity of this enzyme increases during synthesis of the extracellular matrix, which corresponds to the beginning of cell differentiation.[45, 46] The ALP activity was initially assessed at days 3, 7, and 14 upon culturing in the osteogenic medium (Figure 1.9A). Low levels of enzyme activity were detected for all three samples for day 3 cultures, followed by marked increases in ALP activities on days 7 and 14. The incorporation of the virus did not appear to hinder the differentiation potential as the same elevation trends of overall ALP activities were

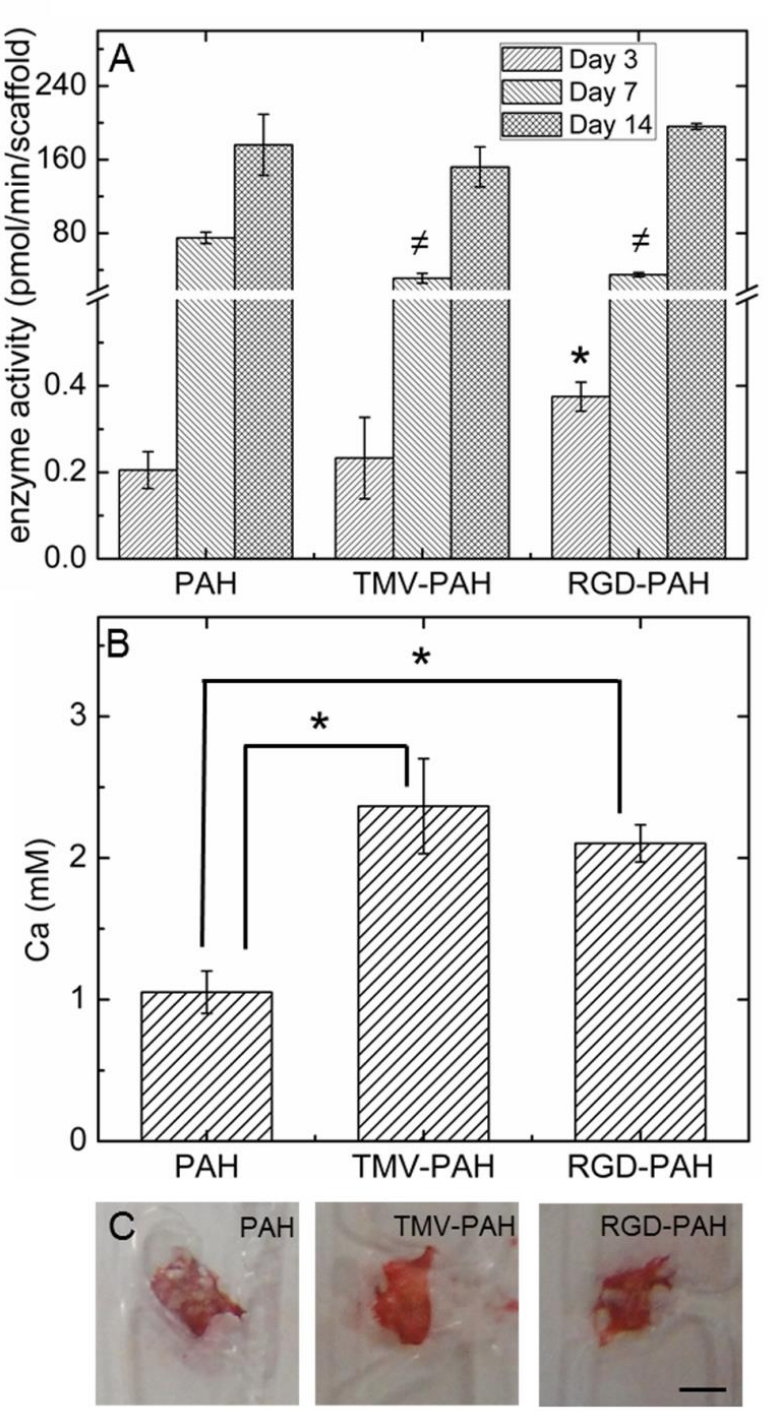

Figure 1.9. Osteogenesis assays of BMSC in porous composite hydrogels. (A) ALP activity assay was performed on day 3, 7, and day 14 of osteogenic culture. Values expressed are mean (n=3) ± S.D., $^{\neq}$*paired equal variance Student t-test, $p < 0.05$. (B) Calcium deposition quantified by ICP-OES on day 6 after background subtraction from control samples with no cells. Values expressed are mean (n=3) ± SEM, *paired equal variance Student t-test, $p < 0.05$. (C) Thin sections of hydrogels stained with Alizarin red on day 14 cultures, scale bar = 2 mm.

measured among the three groups from day 3 to day 14. Interestingly, RGD-PAH seemed to accelerate an early osteogenesis of BMSCs as the ALP activity was significantly higher among three samples on day 3. However, on day 7, the unexpected higher level of ALP activity was observed for PAH compared to the virus-functionalized PAH. Based on the comparison of the three matrices cultures, ALP activity was found to be the same trend, showing an increase in the enzyme activity from day 3 to day 14 in all three hydrogels as the development of bone tissue. Essentially, the incorporation of TMV-RGD1 was shown to promote an early stage differentiation by significantly elevated ALP activity observed on day 3 compared to those from PAH and TMV-PAH.

Although the ALP activity's result from day 7 showed otherwise, the following calcification analysis from ICP-OES showed the significant increase in mineralization in RGD-PAH that was already occurred on day 6. Calcium deposition in three types of hydrogels with BMSC osteogenic culture was quantified by ICP-OES (Figure 1.9B). The average amounts of calcium deposited in both TMV-PAH and RGD-PAH after background subtraction from control samples without cells were higher than in PAH (Figure 1.9B). All three types of hydrogels with BMSCs osteogenic culture were stained with Alizarin red giving intense red color (Figure 1.9C). Although calcium is used as a cross-linking agent, PAH without cells stained lighter pink with the dye (see Appendix B). A higher calcium level of osteogenic culture in TMV- and RGD-PAH could be a consequence of the high calcium binding affinity of TMV.[47, 48] This issue was taken into account as the calcium produced by differentiating cells could be sequestered more in TMV- and RGD-PAH. The high level of calcium accumulation indicated an enhanced bone formation.

Hydroxyapatite is a major mineral component of calcified tissue (bone and teeth). Its composition is a crystalline form of calcium (Ca) and phosphorus (P), with the formula $Ca_{10}(PO_4)_6(OH)_2$.[49] To further confirm the presence of Ca and P in the stem cell impregnated hydrogels, elemental analysis for the two samples were determined. The results indicate deposition of calcium phosphate around the cell areas with higher Ca levels detected for both PAH with and without TMV (Table 1.2). In PAH, the amount of P was less as nondetected in the scaffold.

As BMSCs undergo the phase of the maturation and ECM remodeling, osteocalcin is considered as the most specific marker of mature osteoblasts. Osteocalcin is a calcium binding protein, gets accumulated in mineralized bone, and binds actively to hydroxyapatite crystals promoting bone crystal growth.[31] It actively controls the process of ossification, ECM remodeling, and maturation. We observed this biomarker via immunostaining, which exhibited the intense localization of osteocalcin within 13 days of osteogenic induction culture in all three composite hydrogels. Figure 1.10 illustrated the accumulation of osteocalcin after day 10 (PAH) and day 13 (TMV-PAH and RGD-PAH) and confirmed that virus incorporation into 3D matrices did not impair the differentiation potential of BMSC into osteogenic lineage.

Also, the results from calcium deposition studies including Alizarin red staining, quantification of calcium deposited in the hydrogels by ICP-OES, and elemental analysis using EDX confirmed that differentiated BMSCs underwent mineralization process in composite porous hydrogels under BMP-2 free osteogenic induction. However, unlike what others have reported on similar work with RGD peptide modification in hydrogel systems,[50] the results herein did not show a dramatic increase in ALP activity on early

Table 1.2. Mineralization assay by EDX (Elemental analysis) of BMSC osteogenic culture on day 17 in PAH, TMV-PAH, and RGD-PAH showed peak intensity for calcium and phosphorous around the cell in all three samples.

	Elements	Around cells	Scaffold
PAH	P	9.55	N/D*
	Ca	69.15	56.75
TMV-PAH	P	15.45	17.05
	Ca	283.6	160.65
RGD-PAH	P	23.00	18.00
	Ca	217.85	148.75

*Not detected

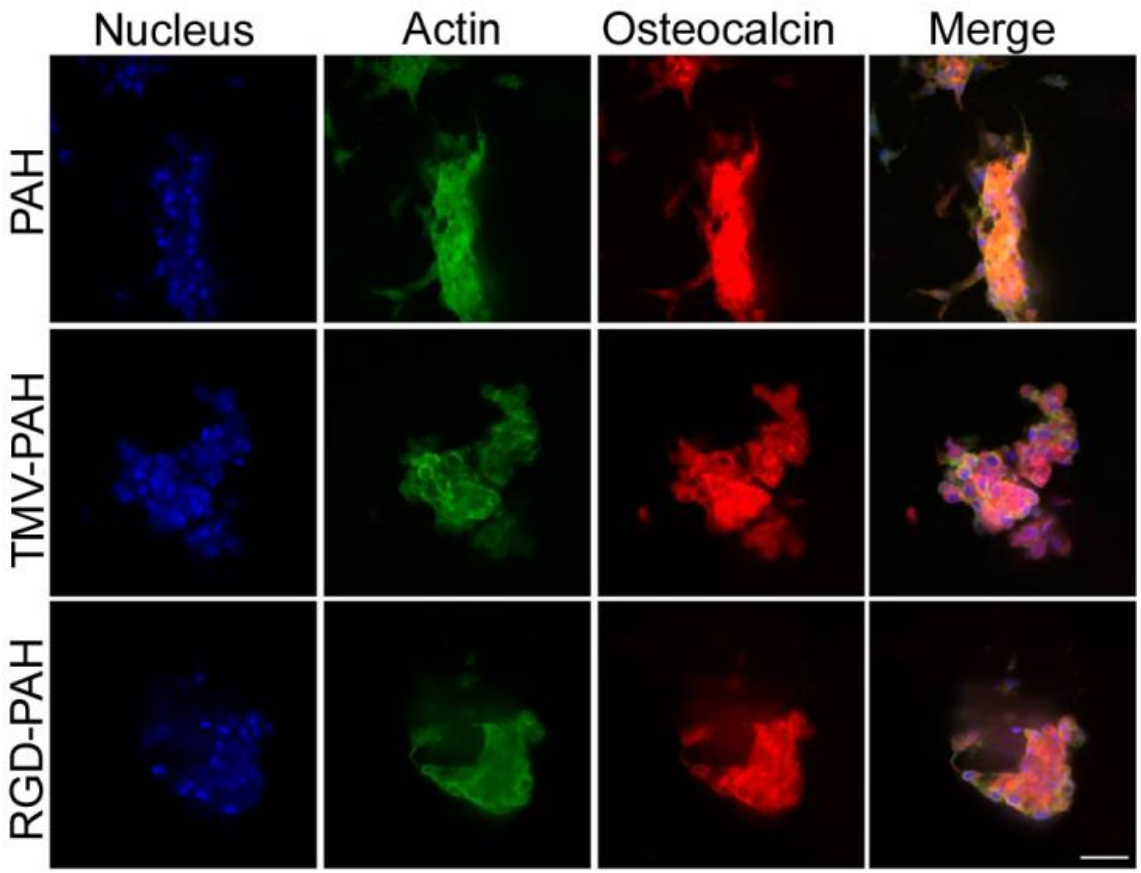

Figure 1.10. Confocal images of differentiated BMSCs in 3D composite hydrogels stained for nucleus (blue), actin (green) and osteocalcin (red). Scale bar = 50 microns.

BMSC differentiation when more biofunctionality was added through TMV-RGD. The possible explanation could be the limited concentration of RGD peptide that was exposed in the hydrogel due to the fairly low percentage (0.1%) of TMV-RGD incorporated in the hydrogel. Yang *et al*. demonstrated that RGD can promote ALP and osteocalcin production of BMSCs, however, in a dose-dependent manner, in peptide covalently incorporated poly(ethylene glycol) diacrylate hydrogel.[51] Therefore, the optimum concentration of TMV and TMVRGD can be further explored to improve the BMSC osteogenesis in this system

Moving forward in a tissue engineering direction, a near future study will be focusing on the improvement of hydrogel synthesis regarding uniformity in size and shape of hydrogels, essentially for further *in vivo* studies, including biocompatibility and *in vivo* bone formation. Besides, with the unique nature of TMV, we can potentially bring other specific ligands to 3D porous composite hydrogel with multivalency directing the stem cell differentiation in other lineages.[16] In addition, there are opportunities to develop this virus-based combinatorial hydrogel functionalization for better therapeutic outcome, for example, conjugation of growth factors and other small molecules to promote stem cell differentiation or vascularization, as well as endogenous stem cell recruitment chemokines to accelerate wound healing process.[52, 53]

1.3 Conclusion

We have successfully synthesized the alginate-based porous composite hydrogels functionalized with biomacromolecules and demonstrated their advantage as vehicles to support the 3D stem cell culture and differentiation. We have shown that TMV surface

can be accessible in 3D porous hydrogels as shown by significant improvement in cell attachment after functionalization by TMV-RGD1. Moreover, the incorporation of TMV and its RGD mutant can facilitate bone differentiation of BMSCs. This study is considered a proof-of-concept for utilizing virus particle to display functionalities onto the 3D alginate porous hydrogel. Together with further biocompatibility and bone formation studies *in vivo*, this system could be even more applicable for tissue engineering biocompatible matrix. This attractive approach could not only allow for the localization, delivery, and differentiation of stem cells but also contribute the advantage of simplicity in matrix modifications.

1.4 Experimental Section

All chemicals were obtained from commercial suppliers and used as received unless otherwise noted. Wild-type TMV (TMV) and its RGD-mutant (TMV-RGD1) were isolated from infected tobacco leaves following previously established protocols.[23]

1.4.1 Synthesis of virus-incorporated porous alginate hydrogels

The synthesis of gas template solid foam was based on the methodology reported by Barbetta *et al*.[28] Briefly, 5% w/v low viscosity sodium-alginate (Protanal® LF 10/60 FT, 30-60 mPas for 1%, kindly provided by FMC Biopolymer UK Ltd.) was dissolved in 2% w/v sodium bicarbonate ($NaHCO_3$) and 4% w/v pluronic F108 solution. Molar equivalent of citric acid with respect to $NaHCO_3$ was added to the mixture while stirring. Stirring was continued for 15 min to allow CO_2 to fully develop. Afterward, the foamy alginate solution was flash frozen in liquid nitrogen and freeze-dried. The resulting solid foam

was soaked in 2 M of $CaCl_2$ for 24 h to induce the formation of the calcium-based physical gel and then dialyzed against large volume of 0.1 M $CaCl_2$. Finally, the solid foam was freeze-dried, resulting in porous alginate hydrogel (PAH). For the TMV modified PAH (TMV-PAH), or mutant TMV-RGD1 modified PAH (RGD-PAH), 0.1% w/v of virus was added to the solution 10 min after adding citric acid. The mixture was stirred for another 5 min.

TMV-PAH was de-crosslinked and dissolved in 0.5 M EDTA, and the solution was analyzed under transmission electron microscopy (TEM) (Hitachi H-8000 microscope) on 300 mesh copper grids coated with carbon and stained with 2% uranyl acetate. The absorbance at 260 nm was measured by UV-Vis spectroscopy to confirm the concentration of TMV in de-crosslinked alginate solution.

1.4.2 Environmental scanning electron microscopy

Environmental scanning electron microscopy (ESEM) images and elemental analysis by EDX were obtained by FEI Quanta 200 electron microscope. Freeze dried samples were cut to about $2 \times 2 \times 2$ mm^3 cubes and mounted on aluminum stubs with carbon tape. For ESEM, samples were observed under a low vacuum with 30 kV of electron acceleration, a spot size of 4-6, and a 6-10 mm working distance. The same condition was used for EDX except the work distance was fixed at 10 mm and at least 3 areas were analyzed. Cell morphology in hydrogels was visualized by ESEM. Day 8 cultured hydrogel samples were prepared following the biological preparation procedure for ESEM. In brief, the samples were fixed in 2.5% glutaraldehyde in 0.1 M cacodylated buffer (pH 7.4) overnight at 4^0C and post-fixed in 1% OsO_4 in cacodylated buffer for 1 h at 4^0C in

dark. The samples, after being washed 3 times with cacodylated buffer, were frozen in liquid N_2 and lyophilized. The lyophilyzed samples were mounted on aluminum stubs using a carbon tape.

1.4.3 Swelling property of PAH

Swelling property of PAH was determined by the final weight divided by the initial weight of the hydrogel. The initial weights (2-3 mg) of freeze dried PAH and TMV-PAH were recorded (μ_0). Hydrogels were immersed in water, and then the weights after hydration of hydrogels were recorded over time (μ_f). Surrounding water was drained and blotted out with Whatman filter paper from hydrated hydrogels before weighing. The study was continued for 4 weeks to observe the stability of the hydrogels. The swelling ratio was defined as μ_f/μ_0.

1.4.4 TMV releasing profile

TMV releasing profile was observed for the stability of TMV-PAH. Fluorescently labeled TMV (TMV-Fl) was prepared by carbodiimide coupling reaction (see Appendix C for the MALDI-TOF analysis of the fluoresceinamine internal modification of wild-type TMV and TMV-Fl emission spectrum) according to the reported protocol[20] and incorporated in alginate hydrogels as previously described. Firstly, the standard curve (Appendix C) of fluorescent intensity from different concentration of TMV-Fl was generated. The reading was measured at 490/530 nm (Ex/Em). Each TMV-PAH ($3 \times 3 \times 2$ mm^3) was submersed in 1 mL 100 mM $CaCl_2$ Tris-buffered saline (TBS) pH 7.4. From each sample, 100 μL of

buffer solution was collected and replaced by the same volume of fresh buffer at different time points.

1.4.5 Mechanical testing

The mechanical properties of porous alginate hydrogels before and after the inclusion of TMV or TMV-RGD1 were compared via unconfined compression testing. Disk-shaped samples (3 mm height, 1.5 mm radius) of each material were maintained in TBS until the time of testing. Each hydrated material sample was placed between flat platens of a mechanical testing system (Bose Electroforce 3200 series instrument) and immediately subjected to displacement-controlled compression of 0.45 mm (displacement rate of 1 mm min^{-1}) without neither water submersion fixture nor water replacement during compression. Sample deformation and load were continuously recorded (50 measurement sec^{-1}) by the system software (Wintest), and subsequently processed to generate true stress versus strain curves. Material incremental moduli were calculated based on average data linearization in two strain regions (0-0.05 and 0.1-0.15) to provide a basis for assessing the effect of TMV or TMV-RGD1 inclusion on the mechanical properties of PAH.

1.4.6 DSC and TGA tests

Modulated differential scanning calorimetry (MDSC) measurements on dry PAH, TMV-PAH, and RGD-PAH were carried out using a TA Q2000-DSC thermal analyzer (TA Instruments, New Castle, DE, USA). Hydrogel samples and TMV alone (5-10 mg, with 0.1 mg accuracy) were packed down and sealed in aluminum solid pans, and an empty

pan was used as reference. The pans were heated at a scan rate of 3°C/min according the following program: equilibrated at 0°C, modulated at ±1°C every 60 sec, kept isothermal for 5 min, and then heated to 220°C. Reversible and non-reversible heat flow signals were separated from the total heat flow signals. The peak melting temperature was determined from the reversing heat flow signal.

Thermogravimetric analysis (TGA) was carried out using a SDT 2960 Simultaneous DTA-TGA thermogravimetric analyzer (TA Instrument). The sample was heated from room temperature to 700°C at a rate of 5°C/min under Helium gas flow. Prior to analysis, the samples were thoroughly dried in a vacuum for overnight.

1.4.7 Bone Marrow Stem Cells (BMSCs) isolation and culture

Primary BMSCs were isolated from the bone marrow of young adult 160-180 g male Sprague-Dawley rats (Charles River Laboratories). The procedures were performed in accordance with the guidelines for animal experimentation by the Institutional Animal Care and Use Committee, School of Medicine, University of South Carolina. Cells were maintained in complete primary media (Dulbecco's Modified Eagle's Medium (DMEM) supplemented with 10% fetal bovine serum (FBS)), kept at 37°C in a CO_2 incubator with 5% CO_2 : 95% air and passaged no more than seven times after isolation.

1.4.8 Cell seeding and attachment studies

Lyophilized PAH, TMV-PAH, and RGD-PAH were cut to $3 \times 3 \times 2$ mm^3 cubes. In each set of experiment, six hydrogels per type of sample were used for these studies. Hydrogels were sterilized in 70% ethanol for 15 min, ethanol was drained on sterile filter

paper and the hydrogels were further sterilized under UV-light for 60 min in laminar airflow hood. Hydrogels were then saturated in complete primary media at 37°C for 60 min, blotted excess media with sterile filter paper, and placed in 12-well non-adhesive plate (6 hydrogels in each well). BMSCs were harvested from 80% confluent culture flask using 0.25% trypsin/EDTA for 5 min and counted and re-suspended in complete primary media. 1.4×10^3 BMSCs were seeded per one volume of hydrogel. Rat BMSCs loaded hydrogels were initially incubated with 200 μL of complete primary media in each well to prevent hydrogels from drying out. After 6 h of an initial incubation, hydrogels were completely submersed in 1 mL of complete primary media in each well. The hydrogels seeded with rBMSCs were cultured at 37°C and 5% CO_2.

Attachment percentages were determined for different types of hydrogels on day 1 after cell seeding by counting floating cells in each well with a hematocytometer. Three separate experiments were carried out in this study.

$$\text{Attachment percentage} = \frac{\text{total seeding cell number-floating cell number}}{\text{total seeding cell number}}$$

1.4.9 Cell viability

CellTiter-Blue® (CTB) cell viability assay (Promega) after day 8 and day 14 of culture was performed for each type of hydrogel. The culture media in each well was replaced by 1 mL of pre-warmed media containing 10% CTB and incubated for 1 h at 37°C and 5% CO_2. The media containing CTB was used without cells as negative controls. The measurement of the CTB product was taken at two time points. First, to detect the cells that attached to the outer surface of hydrogel, the solution was collected and replaced with 1 mL of culture media. The incubation was continued for another 2 h to allow

diffusion of the fluorescent product from the inner part of hydrogel. After 2-hour incubation, the media solution was collected again and replaced with 1 mL of culture media in each well to continue cell culture. The 1:1 mixture of solution from first collection and second collection was measured for fluorescence intensity at 560/590 nm (Ex/Em) using SpectraMax M2 Multi-Mode microplate reader (Molecular Devices). Also, three separate experiments were conducted with each type of sample, which comprised of 6 hydrogels.

1.4.10 Osteogenic culture

After 1 day of cell seeding, complete primary media was replaced by osteogenic media consisting of DMEM supplemented with 10% FBS, 10 mM sodium β-glycerol phosphate, l-ascorbic acid (50 μg/mL), 10^{-2} μM dexamethasone, penicillin (100 units/mL), streptomycin (100 μg/mL), and amphotericin B (1 μg/mL). The osteogenic media was changed every 2 days. The culture was incubated at 37°C and 5% CO_2.

1.4.11 Alkaline phosphatase (ALP) and mineralization assays

Alkaline phosphatase (ALP) activity was determined using pNPP (p-nitrophenyl phosphate) assay (Sigma Diagnostics). After 3, 7 and 14 days, the hydrogels with cells were pre-washed with TBS then incubated with pNPP solution at room temperature for 2.5 h. Absorbance was read using a M2 SpectraMax plate reader at 405 nm indicating ALP activity levels. The enzyme activity was calculated from Beer-Lambert law as follow,

$$\text{Enzyme activity (}\mu\text{moles/min/}\mu\text{g)} = \frac{\text{V (}\mu\text{L)} \times \text{OD405nm (cm}^{-1}\text{)}}{\varepsilon \times \text{incubation time (min)} \times \text{enzyme (}\mu\text{g)}}$$

where ε is the molar extinction coefficient ($M^{-1} \times cm^{-1}$). For p-nitrophenol, ε = 1.78×10^4 $M^{-1} \times cm^{-1}$. OD405nm (cm^{-1}) is the absorbance at 405 nm divided by the light-path length (cm). V is the final assay volume (100 μL).

Alizarin Red S (ARS) staining for Ca^{2+} was performed on day 14 cultures. The hydrogels with cells were washed 3 times with TBS and fixed in 10% buffered formalin overnight and sliced into 1 mm thick samples. The sections were then stained with 0.1% solution of ARS (Sigma-Aldrich) pH 4.1-4.5 for 30 min, washed with 1:1 xylene:acetone solution and placed with toluene mounting solution on glass slides. Control experiments without cells were conducted for PAH, TMV-PAH, and RGD-PAH.

Calcium concentrations were quantified using Varian 720-ES ICP-OES (Inductively Coupled Plasma - Optical Emission Spectrometer) elemental analysis. Standards were created using 0-0.4 mg/L calcium standard solutions. PAH, TMV-PAH and RGD-PAH with similar size and weight were seeded with BMSCs and cultured with osteogenic supplement media until day 6. Samples were washed with sterile Milli-Q water and completely lysed with dissolving solution (0.1% HNO_3, 0.01% TritonX-100, in 100 mM sodium citrate). The dissolved samples were diluted to fit the range of the standard curve. Approximately 4 mL of each diluted sample was fed into the instrument per run. The experiment was performed in triplicates. Control experiments without cells were also performed for PAH, TMV-PAH, and RGD-PAH in the same manner.

1.4.12 Immunostaining

Immunostaining was performed to observe the presence of osteocalcin. rBMSCs culture in PAH, TMV-PAH, and RGD-PAH were terminated after culturing 10 days for PAH

and 13 days for TMV-PAH and RGD-PAH hydrogels in osteogenic media. Hydrogels were washed three times with 100 mM cacodylated buffer and then fixed in 2.5% glutaraldehyde in cacodylated buffer overnight. The fixed samples were then permeablized for 15 min in TBST (0.05% Tween20) and blocked in 2% w/v bovine serum albumin (BSA, Sigma–Aldrich) in TBS for 20 min with gentle agitation at room temperature. After blocking, the hydrogels were incubated for 2 h with primary antibody targeting the osteospecific protein osteocalcin (Santa Cruz Biotechnology). Secondary antibody detection Alexa Fluor® 546 (Molecular Probes, Invitrogen) was used for osteocalcin at 1:100 dilutions in blocking buffer for 1 h at room temperature. In the end, the hydrogels were washed with TBS and counter-stained with DAPI (nuclear staining) and FITC-Phalloidin (actin staining). Images of the stained samples were obtained using Olympus IX81 with DSU confocal mode under 20x oil lens (NA = 0.85). Exposure times were kept constant for all samples (500 ms for DAPI and phalloidin, 1000 ms for osteocalcin).

CHAPTER 2

IN VIVO COMPATIBILITY AND DEGRADABILITY OF TOBACCO MOSAIC VIRUS INCORPORATED HYDROGELS AS SCAFFOLDS FOR TISSUE ENGINEERING

3.1 INTRODUCTION

3.1.1 Virus and virus-like nanoparticles in tissue engineering

Virus nanoparticles are now gaining great interest from different interdisciplinary fields especially in material science as nanoscale building blocks. The major advantage of virus nanoparticles is that they can easily be produced in gram quantities with high uniformity in laboratory. Viral capsids can be in different sizes, shapes and arrangements. They are exceptionally robust in that their surface modifications are amendable by genetic and/or chemical approaches, thereby presenting different types of functionalities.[54, 55] The use of chemical ligands can be complemented by the genetic engineering of virus coat proteins that offer multivalency of specific peptides.[24, 56] Moreover, spatial display of signaling molecules or peptides can be obtained at the nanometer scale leading to the programmable designs for quantitative investigations of cell behaviors.[57, 58] Among viral nanoparticles, plant viruses are considered safer than human pathogen-derived viruses such as adenovirus in terms of handling, processing, and downstream medicinal applications.[59] These properties make the plant viruses attractive tools for biomedical applications including drug delivery and tissue engineering.[60, 61]

Our group had introduced the use of plant viruses as scaffolding materials to probe cellular behaviors. Some of the previous publications focused on the enhanced

bone regeneration from bone marrow stromal cells (BMSCs) using Tobacco mosaic virus (TMV) and its mutants.[16, 17, 25] Along the same line, our attempt has translated into a three dimensional (3D) model using alginate, a well-known biologically inert natural polymer, as the TMV-functionalized 3D hydrogel's base-material. The 3D porous alginate hydrogels (PAH) functionalized with wild-type TMV (TMV-PAH) and its RGD mutant (RGD-PAH) have been developed. This proof-of–concept study indicated that the integration of biofunctionality in 3D hydrogel could be simply achieved by the incorporation of viral nanoparticles which carry the functional units therefore maintain the ability to regulate cell behavior in the hydrogel environment. As shown in our study, RGD-PAH gel had increased cell loading capacity with higher alkaline phosphatase activity in early-stage osteogenesis of BMSCs in comparison to the control hydrogels (PAH and TMV-PAH). We suggested that TMV can be used as a platform to provide a variety of functionalities with nanoscale multivalency for tissue engineering applications.[37]

2.1.2 In vivo toxicity and degradation of plant viruses in biomedicine

In vivo properties, especially any potential toxic effect needs to be taken into account, when developing novel materials for biomedical applications. There have been many studies that reported the *in vivo* characteristics including biodistribution and toxicity of different types of viral nanoparticles used in biomedicine.[62-67] For example, spherical plant viruses, cowpea mosaic virus (CPMV) and cowpea chlorotic mottle virus (CCMV), as well as filamentous bacteriophage M13, showed a broad biodistribution throughout the body, albeit predominantly in the liver and the spleen.[63-66] Blood clearance

kinetics, biodistribution, and histopathology of rod-shaped TMV were also observed by Wu *et al*, 2013. The study demonstrated that radio-iodinated TMV was accumulated mostly in the spleen and the liver of BALB/c mice and U87MG tumor-bearing mice with no overt toxicity. About 97% of TMV particles were eliminated from the blood circulation by the reticulo-endothelial system (RES) within 40 minutes after intravenous (IV) administration of ~1 μg TMV per animal.[67] Liver and spleen are parts of the RES that play a critical role in removing antigens, including structured proteinaceous nanoparticles, from circulation through mononuclear phagocyte system (MPS).[62, 68, 69] Similarly, Steinmetz group studied pharmacokinetic properties of TMV in two different shapes, 300 x 18 nm rods and 54 nm spheres. The rapid clearance of TMV was confirmed in both shapes (rods had longer blood circulation) with blood and tissue biocompatibility. Moreover, PEGylation of TMV could create the stealth layer shielding TMV from recognition of RES leading to the longer circulation of the nanoparticle in blood stream.[62] However, the immune responses for TMV were not addressed.[62, 67] These studies suggested that, even though, the animal's physiologic system recognizes the viral nanoparticles as foreign bodies, these do not necessarily reflect the systemic toxicity.

Antigenicity of TMV has been well established for more than 50 years.[70, 71]This rod-like virus has been used extensively as a model system for studying various aspects of virus-antibody interactions. TMV, when administered with adjuvant, gives very high immunogenicity *in vivo* at doses as low as micrograms immunization per kilogram in rabbits and mice.[72-74] TMV has allowed immunologists to study and develop a system that can enhance immune response to pathogenic antigens for vaccine applications.[75, 76] Gilleland group constructed the genetically modified chimeric TMV by inserting

sequences representing peptide of outer membrane protein F of Pseudomonas aeruginosa between amino acids Ser154 and Gly155 of the TMV coat protein and observed the immunoprotection to the bacteria in a mouse model of chronic pulmonary infection.[77] Nevertheless, the systemic toxicity and immunogenicity of TMV as a functional material in implanted polymeric hydrogels for tissue engineering in animals or human has not been reported.

In our study, we focused on the toxicity of the hydrogels modified with TMV and its mutant in animal model. We studied the potential of using the TMV-functionalized PAH in stem cell bone tissue engineering *in vivo* by two means. First, the biocompatibility and possible toxic effects of the subcutaneously implanted hydrogels were investigated. The antigenicity of TMV in the hydrogel implant was also evaluated. Second, the biodegradability of hydrogels was observed at the endpoint of the animal study to further characterize this plant virus-hydrogel system regarding the suitability of its application for tissue engineering.

3.2 Results and Discussion

3.2.1 In vivo Biocompatibility of Plant Virus as Biomaterial for Tissue Engineering

Our recent discoveries suggested that TMV, as nanoparticle platform, offered a high density of biofunctional ligands that were able to probe different cellular responses including the induction of rapid bone differentiation in both 2D and 3D environments.[16, 25, 36, 37, 55, 78] As reported in our previous paper,[37] we have developed a 3D system of TMV-functionalized macroporous alginate hydrogel that could facilitate bone differentiation of BMSC *in vitro*. By incorporating RGD mutant of TMV to the hydrogel,

cell loading capacity increased by at least 12% and the stem cells expressed greater alkaline phosphatase activity after osteogenic induction. However, questions regarding the *in vivo* toxicity of TMV-modified hydrogel were still unanswered.[37] In this chapter, we performed careful studies mainly focusing on the *in vivo* biocompatibility of the hydrogels functionalized with wild-type TMV and its RGD mutant (Figure 2.1).

TMV is an RNA virus that typically infects plants and considered non-pathogenic in human. Meanwhile, the virus could highly induce the adaptive immune response in mammal.[79, 80] Because of its well-known immunogenicity in mammal, we here evaluated whether TMV, after being incorporated in the 3D biocompatible polymeric hydrogel scaffold, could still cause serious toxicity and/or physical symptoms derived from specific immune response in animal model. The animals were closely observed for the entire experimental period. The surgical wound heeled within 1 week. Grossly, all mice were normally active in eating, drinking, and grooming with no observable hair loss, skin wounds on implanted sites, and aggressive behavior. The body weight of mice with PAH, TMV-PAH, and RGD-PAH implanted were comparable to the mock group (without any implant) as shown in Figure 2.2.

The blood samples from each group of mice in 2 and 4 post-operative weeks were analyzed for total blood count. All animals had blood cell numbers counted in the normal ranges (values shown under the bottom x-axis, Figure 2.3). The host inflammatory responses after the surgery were evaluated by white blood count including total white blood cell (WBC), lymphocyte (LYM), monocyte (MON), and neutrophil (NEU) counts. In this study, these parameters in all mice were shown to fall in the normal range after week 2 and continued to be normal until the end of experiment at week 4 (Figure 2.3).

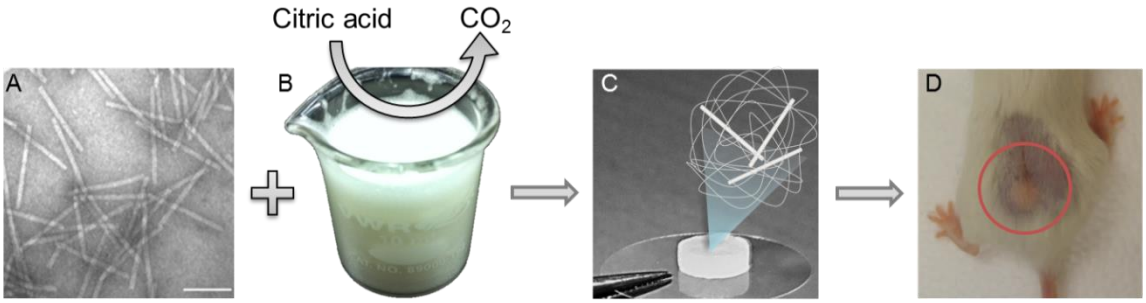

Figure 2.1. Schematic diagram depicted the synthetic procedure virus functionalized composite hydrogel for implantation. Functionalization of composite hydrogels can be achieved through direct mixing of virus solution to the foamy mixture of alginate. (A) TMV particles after purification in 0.1 M potassium phosphate buffer was added and dispersed into the foamy solution B. Scale bar is 200 nm (B) Alginate mixture comprised of low viscosity alginate, Pluronic F108, sodium bicarbonate with an equivalent amount of citric acid to generate gas templated foamy mixture. The mixture was molded, frozen and lyophilized. The lyophilized sample was crosslinked with CaCl2, then lyophilized. (C) The resulting hydrogel was 6.35 mm in diameter and 2 mm in height. (D) After hydrated by sterile PBS overnight, the hydrogel was subcutaneously implanted at the lower back of the experimental animal (circled).

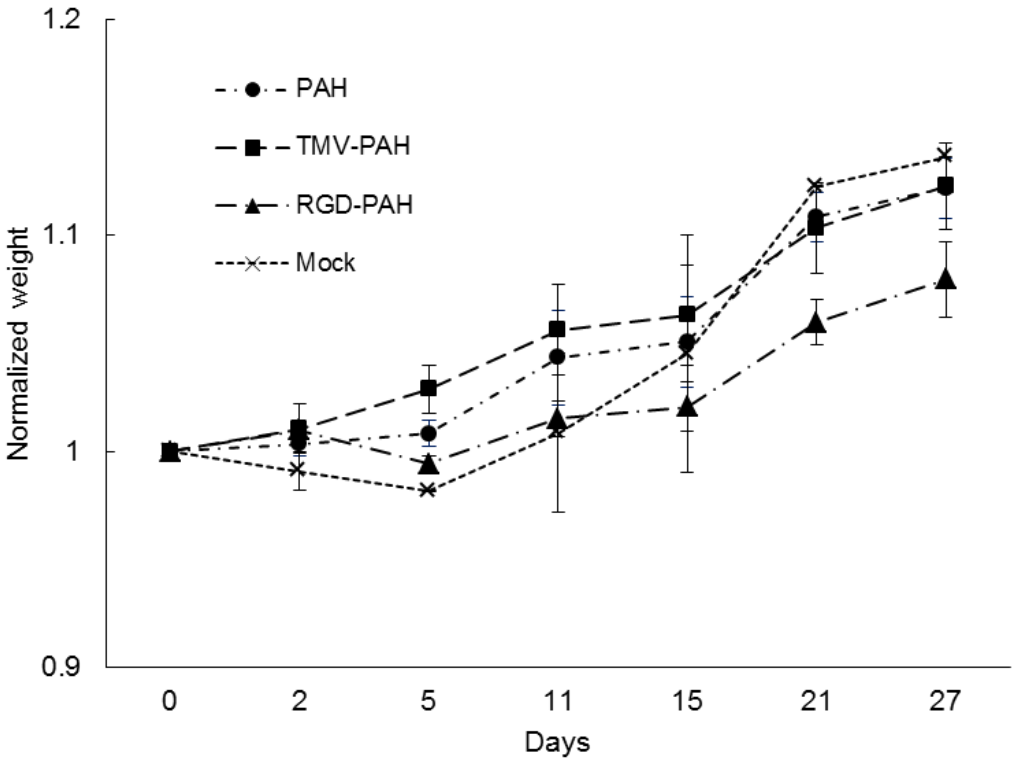

Figure 2.2. Animal growth rates were normal in all mice after implantation of different types of hydrogels. The actual body weight at each time point was normalized with the weight prior to the operation. The mouse weight was monitored along the experimental period of 28 days. All the hydrogel implanted mice were healthy and growing normally according to the mock control. Values expressed are means (n = 6, for day 2 – 14 and n = 3, for day 21 - 28) ± SD. Mock control data analyzed from 2 mocks on the first 2 weeks, but 1 mock after week 2.

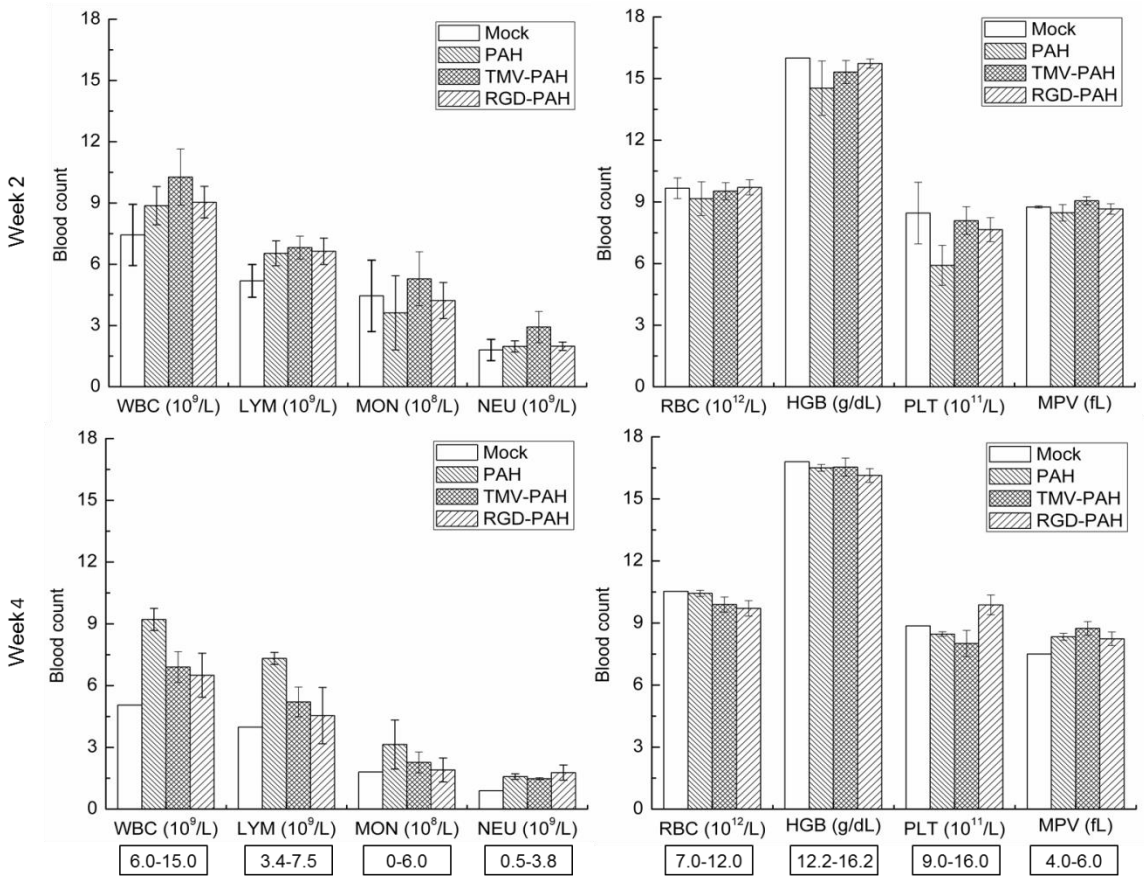

Figure 2.3. Total blood analysis of mice implanted with porous composite hydrogels. The hematology was essentially normal in all animals. The total blood counts were performed at 2 time points (2 and 4 post-operative weeks). The histograms showed the numbers of total white blood cells (WBC), lymphocyte (LYM), monocyte (MON), NEU (neutrophil), red blood cell (RBC), hemoglobin (HGB), platelet (PLT), and mean platelet volume (MPV). The normal range of each parameter for mice was indicated in the boxes below the histograms. Values expressed are means (n = 6, for day 2 – 14 and n = 3, for day 21 - 28) ± SD. Mock control data analyzed from 2 mocks on the first 2 weeks, but 1 mock after week 2.

Other blood parameters that indicate animal health and significant loss of blood such as red blood cell (RBC) and hemoglobin (HGB) were shown to be normal in all animals as well. Even though platelet count (PLT) from every sample was lower than the normal range, as well as the corresponding mean platelet volume (MPV) was shown to be high, this result was consistent with the mock control in both time points (Figure 2.3). The explanation could be an error caused by the automated blood counter instrument that might have counted some aggregates of platelets from each blood sample showing less numbers of PLT and increased number of MVP. The normal spleen weight between 3.0 ± 0.17 and 3.6 ± 0.14 g/kg of total body weight from each animal observed at the end of the experiment indicated that there were no chronic and/or major inflammatory and toxicity reactions in the RES that could cause the spleen enlargement in any group of animals (Table 2.1).[81]

Histological sections of the explants were stained with H&E staining and evaluated the infiltration of inflammatory cells, fibroblast, and new blood vessels into the hydrogels. No significant differences were detected between each gel condition within the same time point. Macrophages and lymphocytes were seen in the tissue around the gel disks at both time points. At week 2, there were some inflammatory cells observed in the peripheral area with 1.0 - 2.0 average score range, as well as the histological scores from week 4 that fell between 1.0 - 1.7. Average scores of 0.3-1.0 indicated mild inflammation observed in the center of the hydrogels from week 2, while they slightly increased with no statistical significance ($p > 0.05$, ANOVA) to 1.0 - 2.0 at week 4. Very few fibrosis was found in all explants (average score = 0.3) at week 2. However, fibroblasts accumulated given statistically higher scores on week 4 ($p < 0.05$, ANOVA).

Table 2.1. Average spleen weights of experimental mice at 8 week endpoint. Healthy mice have normal spleen weight in the range between 0.085 - 0.112 g (calculated from 30 g of total body weight).[33] Values expressed are means (n = 3) ± SD.

Mouse group	Spleen weight (g)
PAH	0.09±0.007
TMV-PAH	0.10±0.011
RGD-PAH	0.09±0.008
Mock	0.09±0.007

New capillaries for which process required oxygenation of transplanted tissues[82] were present in all types of hydrogels from both time-points at average score of 1.0 - 1.3 (Figure 2.4). Inflammatory cell infiltration, fibrosis and neovascularization indicated the normal wound healing progress and emphasized that the macro-porous structure of these hydrogels allowed cell invasion *in vivo*.[27, 83]

The fact that TMV causes humoral immune response in animals and is consequently used as antigen expression system in vaccine has been extensively reported.[79, 80] Since in specific immune response a serious systemic reaction can be induced sequentially from the antigen-antibody complex, we investigated the immunogenicity of TMV-incorporated hydrogels supporting bone differentiation of stem cell. From the ELISA assay, we found that TMV and its RGD mutant within the hydrogels led to non-significant induction of specific anti-TMV Immunoglobulin G (IgG) produced in mice. ELISA revealed lower anti-TMV antibody titers in mouse sera collected from the animals implanted with TMV-PAH and RGD-PAH hydrogels in comparison to the sera from mice that were challenged by native TMV solution (intra-muscular injection) in the same amount of virus presented in the hydrogels (Figure 2.5). This data suggested that there were only limited amount of TMV antigen released from the hydrogels into the circulation system. The result also emphasized *in vivo* safety of this virus-based combinatorial 3D material for tissue engineering.

3.2.2 In vivo Biodegradability of Hydrogels

Biodegradability of materials is one of the requirements for an ideal material applicable to tissue engineering as it is essential to avoid an invasive implant removal procedure

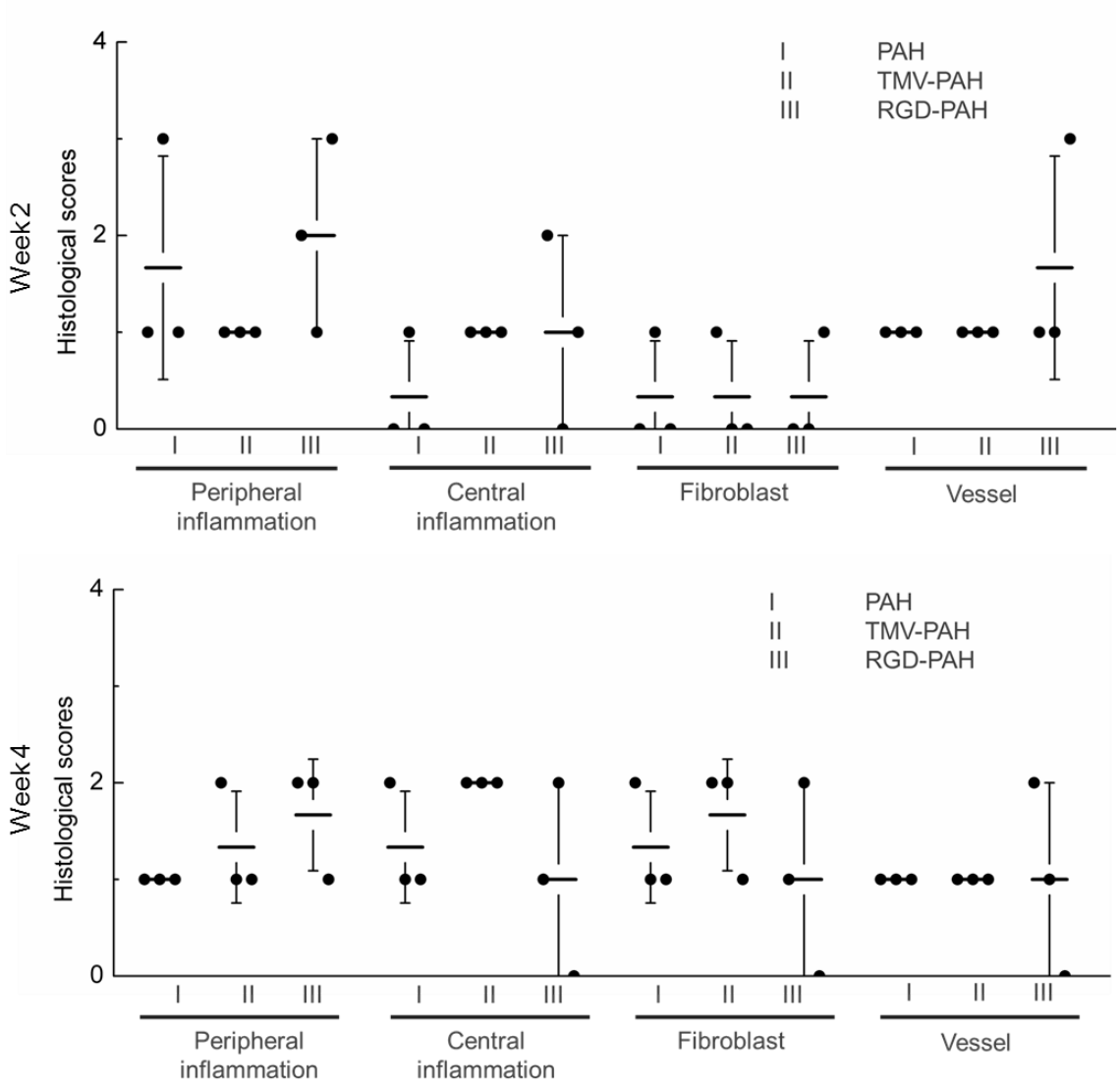

Figure 2.4. Histopathology analysis of hydrogel explants. Histological scoring of three types of hydrogel explants showed similar degree of inflammation from both peripheral and central areas, fibrosis, and vascularization within each time point of 2 and 4 weeks. There were mild to moderate inflammation (average scores 1 - 2) from all the hydrogels. The average fibroblast scores in all types of hydrogel slightly increased from week 2 to week 4. Blood vessel formation was scored 1 on average in all explants from both time points.

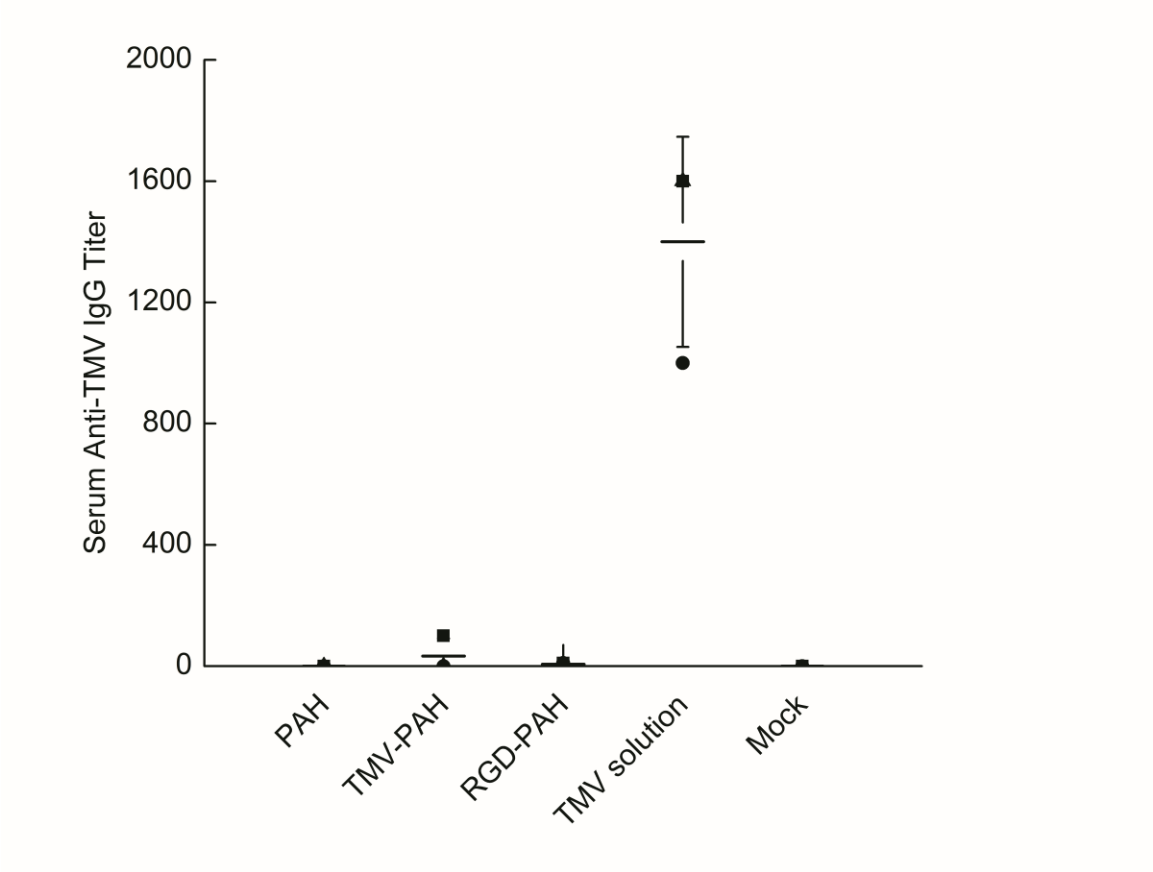

Figure 2.5. Anti-TMV serum titers from mice implanted with different hydrogels. The immune response to TMV in the implant materials was smaller in comparison to the intramuscular injection of native TMV. Comparative serological analysis of the immune response to each type of hydrogels was carried out by ELISA after 4 post-operative weeks. Serum endpoint dilutions for anti-TMV immune response in mice implanted by TMV-PAH and RGD-PAH were lower than ones challenged by single shot of native TMV at the same amount presented in the hydrogels (11 μg). Values expressed are means ± SEM with each scatter plot represents each animal.

after the new functional tissue has been developed in the patient. Moreover, the degradation of the scaffold must closely follow the extracellular matrix (ECM) synthesis and macroscopic tissue development. Thus, the rate of degradation of biomaterial scaffolds is desired to correspond with the development of a type of tissue that they replaced.[84, 85] Here, we tested the hydrogel degradation by measuring the hydrogel size reduced after 4 weeks of implantation and determining the number of hydrogel explants that could be recovered after 8 weeks. Table 2.2 shows that out of 10 samples for each group of hydrogel implant, 4, 6, and 6 of PAHs, TMV-PAHs, and RGD-PAHs, respectively, were completely degraded within 8 post-operative weeks. Moreover, the explants were significantly smaller than the starting hydrogels before implantation. Figure 2.6 represents the photographs of the native hydrogel (Figure 2.6A) and the different hydrogel explants (Figure 2.6B-D). The corresponding dot plot demonstrates the volume reduction calculated from dimensions of each hydrogel explant. Approximately half volume of hydrogels degraded during 4 post-operative weeks regardless of hydrogel type (Figure 2.6 plots). The degradation of these hydrogels could be attributed to the biodegradation of alginate hydrogel, the bulk forming materials used in the study. There were two possible degradation events involving: 1) loss of calcium ion (crosslinker) by diffusion into the surrounding medium and subsequent dissolution; and 2) depolymerization of polymer backbone via β-elimination caused by alkaline hydrolysis.[86-88] Also, Pluronic F108 surfactant might have aided in facilitating faster biodegradation of scaffold as reported by Nsereko and Amiji in which the chitosan alone and chitosan with Pluronic surfactant were compared.[89] In that report, they showed

Table 2.2. Numbers of hydrogel implants recovered from sacrificed mice after 8 post-operative weeks.

Hydrogels	Recovery of Implant
PAH	60%
TMV-PAH	40%
RGD-PAH	40%

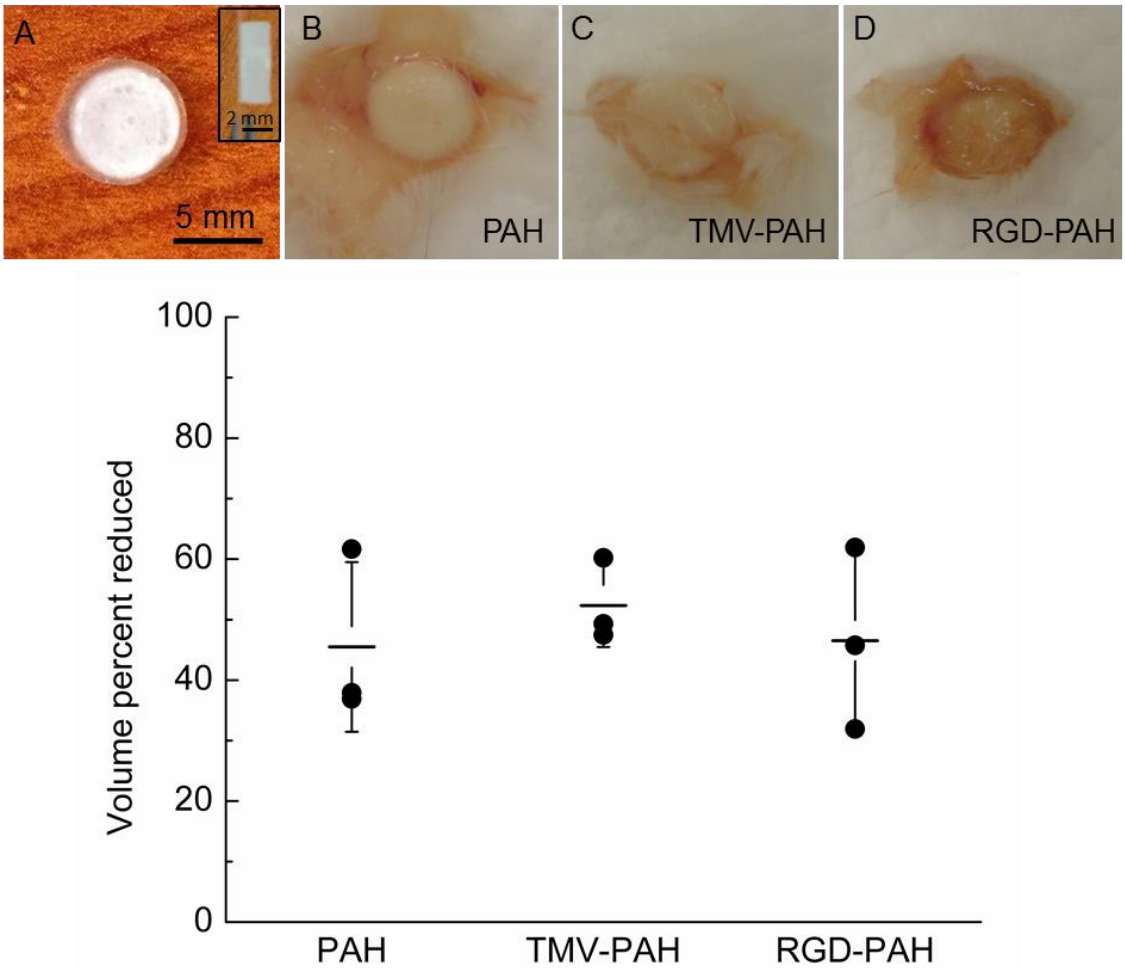

Figure 2.6. *In vivo* degradability of porous composite hydrogels. Photographs illustrated irregular shaped hydrogel explants with size reductions. (A) The hydrogel figure before implant. (B-D) The images of typical explants of PAH, TMV-PAH, and RGD-PAH, respectively. The bottom scattered plots indicated the volume reduction of each explant. Values expressed are means (n = 3) ± SD.

a significant increase in lysozyme degradation profile of the chitosan hydrogel with Pluronic F108 and concluded that the higher porosity of hydrogel resulted from the incorporation of surfactant.[89] However, in our study, we did not observe differences in the *in vivo* degradation of each hydrogel. The detailed degradation profiles of the materials will need to be further explored.

3.3 Conclusion

TMV, as the plant virus nano-scaffolding material, is a versatile tool from natural source for biomedical applications. We hereby conclude that TMV-functionalized porous alginate hydrogel implant is biocompatible in mice. The antigenicity of TMV could be suppressed when immobilized within hydrogels. The hydrogels were degraded in the physiological condition, which is one of the important criteria when developing a scaffold for tissue engineering. This virus-based hydrogel system can be further developed to have a better-controlled biodegradation profile for a less-invasive route of administration (injectable form). Overall, our result highlights the feasibility of incorporating viral nanoparticles in biomaterials for *in vivo* regenerative medicine applications.

3.4 Experimental Section

All chemicals were obtained from commercial suppliers and used as received unless otherwise noted. Wild-type TMV (TMV) and its RGD mutant (TMV-RGD) were isolated from infected tobacco leaves following previously established protocols.[23]

3.4.1 Synthesis of Virus-Incorporated Porous Alginate Hydrogels

The incorporation of TMV and its mutant (TMV-RGD) in porous alginate hydrogel was based on previously reported methods.[37] Briefly, 5% w/v low viscosity sodium alginate (Protanal LF 10/60 FT, 30 − 60 mPas for 1%, kindly provided by FMC Biopolymer UK Ltd.) was dissolved in 2% w/v sodium bicarbonate ($NaHCO_3$) and 4% w/v pluronic F108 solution. Molar equivalent of citric acid with respect to $NaHCO_3$ was added to the mixture while stirring at 500 rpm using overhead stirrer, 115V. Stirring was continued for 15 min at room temperature to allow CO_2 to fully develop. For the PAH modified with TMV (TMV-PAH), or PAH modified with mutant TMV-RGD (RGD-PAH), 0.1% w/v of virus was added to the solution 10 min after adding citric acid. The mixture was stirred for another 5 min. Afterward, the foamy alginate solution was cast in 6.35 mm (0.25 inches) diameter, 2 mm thick aluminum mold and freeze-dried. The resulting solid foam disc was soaked in 2 M of $CaCl_2$ for 24 h to induce the formation of the calcium-based physical gel and then dialyzed against large volume of 0.1 M $CaCl_2$. Finally, the solid foam was freeze-dried, resulting in porous alginate hydrogel (PAH) for implantation in animal study (Figure 2.1).

3.4.2 Animals, Lethality Test and Animal Treatments

The procedures were performed in accordance with the guidelines for animal experimentation by the Institutional Animal Care and Use Committee, School of Medicine, University of South Carolina. NIH guidelines (or for non-U.S. residents similar national regulations) for the care and use of laboratory animals (NIH Publication #85 - 23 Rev. 1985) have been observed. Twelve-week-old male BALB/c mice were

housed at 22 ± 2 °C with a 12-h light/ dark cycle and fed standard rodent chow and water *ad libitum*. Mice were randomly assigned to experimental groups. For *in vivo* biocompatibility tests, each group of animal (3 groups implanted by PAH, TMV-PAH, and RGD-PAH) consisted of 6 mice excepted the positive control group for anti-TMV antibody ELISA that consisted of 3 mice and the non-treatment control (mock) that consisted of 2 mice. A total of 10 mice per each group were used to determine the number of hydrogel explants that could be recovered after 8 post-operative weeks. Disk-shaped hydrogels were implanted subcutaneously to assess biocompatibility. Briefly, under anesthesia with 2-3% Isoflurane in oxygen, a small dorsal incision (~ 1 cm) was made to create a subcutaneous pocket to place the implant along the back of the animal. The skin was closed with surgical sutures. The animals were closely monitored (at least once per week) for signs of distress or abnormal behaviors and measured body weight for the entire experimental period. In the implanted groups, 3 animals in each group were sacrificed at week 2 after implantation and another 3 animals were sacrificed at week 4 at the end of experiment by cervical dislocation. The implanted animals and mocks were bled via retro-orbital bleeding through the anti-coagulant coated glass capillaries every 2 weeks for blood count assay. The serum samples for ELISA were obtained after centrifugation (2,000 g, 15 min, 4 °C) of blood samples collected from every animal just before euthanization and stored at - 80 °C. The implant hydrogels were recovered after the sacrifice of each animal. The size reduction of implanted hydrogels was measured on the explants from week 4 using Vernier Caliper in terms of diameter and height with a subsequent volume calculation. The implanted hydrogels with the surrounding tissues were then preserved in 10% neutral buffered formalin individually in the tissue blocks for

further paraffin embedding and histological assays. The liver, lung, brain, heart, and spleen of all mice were isolated and weighted.

3.4.3 Antibody challenge for ELISA positive control

Administration of TMV in the positive control group was performed by intramuscular injection of 11 µg TMV, which was calculated to match the average amount of TMV presented in each implant hydrogel. TMV in phosphate-buffered saline (pH 7.4) were sterile filtered before injecting into the animals.

3.4.4 Hematological assay

Complete Blood Count (CBC) was preceded right after each blood withdrawal. The blood sample of 10 - 50 µL was transferred into 1 mL BD Microtainer Tube with Dipotassium EDTA. Each tube was subjected to the automated blood counter machine, model VetScan HM5 Hematology System. The numbers of total white blood cell (WBC), neutrophil (NEU), monocyte (MON), lymphocyte (LYM), red blood cell (RBC), hemoglobin (HGB), platelet (PLT), and mean platelet volume (MPV) were recorded and analyzed according to the calibrated instrumental protocol, which indicated the normal range of each parameter specifically for mice.

3.4.5 Paraffin Embedding and Histological Assays

The formalin preserved implanted hydrogels/tissues and organs of all mice were embedded in paraffin blocks individually with proper orientations. Tissue sections (5 µm) were prepared and stained with hematoxylin and eosin (H&E). Based on the amount

of inflammatory cells (basically lymphocytes, neutrophils, macrophages, and so on) observed within the center or peripheral areas of implants, the degree of tissue inflammation was scored as 0, 1, 2, and 3 (normal; none, rarely seen; 1 to 5 per ×40 objective field, slightly increased; 5 to 20 per ×40 objective field, and obviously increased; > 20 per ×40 objective field). Based on the degree of fibrous/connective tissues and capillary blood vessels observed within the center or peripheral areas of implants, the tissue fibrosis and vasculization were scored as 0, 1, 2 and 3 (none, rarely seen; ≤ 2 vessels/ ×40 field, slightly increased; 3 - 10/ ×40, and obviously increased; > 10 vessels/ × 40, respectively). Histological images were taken by using a Nikon microscope and an Olympus digital camera.

3.4.6 Enzyme-Linked Immunosorbent Assay (ELISA)

ELISA was performed no later than 3 months after the sera were collected. In order to coat wells with TMV as an antigen, high protein-binding conical bottom 96-well plate was used. TMV (10 µg/mL, 100 mL) in Phosphate Buffer Saline (PBS) were added to the microwells and incubated for 1 h at room temperature, followed by three PBS washes. Blocking for non-specific binding was performed by adding 100 µL of 1% bovine serum albumin (BSA) and incubating for 30 min at room temperature, followed by three PBS washes. Binding was performed by adding 100 µL of serially diluted antiserum into microwells and incubating for 1 h at room temperature, followed by thorough washes. HRP conjugate anti-mouse IgG (Cayman Chemical Company) diluted at 1:20000 ratio was added and incubated for 30 min at room temperature. Tetramethyl Benzidine (TMB Plus, Amresco) and 1 M H_2SO_4 were added in sequence to the wells according to the

manufacturer's protocol, and the binding efficiency was monitored by measuring absorbance at 450 nm.

CHAPTER 3

BIOCOMPATIBILITY STUDY OF BMSCS INCORPORATED TMV ALGINATE HYDROGELS

3.1 INTRODUCTION

3.1.1 Bone marrow stromal cells in tissue engineering

Bone marrow stromal cells (BMSCs), also sometimes referred to as mesenchymal stem cells (MSCs), are broadly used for regenerative medicine applications.[90, 91] These cells have two important innate abilities. First, MSCs can differentiate into distinctive end-stage cell types, such as those that fabricate specific mesenchymal tissues including bone, cartilage, muscle, bone marrow stroma, tendon/ligament, fat, dermis, and other connective tissues. Second, MSCs, themselves, secrete a broad spectrum of bioactive macromolecules that can aid restructuring microenvironments in sites of tissue injury.[92] Although, numerous preclinical studies have established the therapeutic potential of MSCs in tissue engineering and as cellular protein factory for delivery of cytokines and anticancer agent,[93] to date, MSC immunosuppressive and immunoprivilege properties remain controversial.[94-97] Most of the evidence for MSC immunoprivilege and immunosuppression has been obtained using adaptations of the lymphocyte transformation assays (LTA) and mixed lymphocyte reaction (MLR), respectively. The reliability and sensitivity of these assays is dependent upon the optimization of the assay conditions, and different conditions have yielded conflicting outcomes in some instances.[98] There were some studies reported that MSCs may also behave as

nonprofessional antigen-presenting cells (APCs).[99, 100] An enhancement of lymphocyte proliferation was sometimes seen with MSCs co-cultured.[100]

3.1.2 Virus-functionalized alginate hydrogel scaffolds

In Chapter 1, we have shown that the porous alginate hydrogels (PAH) could be functionalized with tobacco mosaic virus (TMV) and demonstrated their advantage as vehicles to support the 3D stem cell culture and differentiation. TMV, as the plant virus nano-scaffolding material, is a versatile tool from natural source for biomedical applications. In summary, the 3D porous alginate hydrogels (PAH) functionalized with wild-type TMV (TMV-PAH) and its RGD mutant (RGD-PAH) were developed. We have also emphasized that TMV surface can be accessible in 3D porous hydrogels as shown by significant improvement in cell attachment after functionalization by cell binding motif, RGD, via the mutation of TMV. Moreover, the incorporation of TMV and its RGD mutant can facilitate bone differentiation of BMSCs. We reported (Chapter 2) that the virus is biocompatible in the form of porous hydrogel implant using BALB/c mice as the *in vivo* study model. The antigenicity of virus could be suppressed when immobilized and slowly released from the bulk hydrogels. The hydrogels were degraded in the physiological condition, which is one of the important criteria when developing a scaffold for tissue engineering.

Here, we further characterized the *in vivo* properties of this hydrogel system by focusing on the potential of using the TMV-functionalized PAH to incorporate BMSCs in bone tissue engineering. The key objective of this study was to rule out the

biocompatibility and possible toxic effects of the subcutaneously implanted hydrogels when BMSCs were co-delivered with serum-free osteogenic supplemented media.

3.2 Results and Discussion

3.2.1 Ex vivo bone marrow stromal cells loading

To investigate the potentiality of the virus-functionalized hydrogel in stem cell bone tissue engineering application, isolated murine BMSCs from the host strain (BALB/c mouse) were loaded in the hydrogel and primarily induced with non-BMP2 osteogenic induction media before implant. The isolated BMSCs were cultured and expanded *in vitro*. After cells were seeded in the hydrogels, the *in vitro* parallel study of call metabolic activity showed that cells were viable in the hydrogels (Figure 3.1). Moreover, RGD mutant of TMV embedded in the hydrogels clearly enhanced cell adhesion. The results were consistent with the *in vitro* report in which significantly higher metabolic activity of the BMSCs, isolated from Sprague-Dawley rats, in RGD-TMV functionalized hydrogel was shown (Chapter 1).

3.2.2 Immunogenicity of virus in the hydrogel seeded with osteogenic induced BMSCs

Previously in Chapter 2, we demonstrated the remarkable decrease in immunogenicity of TMV incorporated in the hydrogel in BALB/c mice implanted with the materials alone without cells seeded. However, the results did not rule out that immune responses may be

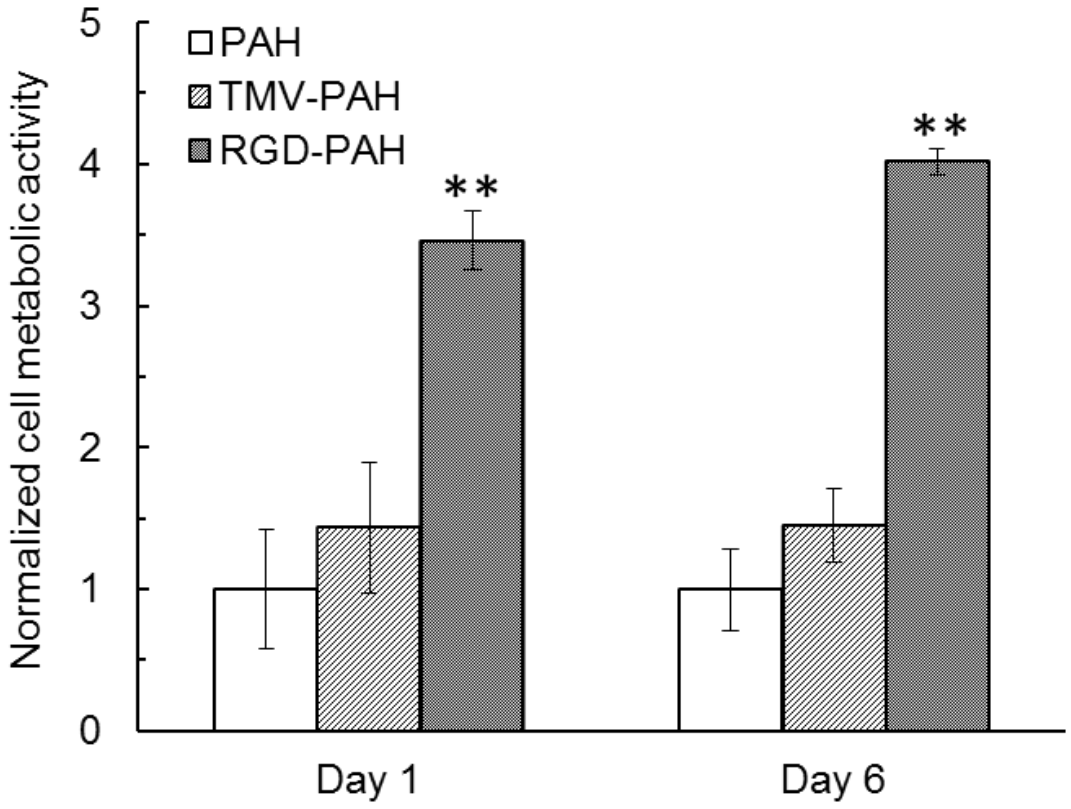

Figure 3.1. CellTiter Blue metabolic activity assay of mBMSCs cultured in different types of hydrogels at different time points, *in vitro*. Values expressed are mean (n = 3) ± SD of RFU that were normalized against PAH for each time point. **p < 0.005, student t test.

elicited in the presence of 1) co-delivered cells or 2) other biological entities due to an adjuvant effect. Although MSCs have been widely reported to have immunomodulatory capacity and an immunoprivileged status,[101-103] for example, strong evidence suggested a delay in B cell maturation and antibody production by MSCs in mice[104, 105] and human cell culture,[106, 107] their interaction *in vivo* is still not well known.[108] Here, we studied the immune response to TMV particles in TMV-PAH and RGD-PAH seeded with mouse BMSCs and saturated with osteogenic induction media. The hydrogels were first soaked in the osteogenic induction media before cell loading. Then the cell-loaded scaffolds were implanted under the skin of the animal. The animals implanted with bare hydrogels (hydrated with PBS), without cells and osteogenic media, were used as control groups for all type of hydrogels. The blood samples collected at the end of the experiment (8 post-implantation weeks) were subjected to ELISA assay. Figure 3.2 showed no differences in anti-TMV titers comparing the controls (no cells) and the hydrogels seeded with BMSCs in osteogenic media. Moreover, regardless of co-delivered cells and media supplements, the ELISA showed negligible immune responses to TMV and TMV-RGD imbedded in the hydrogels. Despite the differences in serum collection time points, this data was consistent with the previous experiment reported in Chapter 2 (sera collected at week 4). Therefore, the result here confirmed that the release of TMV particles happened very slowly over time at the dose that could not elicit a significant immune response.

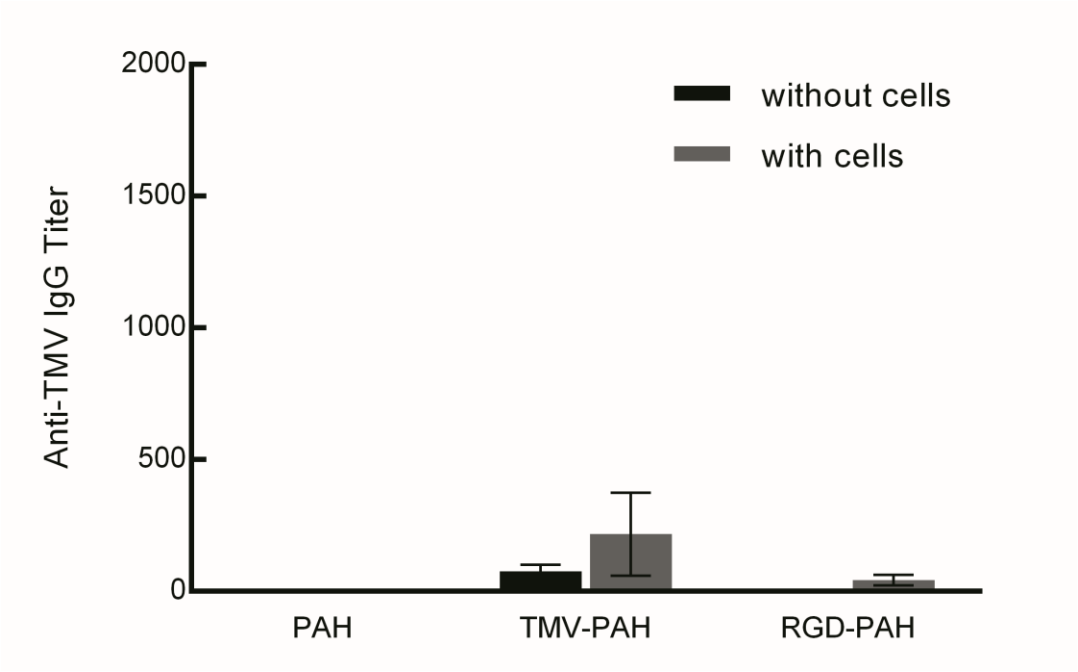

Figure 3.2. Anti-TMV serum titers from mice implanted with different hydrogels seeded with BMSCs. Comparative serological analysis of the immune response to the hydrogels co-delivered with BMSCs and the blank hydrogels was carried out by ELISA after 8 post-operative weeks. Serum endpoint dilutions for anti-TMV immune response in mice implanted by TMV-PAH and RGD-PAH with osteogenic-induced BMSCs were very low with no statistical significances in comparison to the response elicited by the hydrogel alone. Values expressed are means ± SEM.

3.2.3 Histological study

Histological sections of the explants were stained with H&E staining and evaluated the infiltration of inflammatory cells, fibroblast, new blood vessels, and tissue/cell growth in the hydrogels after 8 weeks. For every parameter, no significant differences were detected between each type of hydrogel implant, PAH, TMV-PAH, and RGD-PAH, seeded with BMSCs *ex vivo*. The average histological scores revealed that there were mild to moderate inflammatory cells, fibroblast, and neovascularization at the implantation site (Figure 3.3). However, very rare foam cells were observed within some of the PAH explants, and none were found in TMV-PAH and RGD-PAH (Figure 3.3). It has also been observed that there were few cell growths in the hydrogels possibly from *ex vivo* seeded BMSCs; however, no substantial difference in the degree of cell growths were observed among different hydrogel types. This result was inconsistent with the study of cell adhesion study *in vitro*, which RGD-PAH could attract more cells into the scaffold. This contrary could be justified as following. First, the vascular networks in subcutaneous pocket/tissue are too poor in their natural state to allow the growth and function of tissue graft.[109] Second, the time of implantation was much longer than the incubation time of *in vitro* study. The new extracellular matrix might be generated by the physiological system through the wound healing events in animal body, and overcame the influence from the implant material (RGD-PAH) in cell recruitment. Third, the release of TMV particles due to the degradation of implant materials led to the loss of scaffold functionality over time (Chapter 2). Moreover, the same set of histopathological parameters was assessed comparing between the hydrogels with and without BMSCs. In Figure 3.4, PAH and RGD-PAH showed no statistical differences in terms of

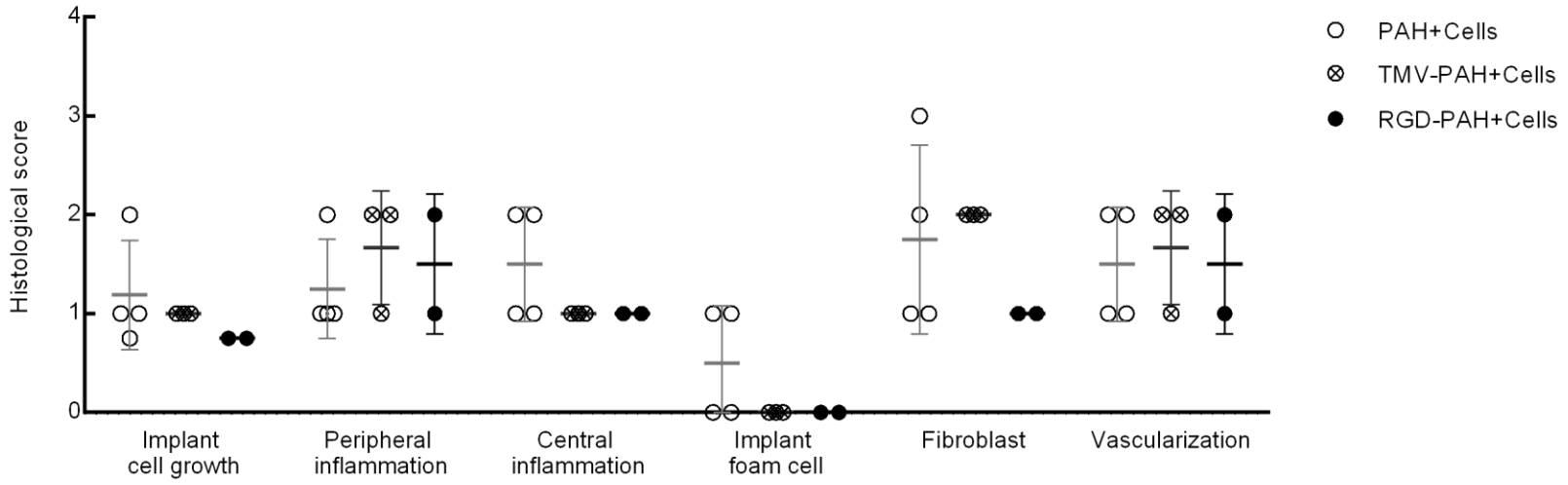

Figure 3.3. Histological score given to hydrogel explants of *ex vivo* BMSC-loaded hydrogels compared implant cell growth, peripheral inflammation, central inflammation, implant foam cell, fibroblast, and vascularization on PAH, TMV-PAH, and RGD-PAH. Each plot represents the response from each animal with mean ± SD shown as a bar.

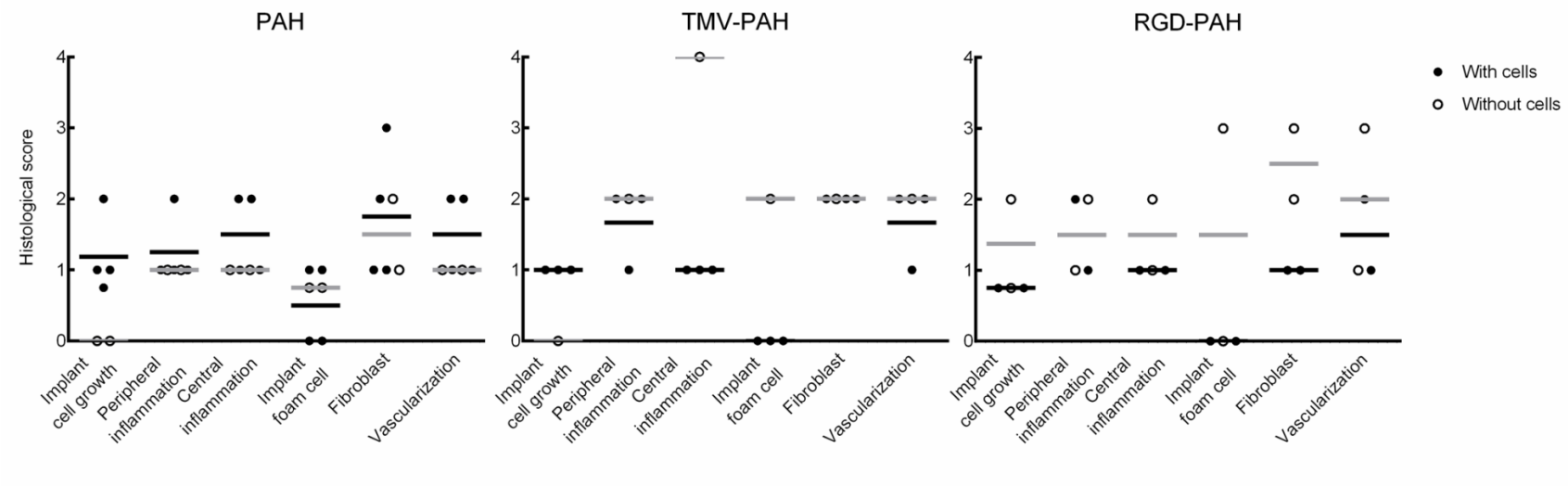

Figure 3.4. For each type of hydrogel implant, histological score compared implant cell growth, peripheral inflammation, central inflammation, implant foam cell, fibroblast, and vascularization on BMSC-loaded and naked implants. Each plot represents the response from each animal with mean ± SD shown as a bar. Grey bars are for the scaffolds without cells. Black bars are for the scaffolds with cells.

inflammations (both peripheral and central), implant foam cells, and vascularization when comparing the blank scaffolds with the cell-seeded scaffolds. To our surprise, bare TMV-PAH induced higher central inflammation and foam cells than the scaffold with co-delivered cells. However, only one animal was used for the control TMV-PAH implant here. To further test for statistical importance of this data, the animal number should be increased.

Some studies suggested that MSCs have antifibrotic properties. Moodley *et al*. reported that locally administered human umbilical cord MSCs reduced fibrosis of bleomycin-induced lung injury in mice by decreasing collagen concentration at the injured site.[110] Leung *et al.* showed that the presence of MSCs can suppress abnormal deposition of collagen I in the nucleus pulposus of intervertebral disc degeneration rabbits, modulating profibrotic mediators MMP12 and HSP47, thus reducing collagen aggregation and maintaining proper fibrillar properties and function.[111] Here, only the RGD-PAH implants exhibited the significant suppression of fibrosis when BMSCs were present. There were no differences in fibrosis between the blank hydrogels and the hydrogels seeded with BMSCs for PAH and TMV-PAH implants. Likewise, the presence of BMSCs caused no differences in vascularization in any types of implants. The cell growths in the cell-loaded implants were compared with the blank implants among each hydrogel type. To our surprise, RGD-PAH showed distinct result to other types of hydrogels. The RGD-PAH without pre-loaded BMSCs exhibited comparable/slightly higher implant cell growth than the hydrogel with initial cell seeding. The possibility could be that the available RGD peptide presented in blank RGD-PAH recruited MSCs that travel through the peripheral blood[112] at the early stage implantation.

3.3 Conclusion

The TMV incorporated porous alginate hydrogel scaffolds were evidenced for the biocompatiblity as *ex vivo* 3D supports for BMSCs and as *in vivo* cell delivery and tissue development platforms. The cell-loaded implants caused insignificant changes in the immunogenicity of TMV particles. Overall, mild to moderate inflammatory responses were observed due to the injury triggered by normal wound healing and implantation of foreign materials with no major differences in degrees of inflammation between the BMSC seeded hydrogel and the control in both virus-functionalized hydrogels and PAH alone. Hence, this virus functionalized hydrogel system is considered a promising candidate as safe and easy incorporating biofunctional material well-suited for stem cell delivery and tissue regeneration. This study is one of the underlying platforms for the development of viral nanoparticle based biomaterials in tissue engineering and regenerative medicine.

3.4 Experimental Section

All chemicals were obtained from commercial suppliers and used as received unless otherwise noted. Wild-type TMV (TMV) and its RGD mutant (TMV-RGD) were isolated from infected tobacco leaves following previously established protocols.[23]

3.4.1 Synthesis of Virus-Incorporated Porous Alginate Hydrogels

The incorporation of TMV and its mutant (TMV-RGD) in porous alginate hydrogel was based on previously reported methods.[37] Briefly, 5% w/v low viscosity sodium alginate (Protanal LF 10/60 FT, 30−60 mPas for 1%, kindly provided by FMC Biopolymer UK Ltd.) was dissolved in 2% w/v sodium bicarbonate ($NaHCO_3$) and 4% w/v pluronic F108 solution. Molar equivalent of citric acid with respect to $NaHCO_3$ was added to the mixture while stirring at 500 rpm using overhead stirrer, 115V. Stirring was continued for 15 min at room temperature to allow CO_2 to fully develop. For the PAH modified with TMV (TMV-PAH), or PAH modified with mutant TMV-RGD (RGD-PAH), 0.1% w/v of virus was added to the solution 10 min after adding citric acid. The mixture was stirred for another 5 min. Afterward, the foamy alginate solution was cast in 6.35 mm (0.25 inches) diameter, 2 mm thick aluminum mold and freeze-dried. The resulting solid foam disc was soaked in 2 M of $CaCl_2$ for 24 h to induce the formation of the calcium-based physical gel and then dialyzed against large volume of 0.1 M $CaCl_2$. Finally, the solid foam was freeze-dried, resulting in porous alginate hydrogel (PAH) for implantation in animal study.

3.4.2 Bone Marrow Stem Cells (BMSCs) Isolation and in vitro Expansion

Primary BMSCs were isolated from the bone marrow of young adult male BALB/c mice. The procedures were performed in accordance with the guidelines for animal experimentation by the Institutional Animal Care and Use Committee, School of Medicine, University of South Carolina. Cells were maintained in complete primary media (Dulbecco's Modified Eagle's Medium (DMEM) supplemented with 20% fetal

bovine serum (FBS)), kept at 37 °C in a 5% CO_2 incubator and passaged no more than six times after isolation.

3.4.3 Cell Seeding and in vitro Cell Viability

For each experimental group of animals, 4 hydrogels of PAH, 3 hydrogels of TMV-PAH and 2 hydrogels of RGD-PAH were prepared for *ex vivo* cell seeding. All hydrogels were sterilized in 70% ethanol for 15 min, ethanol was drained on sterile filter paper and the hydrogels were further sterilized under UV-light for 60 min in laminar airflow hood. For experimental group, hydrogels were then saturated in serum-free osteogenic media at 37 °C for 60 min, blotted excess media with sterile filter paper, and placed in 12-well nonadhesive plate (six hydrogels in each well). The control hydrogels (no cells) were saturated with sterile PBS instead of osteogenic supplemented media. Serum-free osteogenic media contained high-glucose DMEM supplemented with 10 mM sodium β-glycerol phosphate, L-ascorbic acid (50 μg/mL), 10^{-2} μM dexamethasone, 1× ITS, FGF (1 ng/mL), TGFβ (1 ng/mL), EGF (1 ng/mL), penicillin (100 units/mL), streptomycin (100 μg/mL), and amphotericin B (1 μg/mL). BMSCs were harvested from 80% confluent culture flask using 0.25% trypsin/EDTA for 5 min and counted and resuspended in complete primary media. A total of 30×10^3 BMSCs were seeded per one volume (cm^3) of hydrogel. BMSCs loaded hydrogels were initially incubated with 100 μL of serum-free osteogenic media in each well to prevent hydrogels from drying out. After 6 h of an initial incubation, hydrogels were completely submersed in 1 mL of

serum-free osteogenic media in each well. 12 h after cell seeding, cell loaded hydrogels were then implanted to the animals.

For the *in vitro* cell viability assay, the hydrogels were prepared and seeded with mouse BMSCs by the same procedure with the implant hydrogels. The hydrogels seeded with BMSCs were cultured at 37 °C and 5% CO_2. CellTiter-Blue (CTB) cell viability assay (Promega) after days 2 and 6 of culture was performed for each type of hydrogel. The culture media in each well was replaced by 1 mL of prewarmed media containing 10% CTB and incubated for 1 h at 37 °C and 5% CO_2. The media containing CTB was used without cells as negative controls. The measurement of the CTB product was taken at two time points. First, to detect the cells that attached to the outer surface of hydrogel, the solution was collected and replaced with 1 mL of culture media. The incubation was continued for another 2 h to allow diffusion of the fluorescent product from the inner part of hydrogel. After 2 h incubation, the media solution was collected again and replaced with 1 mL of culture media in each well to continue cell culture. The 1:1 mixture of solution from first collection and second collection was measured for fluorescence intensity at 560/590 nm (Ex/Em) using SpectraMax M2 Multi-Mode microplate reader (Molecular Devices). Also, 3 separate experiments were conducted with each type of sample, which is comprised of 4 hydrogels.

3.4.4 Animals, Lethality Test and Animal Treatments

The procedures were performed in accordance with the guidelines for animal experimentation by the Institutional Animal Care and Use Committee, School of

Medicine, University of South Carolina. NIH guidelines (or for non-U.S. residents similar national regulations) for the care and use of laboratory animals (NIH Publication #85 - 23 Rev. 1985) have been observed. Twelve-week-old male BALB/c mice were housed at 22 ± 2 °C with a 12-h light/ dark cycle and fed standard rodent chow and water ad libitum. Mice were randomly assigned to experimental groups. Each group of animal (3 groups implanted by PAH, TMV-PAH, and RGD-PAH) consisted of 6 mice. Disk-shaped hydrogels were implanted subcutaneously. Briefly, under anesthesia with 2 - 3% Isoflurane in oxygen, a small dorsal incision (~ 1 cm) was made to create a subcutaneous pocket to place the implant along the back of the animal. The skin was closed with surgical sutures. The animals were closely monitored (at least once per week) for signs of distress or abnormal behaviors and measured body weight for the entire experimental period. All animals were sacrificed at week 8 after implantation by cervical dislocation. The serum samples for ELISA were obtained after centrifugation (2,000 g, 15 min, 4 °C) of blood samples collected from every animal just before euthanization and stored at -80 °C. The implant hydrogels were recovered after the sacrifice of each animal. The implanted hydrogels with the surrounding tissues were then preserved in 10% neutral buffered formalin individually in the tissue blocks for further paraffin embedding and histological assays. The liver, lung, brain, heart, and spleen of all mice were isolated and weighted.

3.4.5 Paraffin Embedding and Histological Assays

The formalin preserved implanted hydrogels/tissues and organs of all mice were embedded in paraffin blocks individually with proper orientations. Tissue sections (5

μm) were prepared and stained with hematoxylin and eosin (H&E). Based on the amount of inflammatory cells (basically lymphocytes, neutrophils, macrophages, and so on) observed within the center or peripheral areas of implants, the degree of tissue inflammation were scored as 0, 1, 2, and 3 (normal; none, rarely seen; 1 to 5 per × 40 objective field, slightly increased; 5 to 20 per ×40 objective field, and obviously increased; > 20 per × 40 objective field). Implant cell growth and foam cells were also scored with the criteria applied to inflammatory cells. Based on the degree of fibrous/connective tissues and capillary blood vessels observed within the center or peripheral areas of implants, the tissue fibrosis and vasculization were scored as 0, 1, 2 and 3 (none, rarely seen; ≤ 2 vessels/ × 40 field, slightly increased; 3-10/ × 40, and obviously increased; > 10 vessels/ × 40, respectively). Histological images were taken by using a Nikon microscope and an Olympus digital camera.

3.4.6 Enzyme-Linked Immunosorbent Assay (ELISA)

ELISA was performed no later than 3 months after the sera were collected. In order to coat wells with TMV as an antigen, high protein-binding conical bottom 96-well plate was used. TMV (10 μg/mL, 100 mL) in Phosphate Buffer Saline (PBS) were added to the microwells and incubated for 1 h at room temperature, followed by three PBS washes. Blocking for non-specific binding was performed by adding 100 μL of 1% bovine serum albumin (BSA) and incubating for 30 min at room temperature, followed by three PBS washes. Binding was performed by adding 100 μL of serially diluted antiserum into microwells and incubating for 1 h at room temperature, followed by thorough washes. HRP conjugate anti-mouse IgG (Cayman Chemical Company) diluted at 1:20000 ratio

was added and incubated for 30 min at room temperature. Tetramethyl Benzidine (TMB Plus, Amresco) and 1 M H_2SO_4 were added in sequence to the wells according to the manufacturer's protocol, and the binding efficiency was monitored by measuring absorbance at 450 nm.

CHAPTER 4

BONE REGENERATION IN RATS WITH CRANIAL DEFECT BY IMPLANTATION OF TMV FUNCTIONALIZED ALGINATE HYDROGEL SCAFFOLDS

4.1 INTRODUCTION

4.1.1 Rat cranial segmental bone defect model

There are extensive needs for clinical bone replacement from patients with bone loss after resection of tumors, bone loss after trauma, and voids created as a result of fractures. Even though bone has a good healing capacity compared to other tissues, the regeneration potential is limited in the case of large defects such as after tumor resection, major fractures, hip implant revision, or impaired healing capacity of the host.[113, 114] In such cases, the use of bone grafts, derivates, or bone substitutes are indicated to promote healing and regeneration.[114-116] Current clinical methods of treating skeletal defects are autograft and allograft bone transplantation. Autograft bone (bone transplanted from one part of the body to another in the same individual) provides an environment that bone cells like to grow and to make bone tissue. However, the supply of autograft bone is limited. Allograft bone (bone from one person to another including those from cadaveric and living related) has slower rate of healing compared to autograft bone and the possibility of disease transfer. Therefore, material scientists introduced the concept of tissue engineering using biocompatible artificial materials that offer an unlimited supply for treating bone defects. [113, 117]

The translation of many therapeutics, including pharmaceuticals, medical devices and medical strategies, into clinics requires an animal testing. Despite ethical concerns and efforts to develop alternatives to animal experimentation, standardized animal models are crucial components in translational sciences and medical technology development.[118-121] For bone tissue engineering, a number of small animal models exist. Many species have been used for animal models of bone defects, including mice, rats, rabbits, dogs, pigs, sheep and goats, but much of the research has focused on rodent models because of reproducibility, throughput and economic considerations. The rat calvarium or cranium allows for a reproducible defect that can be generated quickly and does not require fixation for stabilization of the skeleton, as is generally required with femoral defects.[122, 123] However, as an anatomical site experiencing less loading than long bones, the functional testing of a bone regeneration strategy intended to withstand biomechanical forces is not feasible in the calvarial defect.[124] Thus, taking into consideration the objective of the biomaterial or bone regeneration strategy, the rat calvarial defect can serve as a rapid, high throughput method for *in vivo* evaluation of bone regeneration. The rat cranial segmental bone defect is a versatile model allows for evaluation of biomaterials and bone tissue engineering approaches within a reproducible, non-load-bearing orthotopic.[125] For critical defects, i.e. defects that would not fully heal spontaneously, or even to accelerate or guide the repair process, the use of bioactive scaffolding material could be of great advantage. Suitable materials can, in fact, fill the cavity or stabilize the defects while exerting beneficial stimuli that promote cell activity and proliferation.[117]

4.1.2 TMV nanoparticle-functionalized porous alginate hydrogel

The goal of this study is to assess the potential for plant virus/polymer hydrogels as materials capable of enhancing bone formation/regeneration. The hydrogel is composed of Tobacco mosaic virus (TMV) as protein templates with a mixture of a natural hydrogel forming polymer that is biocompatible and biodegradable, sodium alginate (sugar-based polymer derived from algae/seaweed). Alginate has been well established as a hydrogel forming polymer that is used extensively in biomedical applications. However, alginate itself cannot guide cells towards bone differentiation, unless complex mixtures of protein materials (i.e. growth factors, cell binding sequences) are incorporated. Therefore, we rationalized that TMV can supplement the polymer backbone to promote bone formation. There are two rationales for using the plant virus. One, the plant virus cannot infect mammalian cells. Historically and at present, there have been no reports of TMV infections in mammals. Even in the case that the plant virus was to enter the mammalian cells, it does not have the proper material to replicate itself inside the mammalian cells.[36, 126-128] The virus solution can further be purified to be pathogen-free by sterile filtration. Second, a large number of functionalities (cell anchorage sites, growth factors) can be placed on the virus at the nanometer scale.[23, 24] The ability to place specific functional groups (cell anchorage sites, growth factors) at nanometer scales within the hydrogel has been an important direction for tissue engineering. [23, 24 23, 24 23, 24 23, 24 23, 24 23, 24] Currently, the preparation of complex hydrogels is a tedious process that involves multiple steps to position the cell anchorage sites and growth factors within the hydrogel. By incorporating cell-binding ligands on the external surface of TMV, we have shown that TMV can act as nanometer sized building blocks that the plant virus act as nanometer sized materials that

can support mesenchymal stem cells and dramatically improve the transformation of cells into bone-like cells *in vitro*.[16, 17, 37] We did not observe any decrease in cell survival even with very high doses of TMV. Additionally, from our previous studies reported in Chapter 2 for biocompatibility (subcutaneous) of TMV and its mutant (TMV-RGD) incorporated alginate hydrogel scaffold in mice, we did not observe any serious immune responses in comparison with the control group (mice subcutaneously implanted with alginate-alone scaffold). Therefore, the proposed hydrogel will possibly provide a new way to prepare biomaterials for bone repairing applications.

4.2 Results and Discussion

4.2.1 Surgical recovery of animals

The survival surgery of cranial bone defect creation with subsequently hydrogel implantation was carried out. Mean surgery time was 10 minutes (SD = 4). One out of the 21 animals did not gain consciousness and died after the surgery. Animal's weight was measured immediately after the cranial defect survival surgery on each animal to monitor post-surgery weight loss. Figure 4.1A showed that all rats lost less than 5% of its initial weight measured before the operation. Blood loss during surgical procedure was also estimated to be less than 1 mL in all rats. The animals were closely monitored within the first 6 hours after and weighed every day for the first post-operative week and at least once every consecutive week, continuously for the entire experimental period. Postoperatively, the rats recovered quickly, gaining their baseline weight and returning to routine activities such as grooming, eating and drinking in less than 48 hours. The

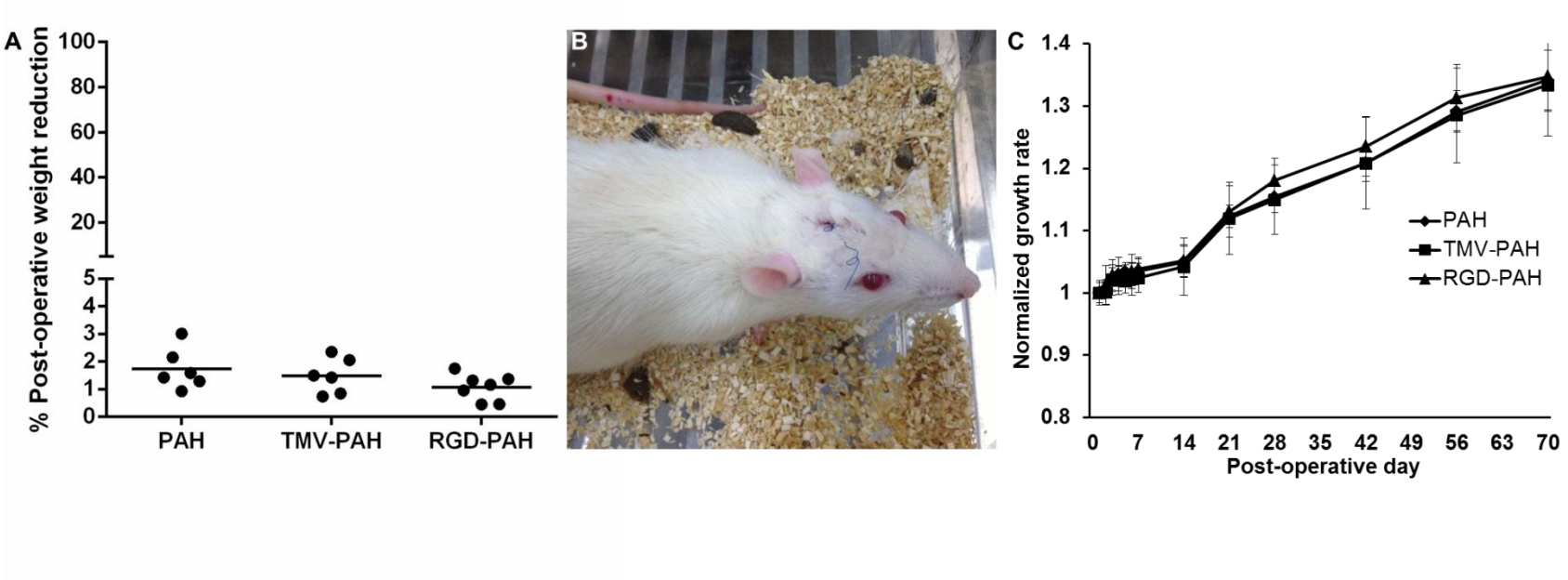

Figure 4.1. Animal post-operative care and monitoring. (A) All experimental animals only lost less than 5% of their original weights after the surgery. The dot plot represented each animal with mean shown as a bar (n = 6, for PAH and TMV-PAH and n = 7, for RGD-PAH). (B) The rats recovered quickly, the surgical wound healed completely and the suture material fell off spontaneously within 2 weeks. (C) All rats maintained their normal growth rates for the entire experimental period. Values expressed are means (n = 6, for PAH and TMV-PAH and n = 7, for RGD-PAH) ± SD.

surgical wound heeled within 1.5 weeks without post-surgical bleeding or wound infection. The surgical suture fell off spontaneously from the surgical site after the wound healed completely (Figure 4.1B). From gross observations after cranial defect operation and implantation, all animals were normally active in eating, drinking, and grooming with no observable hair loss and aggressive behavior. The growth rate was evaluated by body weight of rats at each time point normalized with their original weight before implantation with PAH, TMV-PAH, and RGD-PAH. Comparing to the normal growth rate of Sprague Dawley rats.[129] All experimental animals grew normally with no weight loss as shown in Figure 4.1C.

4.2.2 Systemic inflammatory and immunogenic responses

Complete blood count was analyzed from whole blood samples from each group of rats at every week for 4 weeks, and then every other week until termination after 10 post-operative weeks. Figure 4.2 and 4.3 showed different blood counts in normalization to the initial numbers that were analyzed from whole blood collected from a 8-week old normal Sprague Dawley rat. The host inflammatory responses after the surgery were evaluated by white blood count including total white blood cell (WBC), lymphocyte (LYM), monocyte (MON), and neutrophil (NEU) counts. Overall, all animals had slightly low WBC, LYM, and NEU comparing to the normal rat. However, the comparison had no statistical difference for each parameter in each time point except for PAH group. Rats implanted with PAH had significant lower WBC at week 1, 3, 8, and 10, and LYM at week 3 and 10 compared to normal rat ($p < 0.01$, multiple t-test). MON count from all

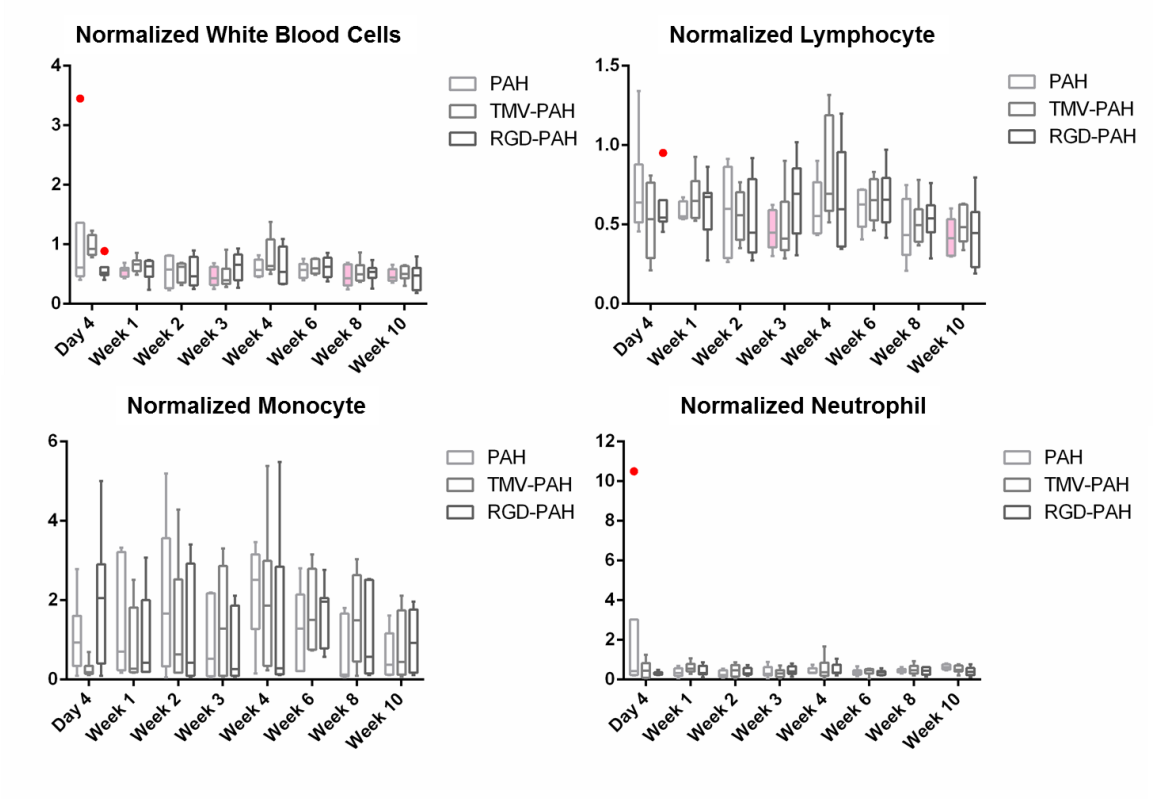

Figure 4.2. White blood count analysis of all rats with bone substitute implants. The total blood counts were monitored at 8 time points (day 4, week 1, 2, 3, 4, 6, 8 and 10, post-operatively). The histograms showed the numbers of total white blood cells (WBC), Lymphocyte (LYM), Monocyte (MON), NEU (neutrophil) normalized with the values measured from non-treated rat. Each bar indicated min to max with mean as the middle horizontal bar (n = 6, for PAH and TMV-PAH and n = 7, for RGD-PAH) ± SD. From t-test analysis comparing control (non-treatment) and experimental value, the filled bars represented statistical significance, $p<0.05$. Red dots represented outliers.

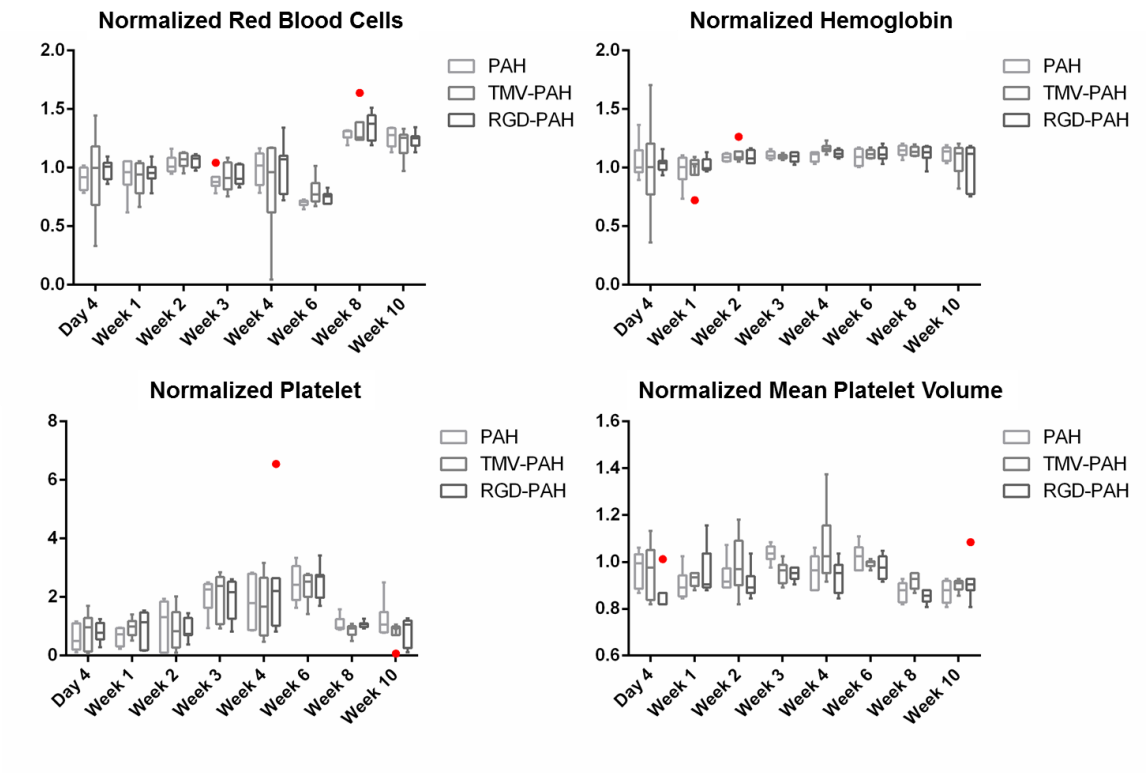

Figure 4.3. Hematology analysis of all rats with bone substitute implants. The total blood counts were monitored at 8 time points (day 4, week 1, 2, 3, 4, 6, 8 and 10, post-operatively). The histograms showed the numbers of red blood cell (RBC), hemoglobin (HGB), platelet (PLT), and mean platelet volume (MPV) normalized with the values measured from non-treated rat. Each bar indicated min to max with mean as the middle horizontal bar (n = 6, for PAH and TMV-PAH and n = 7, for RGD-PAH) ± SD. From t-test analysis comparing control (non-treatment) and experimental value, the filled bars represented statistical significance, $p < 0.05$. Red dots represented outliers.

rats was comparable with value shown in normal rat's blood (no significant difference, multiple t-test). There were also no significant differences in all white blood counts when compared between each group of hydrogel implant. There were 2 outliers on day 4 white blood counts: one, from RGD-PAH implanted group expressed increased numbers of LYM and the corresponding WBC; another, from PAH implanted group exhibited high NEU and its corresponding WBC. However, both rats had white blood counts leveled out to the values comparable to all other rats after 1 post-operative week (Figure 4.2).

Other blood parameters that indicate animal health and significant loss of blood such as red blood cell (RBC), hemoglobin (HGB), platelet count (PLT), and mean platelet volume (MPV) were shown to be comparable to the values measured from non-treated rat's blood in all animals that were implanted with different types of hydrogels. Even though there were some outliers appeared at different time points for each parameter, those outliers seemed to obtain only temporal changes in particular blood counts that returned to the normal values at the later time point (Figure 4.3).

Organ weight can be the most sensitive indicator of an effect of drug toxicity, as significant differences in organ weight between treated and control animals may occur in the absence of any morphological changes.[130] The spleen and liver are main target organs for various nanomaterials in the circulatory system, because these organs are part of the reticulo-endothelial system (RES) that has removing foreign agents from the circulation as one of its functions. [131-133] In this study, we utilized viral nanoparticles in providing biofunctionality to hydrogel to create extracellular matrix preferable for cell attachment and growth. It was critical to evaluate the spleen enlargement that might occur from the immunogenic and/or elimination reaction of the body towards viral nanoparticles

presented in the hydrogel implants. Figure 4.4 showed that the spleen weights measured after the animal sacrifice (at the age of 22 weeks) were not significantly different among all groups. The corresponding mean spleen weight of all rats was 1495 ± 236 mg/kg of total body weight, which was not statistically different from the value reported in the literatures ($p > 0.05$, t-test). The mean normal spleen weight of male Sprague Dawley rat ± SD calculated from a generalized Michaelis–Menten (GMM) model, used to fit organ weights versus age in a previous study reported by Schoeffner *et al*., equaled to 1029 ± 191 mg/kg of total body weight.[134-136] From each animal observed at the end of the experiment, there were no chronic and/or major inflammatory and toxicity reactions in the RES that could cause the spleen enlargement in any group of animals.

In chapter 2, we have discussed the immunogenicity of TMV in the hydrogels implanted subcutaneously at lower back of BALB/c mice. The assay showed non-significant induction of specific anti-TMV Immunoglobulin G (IgG) produced in mice. Here, with the distinct rat cranial defect model, we re-evaluated the humoral immune reaction causing by TMV and its RGD mutant in the hydrogels after the bone defect replacement by TMV-PAH and RGD-PAH. From the ELISA assay, we found that TMV and its RGD mutant within the hydrogels led to average anti-TMV titer at peak time (week 8) below 1000. ELISA revealed higher anti-TMV antibody titers in rat sera collected from the animals implanted with TMV-PAH than those implanted with RGD-PAH hydrogels (Figure 4.5A). This observation might be due to the experimental design. The ELISA was performed based solely on wild-type TMV (used as antigen coated on ELISA plate). This could lead to the lower sensitivity in titer detection for the RGD-PAH group. Since it is not clear whether the antigen binding site of antibody produced against

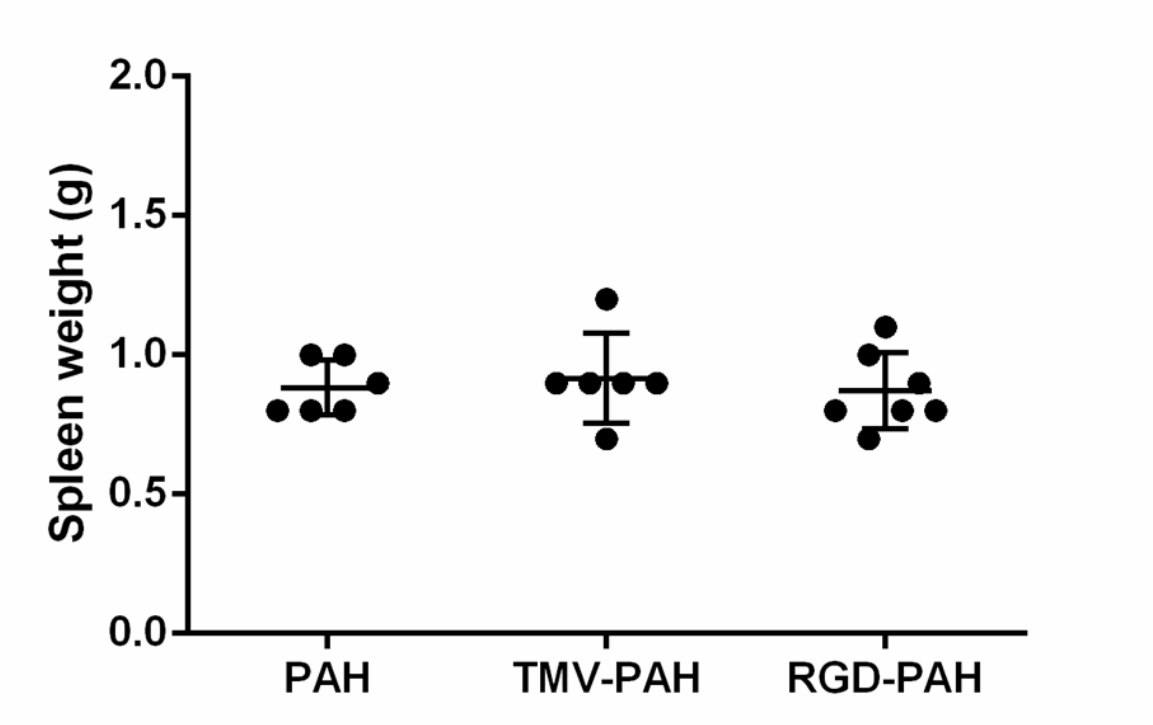

Figure 4.4. Rat spleen weight at 10 week endpoint. Values expressed are means (n = 6, for PAH and TMV-PAH and n = 7, for RGD-PAH) ± SD.

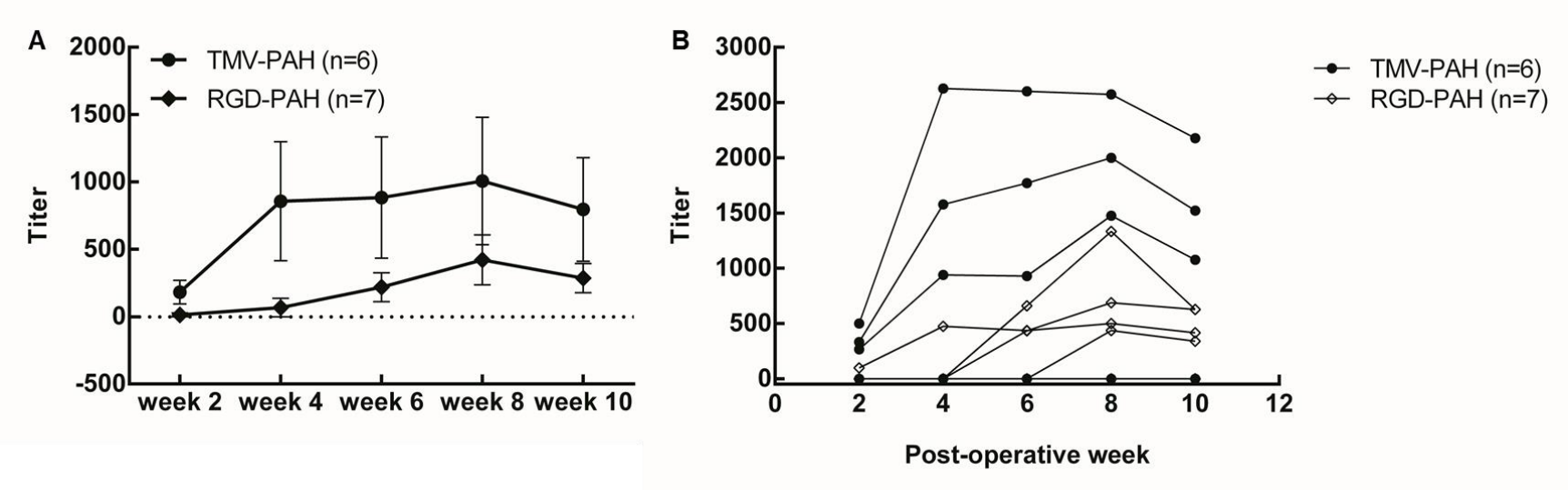

Figure 4.5. Immune response to TMV (Anti-TMV titer) in the rats with bone substitute implant materials. Comparative serological analysis of the immune response to each type of hydrogels was carried out by ELISA at different time points including 2, 4, 6, 8, and 10 post-operative weeks. TCID50 was shown as a titer for each plot. (A) Values expressed are means (n = 6, for TMV-PAH and n = 7, for RGD-PAH) ± SEM. (B) Each rat responded differently in terms of the titer level and the progression of anti-TMV IgG production. Each line connected the values analyzed from the same rat at different time points.

TMV wild-type and TMV-RGD1 share the same structure, the assay could have been optimized using different coating for ELISA on sera collected from different groups of animals. TMV-RGD1 mutant could have been used as the coating antigen to detect the titer for the rats in RGD-PAH group. Another possibility could be the difference of release profile between the wild-type TMV and the RGD mutant that escaped from the hydrogel scaffold into the circulation. The detailed studies on *in vivo* bioavailability and fate of both types of TMV releasing from the hydrogels would be carefully designed and preceded. Figure 4.5B shows that 3 out of 6 animals implanted with TMV-PAH expressed anti-TMV antibody as early as week 2, and the titers were continued to increase to reach their maximum within week 8. Among 7 rats implanted with RGD-PAH, 4 rats produced antibodies against TMV. However, the initial time points that the titers were first detected varied from week 2 to week 8. Interestingly, the titers decreased after week 8 in all rats that showed positive immune response from ELISA. This data suggested that there were only limited amount of TMV antigen released from the hydrogels into the circulation system. The result also emphasized *in vivo* safety of this TMV-based combinatorial 3D material for tissue engineering.

4.2.3 *Local inflammatory responses towards hydrogel implant*

Histological sections of the explants were stained using Masson's trichrome staining method and evaluated the inflammation, fibrosis and connective tissue formation, and vascularization in the hydrogels. No significant differences were detected between each gel condition. Figure 4.6 showed that RGD-PAH had significantly higher scores on

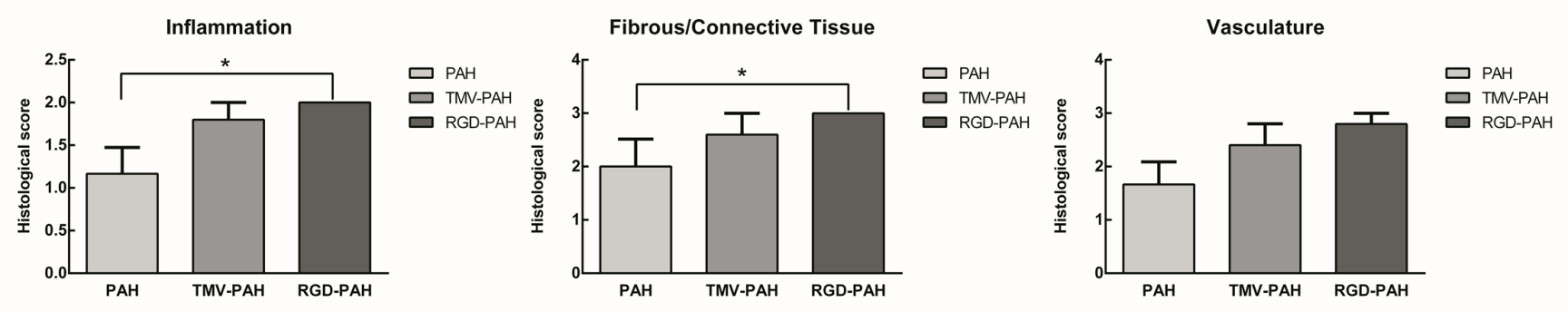

Figure 4.6. Histopathological analysis of bone substitute hydrogel implants. Histological scoring of three types of hydrogels in tissue excises showed different degree of inflammation, fibrosis, and vascularization after 10 week of implantation. Values expressed are means (n = 6, for PAH and n = 5, for TMV-PAH and RGD-PAH) ± SEM. * $p < 0.05$.

inflammation and fibrosis comparing to the control PAH (t-test, $p < 0.05$), yet obtained slightly higher scores than TMV-PAH with no statistical significance. Similarly, the average scores evaluated based on both histopathological parameters for TMV-PAH were slightly higher, but not significant, than those for PAH control. The same score trend among three types of hydrogels was observed with the vasculature analysis, but the differences were not statistically significant (t-test, $p > 0.05$), as well. The descriptive statistics of each histopathological variable was demonstrated in Table 4.1. There were inflammatory cells observed in the following hydrogel implants with average scores of 1.2 (PAH), 1.8 (TMV-PAH), and maximum 2.0 (RGD-PAH). The average scores of 2.0, 2.6, and 3.0 for PAH, TMV-PAH, and RGD-PAH, respectively, were given to the extent of connective and fibrous tissue (min - max = 0 - 3) formed in the hydrogels. Interestingly, every sample from RGD-PAH group scored maximum for inflammation and fibrosis variables, and gained a minimum of 2 scored for vasculature. The average scores for new blood vessels formed in each type of hydrogel (min - max = 0 - 3) are 1.7 for PAH, 2.4 for TMV-PAH, and 2.8 for RGD-PAH. Based on histological analysis of bone excises at the defect area, the animals that were treated with hydrogels incorporated with TMV and its RGD mutant tended to induce more physiological reactions towards implant materials including inflammatory cells infiltration, fibrosis, and neovascularization. One possible explanation could be that TMV might be able to induce more cytokine production from the migrating cells at the implantation site that could lead to more inflammatory cells recruited. The previous report by Sitasuwan *et al*. suggested that some cytokine-induced neutrophil chemoattractant-1 (CINC-1), CINC-2, macrophage inflammatory protein-3α (MIP-3α), and vascular endothelial growth factor

Table 4.1. Descriptive statistics of variables according to the type of hydrogel implant.

Variable	Hydrogel Implant	n	Average	SEM	95% CI of mean		Min	Max
					Lower	Upper		
Inflammatory	PAH	6	1.2	0.3	0.4	2.0	0	2
	TMV-PAH	5	1.8	0.2	1.2	2.4	1	2
	RGD-PAH	5	2.0	0	2.0	2.0	2	2
Fibrous/Connective Tissue	PAH	6	2.0	0.5	0.7	3.3	0	3
	TMV-PAH	5	2.6	0.4	1.5	3.7	1	3
	RGD-PAH	5	3.0	0	3.0	3.0	3	3
Vasculature	PAH	6	1.7	0.4	0.6	2.8	0	3
	TMV-PAH	5	2.4	0.4	1.3	3.5	1	3
	RGD-PAH	5	2.8	0.2	2.2	3.4	2	3

(VEGF) were detected from the conditioned media for the bone marrow stromal cells grown on TMV coated substrate.[36] CINC-1 and MIP-3α recruit neutrophils and monocytes that result in the induction osteogenesis.[137] Cytokines and growth factors secreted by infiltrated inflammatory cells including neutrophils, monocyte-derived macrophages, and lymphocytes are the molecular messengers that promote inflammatory events, such as neutrophil and macrophage recruitment, as well as wound healing events, such as connective tissue synthesis and vasculature. [27, 83, 138, 139] Moreover, the RGD peptide introduced by the incorporation of TMV-RGD1 into the hydrogel implant could induce even more material-host interaction. Even though, it has not been conclusive whether RGD can regulate *in vivo* cell adhesion to biomaterials as it does *in vitro*.[140] Our observation was consistent with many reports in RGD-functionalized materials promoting materials and surrounding cells interaction *in vivo*. For example, Shu *et al*. reported that the inclusion of covalently attached RGD peptides onto hyaluronan-based hydrogels could enhance the formation of fibrous tissue *in vivo*, with increased production of procollagen by the fibroblasts in the newly formed fibrous tissue at 4 weeks after animal treatment.[141] However, the future study with larger animal numbers should be performed in order to confirm these results and obtain more statistically significant analyses.

4.2.4 Bone healing analysis

The new bone formation after the hydrogel implantation was evaluated by two methods; 1) micro computed tomography (microCT) and 2) histological analysis of tissue excises

using Masson's trichrome staining technique. Microcomputed tomography (MicroCT) is an X-ray–based imaging method that offers access to the 3D microarchitecture of bone. A computer combines a stack of virtual cross-sections, interpolating sections along different planes, to inspect the internal structure of the object. A quantitative 3D histomorphometric evaluation (i.e., determination of the volume of bone mass and of the microarchitecture indices of the newly formed bone) can then be performed on a cubic volume or on an irregularly shaped volume of interest.[142, 143] Here, we scanned the regenerated bone tissue excises and quantified the new bone formed in each type of hydrogel implants using the microCT scanner. First, measurement of the angle for rotation and reconstruction of the 2D images were performed to ensure that all parts of the samples were scanned properly. All 2D constructs were shown in Appendix D. Figure 4.7 showed that RGD-PAH samples gave the most average bone volume following with TMV-RGD. PAH samples had the least mean bone volume quantified by microCT. Nevertheless, with statistical t-test analysis, the regenerated bone volume differences among three types of hydrogels lacked of significance. Therefore, more replicate samples may be investigated to make this conclusion definitive.

The same samples were then subjected to histopathological analysis. Masson's trichrome is to show the bone and non-mineralized osteoid seen in blue (aniline blue) and red (biebrich-scarlet), respectively. Figure 4.8 illustrated the representative image from each type of hydrogel sample corresponding to the bone density rank that obtained highest frequency (rat number) within each hydrogel type. The insets of Figure 4.8 depicted descriptive statistical analysis showing the frequency of each level of bone tissue formed. For example, the histological image of RGD-PAH shown in the right panel

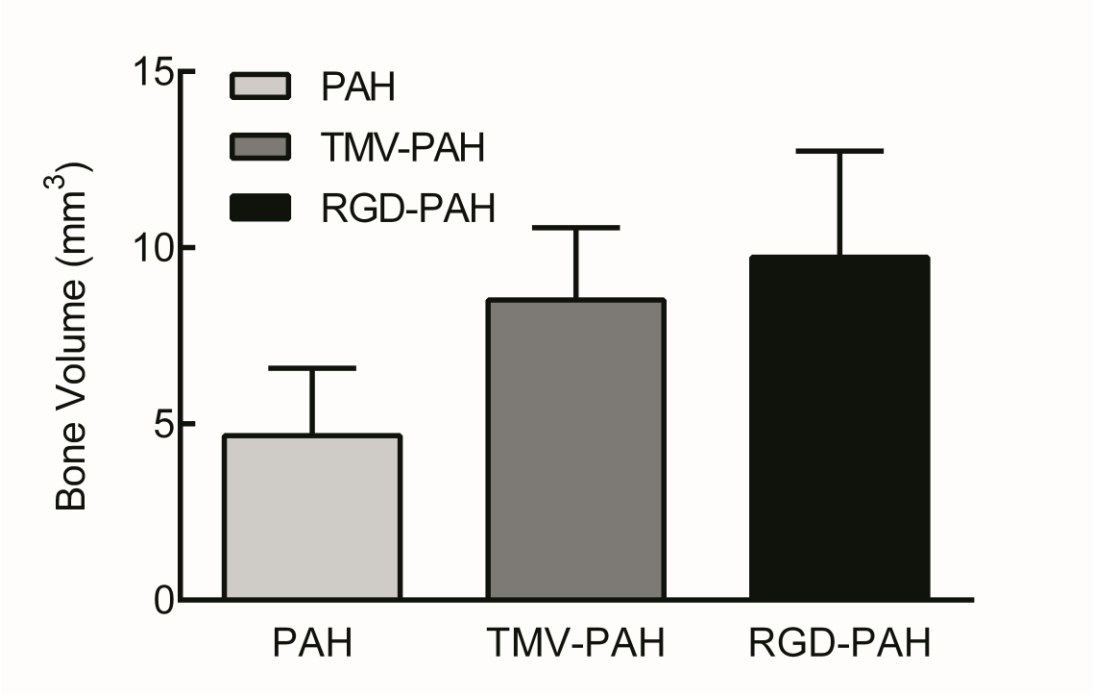

Figure 4.7. Bone regeneration in critical size defect areas with porous hydrogel bone substitutes. The bone volume regenerated in each type of hydrogel was quantified using micro computed tomography (microCT). Values expressed are means (n = 6, for PAH and n = 5, for TMV-PAH and RGD-PAH) ± SEM.[2]

[2] microCT scanned and analyzed by Amy Cheng, Garcia Lab at Georgia Institute of Technology.

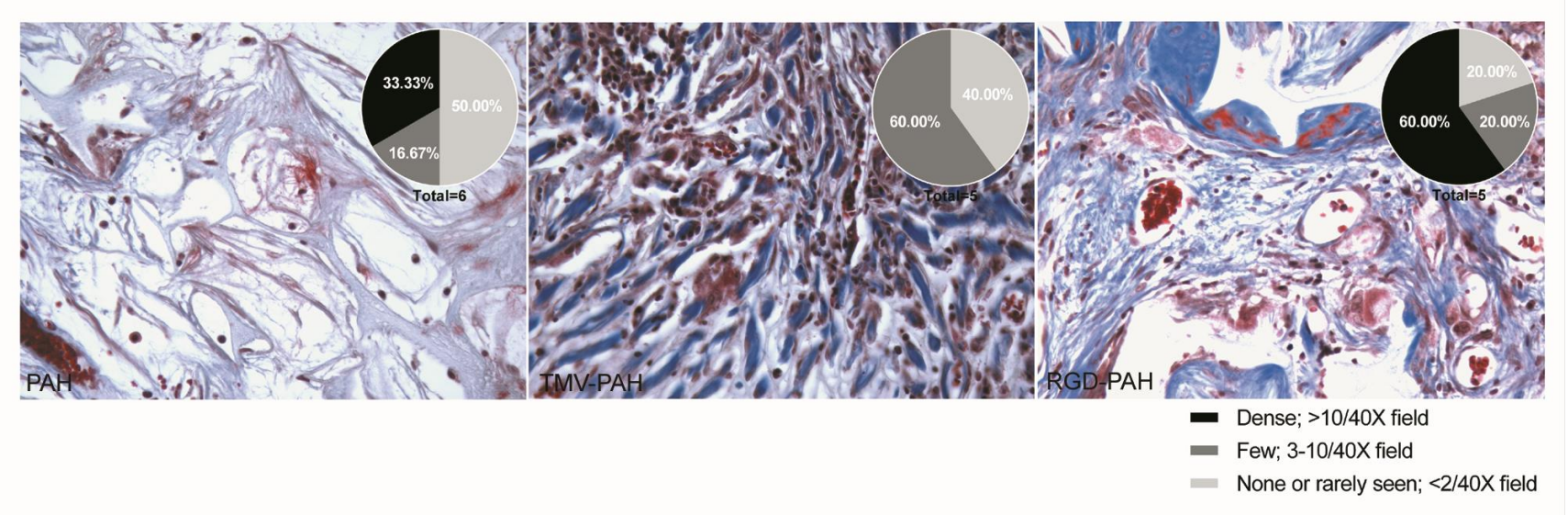

Figure 4.8. Histological analysis of regenerated bone at defect sites filled with hydrogel implants. Histological sections cut coronally through the defect after 10 weeks of implantation. The sections are stained with Masson's trichrome and imaged at × 40 magnification. The regenerated bone was characterized by the presence of a collagen-rich matrix stained blue. The inset pie charts represented the rat numbers that developed different degree of bone regeneration at the defect site.

of Figure 4.8 corresponded to the sample that was stained dense bone tissue (weighted 60% of total rats treated with RGD-PAH). Figure 4.8 showed that the rats that received RGD-PAH implants had more probability to regenerate higher density of bone. Following by the group that was treated with TMV-PAH, 60% of the animals in this group could regenerate few or medium bone tissue. The group with PAH alone had the most probability in having none or rarely seen bone formation. This analysis suggested that by incorporating TMV particle into the hydrogel scaffold, the bone regeneration could be enhanced. Moreover, TMV-RGD1 mutant further improved the new bone formation bridging the cranial bone defects. This result also corresponded to the histological analysis from previous section. Among combinations of hydrogel types, Pearson's statistical correlation test showed correlations between bone tissue formation in the hydrogel implants and two isolated histopathological variables including fibrous/connective tissue (correlation coefficient; $r = 0.6$) and neovascularization ($r = 0.6$). This study suggested, in consistence with many other studies, that RGD, when attached to the implanted scaffolding materials, played an important role in cell recruitment that could eventually help promote bone regeneration.[144-146]

4.3 CONCLUSION

The viral particle functionalized PAHs were comparatively investigated in terms of inflammation and healing of confined critical size cranial bone defects in rats. *In vivo*, TMV- and RGD- PAH permitted the healing of critical size defects in the cranial segmental bone of rats, as did the PAH control gel, but, unlike the latter, RGD-PAH

improved bone remodeling and maturation. The hydrogels elicited neither a systemic inflammatory reaction, nor a severe immunogenic adverse effect. Therefore, virus-based combinatorial porous alginate hydrogel is potentially useful as bone replacement material in reconstructive orthopaedic surgery, being a readily available biomaterial able to improve bone healing and maturation. However, more animal research with other model of bone defects (e.g., tibia and femur) and other higher animal may be needed before translation to clinic.

4.4 Experimental Section

All chemicals were obtained from commercial suppliers and used as received unless otherwise noted. Wild-type TMV (TMV) and its RGD mutant (TMV-RGD) were isolated from infected tobacco leaves following previously established protocols.[23]

4.4.1 Synthesis of Virus-Incorporated Porous Alginate Hydrogels.

The incorporation of TMV and its mutant (TMV-RGD) in porous alginate hydrogel was based on previously reported methods.[37] Briefly, 5% w/v low viscosity sodium alginate (Protanal LF 10/60 FT, 30 − 60 mPas for 1%, kindly provided by FMC Biopolymer UK Ltd.) was dissolved in 2% w/v sodium bicarbonate ($NaHCO_3$) and 4% w/v pluronic F108 solution. Molar equivalent of citric acid with respect to $NaHCO_3$ was added to the mixture while stirring at 500 rpm using overhead stirrer, 115V. Stirring was continued for 15 min at room temperature to allow CO_2 to fully develop. For the PAH modified with TMV (TMV-PAH), or PAH modified with mutant TMV-RGD (RGD-PAH), 0.1% w/v of

virus was added to the solution 10 min after adding citric acid. The mixture was stirred for another 5 min. Afterward, the foamy alginate solution was cast in 6.35 mm (0.25 inches) diameter, 2 mm thick aluminum mold and freeze-dried. The resulting solid foam disc was soaked in 2 M of $CaCl_2$ for 24 h to induce the formation of the calcium-based physical gel and then dialyzed against large volume of 0.1 M $CaCl_2$. Finally, the solid foam was freeze-dried, resulting in porous alginate hydrogel (PAH) for implantation in animal study.

4.4.2 Animals, Lethality Test and Animal Treatments.

The procedures were performed in accordance with the guidelines for animal experimentation and the protocol approved by the Institutional Animal Care and Use Committee, University of South Carolina. NIH guidelines (or for non-U.S. residents similar national regulations) for the care and use of laboratory animals (NIH Publication #85 - 23 Rev. 1985) have been observed. Twelve-week-old male Sprague-Dawley rats were housed at 22 ± 2 °C with a 12/12 h light/ dark cycle and fed standard rodent chow and water ad libitum. Twenty-one rats were randomly assigned to experimental groups. Two groups that were implanted by TMV-PAH, and RGD-PAH consisted of 7 rats each. Another group implanted by PAH consisted of 6 rats. Disk-shaped hydrogels were implanted to fill the cranial bone defects created in the surgery. Rats were given 2 - 4 mg/kg of Carprofen 2 - 4 hours before surgery subcutaneously for analgesia. Procaine penicillin (60,000IU) was given SQ for infection prophylaxis. Instruments were autoclaved prior to use to minimize risk of post-surgical infection and cross contamination. The animal was anesthetized with 3% isoflurance in oxygen. After the

appropriate plane of anesthesia was obtained, the fur over each animal's cranium was shaved and the skin was cleansed with normal saline to remove loose hair. A dry heating pad was used to keep the animal warm during surgery. A midline incision was made from the middle of the nasofrontal area to the external occipital protuberance, utilizing a sterile No. 15 scalpel blade. Full-thickness skin flaps will be reflected laterally with a periosteal elevator to expose the calvaria. An 8-mm craniotomy was performed in all animals utilizing a dental handpiece system at low speed and with copious sterile saline irrigation to remove loose debris and to avoid generation of frictional heat at the surgical site. Bone defects were standardized by using an 8-mm diameter trephine bur to outline the treatment area. A PTFE barrier membrane (Osteogenics Biomedical, Lubbock, TX) was inserted to form a barrier on top of the dura. Next, the hydrogel scaffold was carefully placed into the defect and the second PTFE membrane was placed over the defect and under the periosteum. The periosteum was repositioned and closed utilizing continuous interlocking sutures using Nylon suture material. Postoperative analgesia to relieve pain with carprofen (2 - 4 mg/kg) was given orally at least once every 24 hours for 48 hours. The animals were weighed immediately before/after surgery and daily afterward for the first 2 days. Then they were weighed once a week until the experiment ended. Signs of pain or distress were monitored daily after surgery.

Blood withdrawal was performed on day 4, weekly at the first 4 weeks, and biweekly until the end point at week 10, after the surgery. Blood samples from all animals were subjected to total blood count and antigen-antibody ELISA assay specific to TMV. Three-hundred microliters of blood was withdrawn from the tail vein while the

animals were restrained using a restraint tube. After iodine scrub, a butterfly needle was inserted into the vein. The blood was then collected into the collection tube.

At 10 week time point, the animals were euthanized. The implants were recovered together with their surrounding tissues. The excised implants with the surrounding tissues were then preserved in 10% neutral-buffered formalin for subsequent analyses. The spleen of every rat was isolated and weighted.

4.4.3 Micro computed tomography

The samples and the surrounding bone tissues were fixed in a 10% formalin solution for micro-computed tomography (Micro-CT, Skyscan 1076, Skyscan, Belgium) analysis and histopathology study 1 and 2 months after implantation. MicroCT was used to observe the new bone formation in the defected skull site. Each sample was fixed on the object stage, and imaging was performed on the sample for 360° of rotation with an exposure time of 20 min. MicroCT images were reconstructed over the region of interest (ROI) using CTAn (Skyscan) and CTVol (Skyscan) to make 3D images.

4.4.4 Hematological assay.

Complete Blood Count (CBC) was preceded right after each blood withdrawal. The blood sample of 10-50 µL was transferred into 1 mL BD Microtainer Tube with Dipotassium EDTA. Each tube was subjected to the automated blood counter machine, model VetScan HM5 Hematology System. The numbers of total white blood cell (WBC), neutrophil (NEU), monocyte (MON), lymphocyte (LYM), red blood cell (RBC), hemoglobin (HGB), platelet (PLT), and mean platelet volume (MPV) were recorded and

analyzed according to the calibrated instrumental protocol, which indicated the normal range of each parameter.

4.4.5 Paraffin Embedding and Histological Assays.

The formalin preserved implanted hydrogels/tissues of all rats were decalcified using 10% formic acid in formalin for 1 week and then embedded in paraffin blocks individually with proper orientations. Tissue sections (5 μm) were prepared and stained with Masson's trichrome. Based on the amount of inflammatory cells (basically lymphocytes, neutrophils, macrophages, and so on) observed within areas of implants, the degree of tissue inflammation was scored as 0, 1, and 2 (normal: none or rarely seen, slightly increased: 5 to 20 per × 40 objective field, and obviously increased: > 20 per × 40 objective field). Based on the degree of fibrous/connective tissues and capillary blood vessels observed within the areas of implants, the tissue fibrosis and vasculization were scored as 0, 1, 2 and 3 (none, rarely seen; ≤ 2 vessels/ × 40 field, slightly increased; 3 - 10/ × 40, and obviously increased; > 10 vessels/ × 40 field, respectively). Bone regeneration was evaluated on the same tissue sections and given the degree of new bone formation as follows: none or rarely seen; ≤ 2 per × 40 field, few or moderate; 3 - 10 per × 40 field, and dense; > 10 per × 40 field. Histological images were taken by using a Nikon microscope and an Olympus digital camera.

4.4.6 Enzyme-Linked Immunosorbent Assay (ELISA).

The serum samples for ELISA were obtained after centrifugation (2,000 g, 15 min, 4 °C) of blood samples collected from every animal and stored at -80 °C. ELISA was

performed no later than 3 months after the sera were collected. To coat wells with TMV antigen, high protein-binding conical bottom 96-well plate was used. Wild-type TMV (10 µg/mL, 100 mL) in phosphate buffer saline (PBS) was added to the microwells and incubated for 1 h at room temperature, followed by three PBS washes. Blocking for non-specific binding was performed by adding 100 µL of 1% bovine serum albumin (BSA) and incubating for 30 min at room temperature, followed by three PBS washes. Binding was performed by adding 100 µL of serially diluted antiserum into microwells and incubating for 1 h at room temperature, followed by thorough washes. HRP conjugate anti-mouse IgG (Cayman Chemical Company) diluted at 1:20000 ratio was added and incubated for 30 min at room temperature. Tetramethyl benzidine (TMB Plus, Amresco) and 1 M H_2SO_4 were added in sequence to the wells according to the manufacturer's protocol, and the binding efficiency was monitored by measuring absorbance at 450 nm.

CHAPTER 5

CHONDROGENIC DIFFERENTIATION OF BONE MARROW STROMAL CELLS IN THREE-DIMENSIONAL CULTURES

5.1 INTRODUCTION

5.1.1 Hydrogels as scaffolds for chondrogenesis of bone marrow stromal cells

Cartilage tissue engineering has been of significant interest with incessant efforts in research and development because damaged human articular cartilage lacks the ability for self-repair.[147-149] Current clinical methods to repair defective cartilage are limited in their ability to regenerate functional cartilage both in terms of composition and mechanics.[149] In replicating the native cartilage microenvironment, hydrogels provide cell support and display high water retention.[150] Many studies have evidenced that hydrogel-based biomaterials can offer an instructive three-dimensional (3D) microenvironment for chondrogenesis of stem cells *in vitro*, and can serve a delivery system for cell-based therapies *in vivo*.[150-152]

Bone marrow stromal cells (BMSCs) have emerged as a clinically relevant cell source for regenerative medicine due to their potential to differentiate into several mesenchymal lineages including cartilage, bone, and fat.[153, 154] The multipotent differentiation of BMSCs is regulated by both soluble and physical factors present in the extracellular microenvironment, including cell-cell and cell-matrix interactions, features that can be engineered into a range of natural and synthetic biomaterial scaffolds.[155]

The scaffolds not only provide structural support for chondrogenesis of BMSCs, but also control the differentiation through the design that imitates components of the natural extracellular microenvironment.[156, 157]

5.1.2 Tobacco mosaic virus as bionanoparticle to functionalize hydrogels

Here, we utilized the tobacco mosaic virus (TMV) as a functional nano-scaffolding material to decorate the hydrogel with multivalent RGD peptide, i.e. a common integrin-binding motif, through its RGD mutant. RGD has been shown to influence both chondrogenesis and osteogenesis in alginate hydrogels in dose-dependent manner.[156, 158, 159] The degree of cellular adhesion to the environment (e.g., through changes in ligand density) regulates integrin clustering, cytoskeletal organization, overall morphology, and, specifically in the case of stem cells, differentiation.[160-163] In Chapter 1, we explored the use of this virus functionalized hydrogels by studying the cell adhesion and osteogenic differentiation of BMSCs in 3D environment. The porous alginate hydrogel (PAH) scaffold was modified with TMV (TMV-PAH) and TMV-RGD1 mutant (RGD-PAH). The virus-functionalized hydrogels were cyto-compatible *in vitro* (Chapter 1), and biocompatible in mice and rats (Chapter 2 - 4). The RGD motif presented in the hydrogel was shown accessible to the cells by the increase in cell binding. Moreover, the hydrogels allowed the osteogenic differentiation with higher degree of mineralization in virus-functionalized hydrogels. In this chapter, we laid the concept of easy-to-functionalize hydrogel scaffold with controllable RGD dose and multivalency via viral nanoparticle on chondrogenesis of BMSC in 3D culture and characterization.

5.2 Results and Discussion

5.2.1 Chondrogenesis primer optimization

In this chapter, gene expression for 4 chondrogenesis marker proteins including Aggrecan, COMP (Cartilage Oligomeric Matrix Protein), Collagen II, and Sox9 were proposed to be used for characterization of the cartilage differentiation of BMSCs in 3D porous hydrogel scaffolds. First, Aggrecan is a cartilage-specific proteoglycan core protein (CSPCP) or chondroitin sulfate proteoglycan 1 that performs as an integral part of the extracellular matrix (ECM) in cartilaginous tissue. This molecule is important in the proper functioning of articular cartilage because it provides a hydrated gel structure (via its interaction with hyaluronan and link protein) that endows the cartilage with load-bearing properties. It is expressed by chondrocytes and is also crucial in chondroskeletal morphogenesis during development.[164] Second, cartilage oligomeric matrix protein (COMP) is a non-collagenous ECM protein expressed primarily in cartilage, ligament, and tendon. The molecular functions of COMP include: binding other ECM proteins, catalyzing polymerization of type II collagen fibrils, and regulation of chondrocyte proliferation.[165] Third, the synthesis of type II collagen is initiated as mesenchymal cells differentiate into chondrocytes. The level of cytoplasmic type II collagen mRNA progressively increases during the course of chondrogenesis, which parallels the progressive accumulation of cartilage matrix by cells.[166] These three protein markers mentioned are considered as the essential parts of the cartilage ECM. Another important chondrogenic protein marker, Sox9 is a transcription factor with a high-mobility group (HMG-box) DNA-binding domain exhibiting a high degree of homology with that of the mammalian testis-determining factor, SRY. During chondrogenesis, Sox9 is expressed in

all chondroprogenitors and all differentiated chondrocytes. This transcription factor is required in several successive steps of the chondrocyte differentiation pathway during endochondral bone formation *in vivo* and for the proper progression of cells through the sequential steps of this process. Akiyama *et al.* emphasized that Sox9 is needed for the commitment of undifferentiated mesenchymal cells to a chondroprogenitor.[167] To study these genes, we first verified the primers and optimized the reverse transcription polymerase chain reaction (RT-PCR) condition using the commercial cartilage cDNA.

The primer sequences for these genes were listed in Table 5.1. Figure 5.1 represented the corresponding RT-PCR products on agarose gel suggesting the validity of the primers and the respective RT-PCR condition for Sox9 (lane B), COMP (lane C), Aggrecan (lane D), and GAPDH (lane E). However, the RT-PCR product of Collagen II could not be synthesized from the same batch of cDNA (lane A), even with the increased dose of primers (up to 0.4 μM) and/or greater cDNA concentration.

5.2.2 Chondrogenesis gene expression

The genes related to chondrogenesis were studied from the differentiated BMSCs in PAH, TMV-PAH, and RGD-PAH cultured with chondrogenic media. Figure 5.2 showed the quantitative PCR results from day 18 culture normalized with non-induced BMSCs day 0. Overall, there were insignificant upregulations of all chondrogenic marker genes for Aggrecan, COMP, and Sox9 with no statistical significance among different types of hydrogels. The standard deviation (SD) expression of each gene normalized with

Table 5.1. Primers used for RT-PCR and RT-qPCR to measure chondrogenesis gene expression.

Gene	Sequence (5'-3')	Reference
GAPDH	Forward: ACTAAAGGGCATCCTGGGCTACACTGA	17
	Reverse: TGGGTGGTCCAGGGTTTCTTACTCCTT	
Aggrecan	Forward: GGCCTTCCCTCTGGATTTAG	[168]
	Reverse: CCGCACTACTGTCCAAC	
COMP	Forward: TGACTTCGATGCTGACAAGG	[168]
	Reverse: GAACGATCTCCATTCCCTGA	
Sox9	Forward: CTGAAGGGCTACGACTGGAC	[168]
	Reverse: TACTGGTCTGCCAGCTTCCT	
Collagen II	Forward: AGGGGTACCAGGTTCTCCATC	[169]
	Reverse: CTGCTCATCGCCG CGGTCCGA	

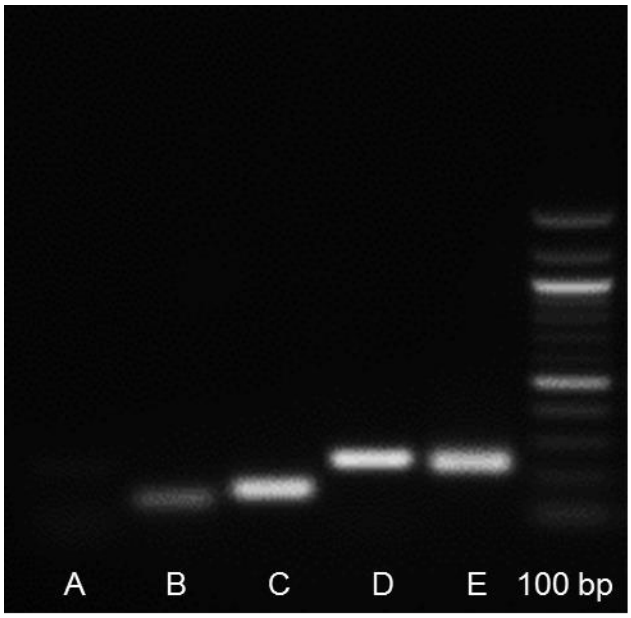

Figure 5.1. Agarose gel image of RT-PCR products derived from cartilage cDNA used for primer and PCR optimization. Gel image showed the PCR products of house-keeping gene (lane E), Aggrecan (lane D), COMP (lane C), and Sox9 (lane B). There was no product appeared for Collagen II gene (lane A).

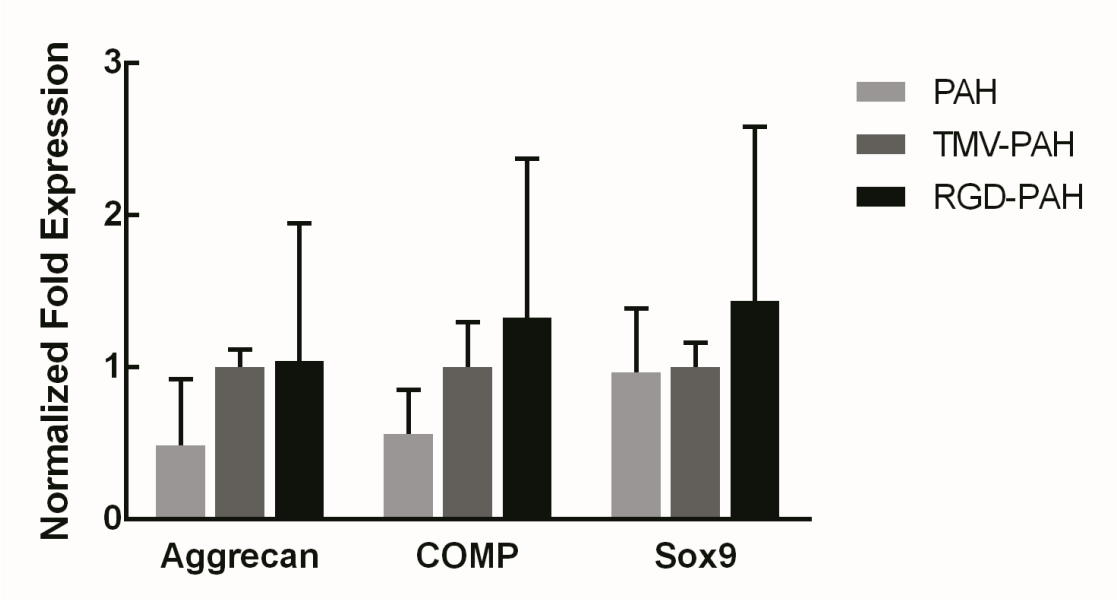

Figure 5.2. Gene expression levels of chondrogenesis markers after chondrogenic induction of BMSCs cultured in PAH, TMV-PAH, and RGD-PAH for 18 days.

housekeeping gene (GAPDH) and among triplicate samples were very high due to the poor quality and quantity of messenger RNA extracted from the hydrogels. Aiming for a quality RNA extraction from polysaccharide based scaffolds is extremely challenging.[170-172] However, the improvement in RNA purification method is required for more conclusive data.

5.2.3 *Collagen II immunohistochemical staining*

Immnofluorescence imaging in Figure 5.3 showed that the chondrogenic-induced BMSCs cultured in TMV-PAH and RGD-PAH stained positive for type II collagen after 18 days with higher fluorescence intensity than it appeared in PAH. It is likely that TMV and RGD-TMV could enhance the differentiation of BMSCs into chondrocyte. With very limited data, thus far, a possible justification at this point could be that TMV particles might induce the chondrogenesis through the stimulation of bone morphogenic protein-2 (BMP-2) as it has been suggested by Sitasuwan *et al*. in osteogenesis of BMSCs.[17] Likewise, the BMPs have been identified by virtue of their ability to promote cartilage formation, especially in commitment and condensation during chondrogenesis.[173-175] Therefore, more detailed study in expression of BMPs is necessary to rule out this hypothesis.

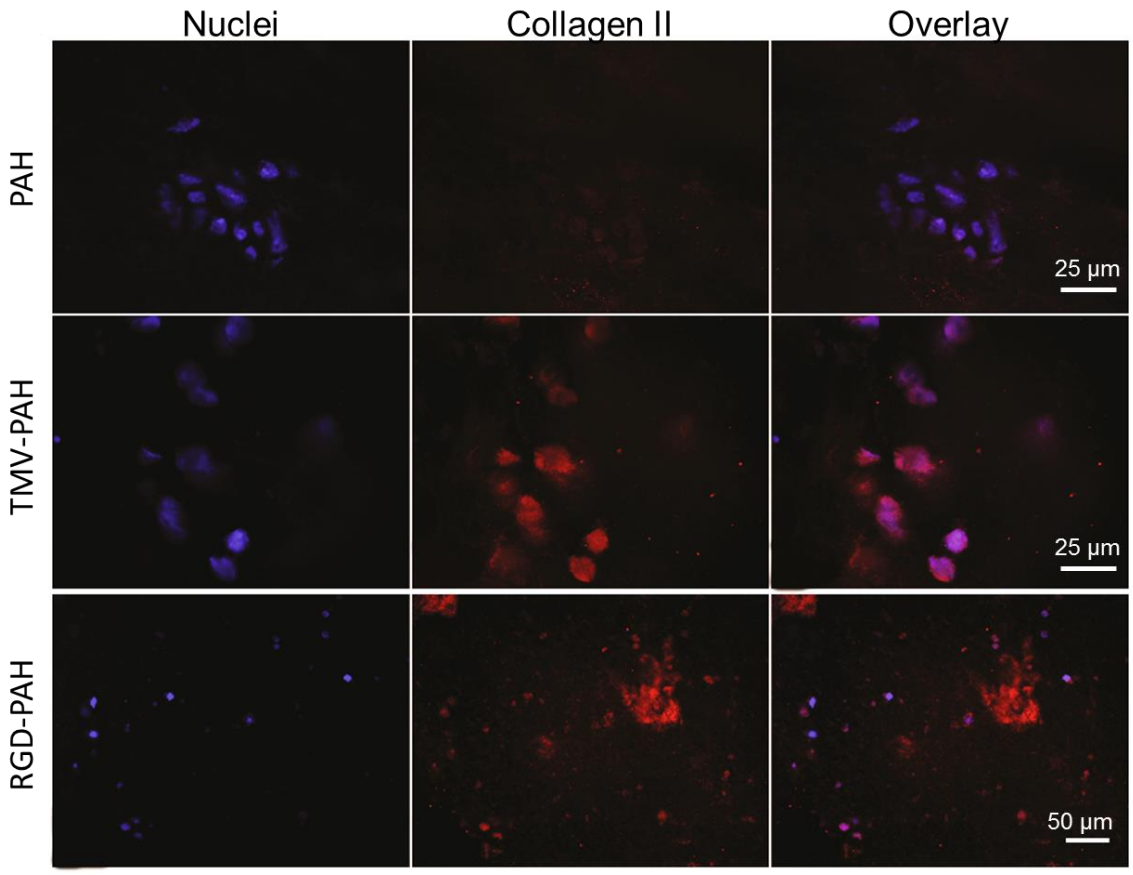

Figure 5.3. Immunofluorescence images of chondrogenic differentiated BMSCs in 3D virus functionalized hydrogels stained for nucleus (blue) and Collagen II (red).

5.3 Conclusion

In this chapter, we have verified the primers and the PCR condition used for chondrogenic gene study including Aggrecan, COMP, and Sox9. When BMSCs were culture with chondrogenic supplemented media in 3D hydrogels with virus nanoparticles (TMV-PAH and RGD-PAH), collagen II was accumulated and that could eventually lead to the cartilage-like tissue formation with the ECM components secreted during the differentiation and the 3D supports provided by the hydrogel scaffolds. However, the appropriate solid data should be continued to explore in order to make the argument conclusive. In conclusion, this virus functionalized porous alginate hydrogel system is considered a prototypical concept for the development of biomaterials to study the regulation of multivalent-displayed biofunctionality or specific scaffold chemistry towards cartilage differentiation of stem cells in 3D.

5.4 Experimental Section

All chemicals were obtained from commercial suppliers and used as received unless otherwise noted. Wild-type TMV (TMV) and its RGD-mutant (TMV-RGD1) were isolated from infected tobacco leaves following previously established protocols.[23]

5.4.1 Synthesis of virus-incorporated porous alginate hydrogels

The synthesis of gas template solid foam was based on the methodology reported by Barbetta *et al*.[28] Briefly, 5% w/v low viscosity sodium-alginate (Protanal® LF 10/60 FT, 30 - 60 mPas for 1%, kindly provided by FMC Biopolymer UK Ltd.) was dissolved in

2% w/v sodium bicarbonate ($NaHCO_3$) and 4% w/v pluronic F108 solution. Molar equivalent of citric acid with respect to $NaHCO_3$ was added to the mixture while stirring. Stirring was continued for 15 min to allow CO_2 to fully develop. Afterward, the foamy alginate solution was flash frozen in liquid nitrogen and freeze-dried. The resulting solid foam was soaked in 2 M of $CaCl_2$ for 24 h to induce the formation of the calcium-based physical gel and then dialyzed against large volume of 0.1 M $CaCl_2$. Finally, the solid foam was freeze-dried, resulting in porous alginate hydrogel (PAH). For the TMV modified PAH (TMV-PAH), or mutant TMV-RGD1 modified PAH (RGD-PAH), 0.1% w/v of virus was added to the solution 10 min after adding citric acid. The mixture was stirred for another 5 min.

5.4.2 Bone Marrow Stem Cells (BMSCs) isolation and culture

Primary BMSCs were isolated from the bone marrow of young adult 160-180 g male Sprague Dawley rats (Charles River Laboratories). The procedures were performed in accordance with the guidelines for animal experimentation by the Institutional Animal Care and Use Committee, School of Medicine, University of South Carolina. Cells were maintained in complete primary media (Dulbecco's Modified Eagle's Medium (DMEM) supplemented with 10% fetal bovine serum (FBS)), kept at 37°C in a CO_2 incubator with 5% CO_2 : 95% air and passaged no more than seven times after isolation.

5.4.3 Cell seeding and chondrogenic culture

Lyophilized PAH, TMV-PAH, and RGD-PAH scaffolds were cut to $3 \times 3 \times 2$ mm^3 cubes. For quantitative real-time RT-PCR, each set of experiment (N) contained six hydrogels per type of scaffold. For immunostaining experiment, one hydrogel per sample was used. Hydrogels were sterilized in 70% ethanol for 15 min, ethanol was drained on sterile filter paper and the hydrogels were further sterilized under UV-light for 60 min in laminar airflow hood. Hydrogels were then saturated in chondrogenic supplemented media at 37°C for 60 min, blotted excess media with sterile filter paper, and placed in 12-well non-adhesive plate. BMSCs were harvested from 80% confluent culture flask using 0.25% trypsin/EDTA (Cellgro) for 5 min and counted and re-suspended in complete primary media. 4×10^3 BMSCs were seeded per one volume (mm^3) of hydrogel. Rat BMSCs loaded hydrogels were initially incubated with 200 μL of chondrogenic media in each well to prevent hydrogels from drying out. After 6 h of an initial incubation, hydrogels were completely submersed in 1 mL of chondrogenic media in each well. The hydrogels seeded with BMSCs were cultured at 37°C and 5% CO_2.

Chondrogenic supplemented media comprised of DMEM (Hyclone, Thermo scientific), 1% fetal bovine serum (Atlanta biologicals), 1 × Penicillin-Streptomycin-Amphotericin B (from MP Biomedicals,100 U/mL penicillin and 1000 U/mL streptomycin solution, 0.25 μg/mL amphotericin B antimycotic), 100 nM dexamethasone (Enzo Life Sciences), 10 ng/mL TGF β1 (R&D System), 50 μg/mL ascorbic acid (Sigma-Aldrich), 1 mM sodium pyruvate (Hyclone, Thermo scientific), 1 × ITS^{+3}(from Sigma-Aldrich, contains 1.0 mg/ml insulin from bovine pancreas, 0.55 mg/mL human transferrin

(substantially iron-free), 0.5 μg/mL sodium selenite, 470 μg/mL linoleic acid, 470 μg/mL oleic acid and 50 mg/mL bovine serum albumin), 2 mM l-glutamine (Hyclone, Thermo scientific) and 40 μg/mL l-proline (Sigma-Aldrich).[176, 177] Medium was replaced thrice in a week and cultures were harvested at day 18.

5.4.4 RT-PCR

Rat cartilage cDNA (Zyagen) was used to verify the primers for cartilage related genes including Aggrecan, COMP, Sox9, and Collagen II and to optimize the quantitative real-time RT-PCR condition. RT-PCR was then achieved by the method described as: 45 cycles of PCR (95°C for 20s, 60°C for 15 s, and 72°C for 15 s), after initial denaturation step of 5 minutes at 95°C, by using 0.1 μL of Taq DNA polymerase, 0.5 μL of 10 mM dNTP Mix, 2.5 μL of 10X PCR Buffer, without Mg, 2 pmol/μL of each forward and reverse primers and 30 ng cDNA templates in a final reaction volume of 25 μL. The primer sequence used was listed in Table 5.1. The PCR product was then subjected to standard agarose DNA gel electrophoresis.

5.4.5 Quantitative real-time RT-PCR analysis (RT-qPCR)

The chondrogenic cell cultures were terminated after 18 days. At the termination time point, the hydrogels were flash frozen then immediately disrupted by high speed homogenization in the prechilled RNAzol® RT reagent (MRC). The tissue homogenizer probe was rinsed with RNase-free water and 10% sodium lauryl sulfate between each sample processing to prevent cross-contamination. Total RNA was subsequently

extracted following manufacturers' protocols of RNAzol® RT (MRC). The resulting RNA was reverse transcribed by using qScript™ cDNA Supermix (Quanta Biosciences). The number of samples for each experiment (n) was six and each experiment was repeated (N) three times. The quality and quantity of the extracted RNA was analyzed using Bio-Rad Experion (Bio-Rad Laboratories) and was reverse transcribed by using qScript™ cDNA Supermix (Quanta Biosciences). RT-qPCR (iQ5 real-time PCR detection system Bio-Rad Laboratories) was done by the method described as: 45 cycles of PCR (95°C for 20s, 60°C for 15 s, and 72°C for 15s), after initial denaturation step of 5 minutes at 95°C, by using 12.5 µL of iQ5 SYBR Green I Supermix, 2 pmol/µL of each forward and reverse primers and 2 - 5 µL cDNA templates in a final reaction volume of 25 µL. Glyceraldehyde 3-phosphate dehydrogenase (GAPDH) was used as the housekeeping gene. Data collection was enabled at 72°C in each cycle and CT (threshold cycle) values were calculated using the iQ5 optical system software version 2.1. Quantification of gene expression was based on the CT value for each sample which was calculated as the average of three replicate measurements for each sample analyzed using the same software. The primers used for RT-qPCR are shown in Table 5.1. The primers were synthesized commercially (Integrated DNA Technologies, Inc.), and evaluated for an annealing temperature of 60°C.

5.4.6 Immunohistochemistry staining for type II collagen

Immunostaining was performed to observe the presence of collagen II. rBMSCs culture in PAH, TMV-PAH, and RGD-PAH were terminated after culturing 18 days in

chondrogenic media. Hydrogels were washed three times with 100 mM cacodylated buffer and then fixed in 2.5% glutaraldehyde in cacodylated buffer overnight. The fixed samples were then permeablized for 15 min in TBST (0.05% Tween20) and blocked in 2% w/v bovine serum albumin (BSA, Sigma–Aldrich) in TBS for 20 min with gentle agitation at room temperature. After blocking, the hydrogels were incubated for 2 h with primary antibody targeting the type II collagen (Sigma-Aldrich) at 1:100 dilution. Secondary antibody detection Alexa Fluor® 546 (Molecular Probes, Invitrogen) was used at 1:200 dilutions in blocking buffer for 1 h at room temperature. In the end, the hydrogels were washed with TBS and counter-stained with DAPI (nuclear staining). Images of the stained samples were obtained using Olympus IX81 with epi-flour mode under 20x objective lens (for PAH and TMV-PAH) and 10x objective lens (for RGD-PAH). Exposure times were kept constant for all samples (50 ms for DAPI and 1000 ms for collagen II).

CHAPTER 6

IN SITU CROSSLINKING HYDROGELS WITH CYSTEIN-ADDED MUTANT OF TOBACCO MOSAIC VIRUS FOR STEM CELL ENCAPSULATION AND CULTURE

6.1 INTRODUCTION

6.1.1 Viral nanoparticle as a versatile nano-sized biomaterial in biomedicine

Plant viruses or virus like particles (VLPs) are becoming attractive platforms in variety of biomedical applications. Due to the simplicity of their genome, viruses use repetitive protein units to construct their capsids, which lead to highly organized structures on the surface.[178] This can provide a highly ordered platform to display various functionalities in high density. By designing the plant virus with simple functional groups, previous reports have shown that the tobacco mosaic virus (TMV), as nanometer sized building block, can support mammalian cells and dramatically improve the transformation of bone marrow derived mesenchymal stem cells (BMSCs) into bone-like cells in the laboratory. [36, 37] Moreover, Sitasuwan *et al*. reported the acceleration of bone differentiation with overexpressed BMP-2 gene in osteogenic induced BMSCs when grown on wild-type TMV based substrate.[17] Our aim was to implement these tissue responses in 3D hydrogel system in an injectable format for cartilage tissue engineering. The design of this study based on the covalent crosslinking of TMV particles onto the polymer backbone of injectable hydrogel. The polymer backbone functionalized with (meth)acrylate groups that can undergo Michael addition reaction with thiol molecules. Native TMV particles are nearly unreactive towards thiol-selective reagents including meth(acrylate).[38]

Therefore, in this chapter, we utilized a cysteine added mutant of TMV (TMV-1Cys) to serve the crosslinking purpose. Cys mutant of TMV has been successfully expressed in tobacco plants and purified in large quantities to utilize the virus platform in various application including vaccine carrier[76], DNA microarrays[179, 180], and battery electodes.[181]

6.1.2 Hyaluronic acid as a hydrogel-forming biopolymer

Hyaluronic acid (HA) is a mucopolysaccharide that binds to water giving it a stiff viscous quality similar to "Jello". It is natively found in most connective tissues and is particularly concentrated in human synovial fluid, the vitreous fluid of the eye, umbilical cords, nasal cartilage and rooster combs.[182] It is naturally synthesized by a class of integral membrane proteins called hyaluronan synthases, and degraded by a family of enzymes called hyaluronidases that are found throughout the body or through oxidative mechanisms to yield oligosaccharides and glucuronic acid.[183, 184] The biological functions of HA include maintenance of the elastoviscosity of liquid connective tissues such as joint synovial and eye vitreous fluid, control of tissue hydration and water transport, supramolecular assembly of proteoglycans in the extracellular matrix (ECM), and numerous receptor-mediated roles in cell detachment, mitosis, migration, tumor development and metastasis, and inflammation.[185-189] HA is a linear chain polymer of repeating units of disaccharide, β-1,4-D-glucuronic acid–β-1,3-*N*-acetyl-D-glucosamine.[182, 190] The polymer possesses properties desirable for tunable scaffolds for tissue engineering as a wide range of molecular weights can be obtained, as well as the presence of chemically modifiable groups (hydroxyl and carboxyl groups) on the

backbone. Functionalized HA with reactive groups such as methacrylates and acrylates has been utilized to form HA-based hydrogels for controlling stem cell differentiation.[191-194] HA hydrogel can also be further engineered to obtain different physical and chemical properties. For example, gelation time and mechanical property of the hydrogel could be tailored by altering the degree of modification of HA (methacrylation of HA) and/or the concentration of HA.[195]

6.1.3 Injectable hydrogel for cell encapsulation and tissue engineering

In situ gelling hydrogel system is currently of significant interest for tissue engineering applications due to its advantages over the pre-formed hydrogel scaffold. The key benefits include 1) cell encapsulation occurred as the gelation progress eliminating a concern over limited cell penetration into scaffold; 2) better cell-material contact closely resembling the natural tissue environment; 3) *in situ* molding feature capable of filling irregular shape defect and providing better tissue integration; and 4) minimally invasive route of administration improving patient compliance.[84, 196-198] Injectable hydrogel requires that the gel precursors can be gelled under mild conditions driven by physical changes like pH value, temperature, ionic concentration, and/or chemical crosslink reactions.[17] Here, we used hyaluronic acid (HA) as the hydrogel forming polymer to design the virus-incorporated injectable hydrogel. HA backbone was modified to have the reactive methacrylic group and the gel could be formed the physiological condition *in situ* upon addition of dithiothreitol (DTT) crosslinker via thiol-ene Michael addition reaction.[190, 195] The incorporation of TMV could be proceeded through the same thiol-ene reaction between thiol group of TMV-1Cys mutant and the methacrylated HA polymer.

Together with the previous observation that 2D TMV coated substrate could regulate early stem cell differentiation, we hypothesized that TMV displayed in a 3D hydrogel system could affect the hydrogel material properties and direct cell responses. In this study, we characterized the physical properties of hydrogels including viscoelasticity and gelation behaviors, the cross-linked TMV particles within the hydrogel, and the stem cell response after encapsulation in the TMV-based hydrogel.

6.2 Results and Discussion

6.2.1 HA-methacrylate synthesis and chemical characterization

Firstly, to fabricate the hydrogels, HA was functionalized with methacrylate groups using a simple, one-step reaction with methacrylic anhydride. Methacrylate groups were then crosslinked via a rapid Michael addition reaction with thiol-containing molecules. In our experiment, the cysteine-containing coat protein subunits of TMV-1Cys and dithiothreitol (DTT; a small molecule crosslinker) were used as the crosslinkers (Figure 6.1). Thiol-(meth)acrylate Michael addition is an efficient reaction that may be completed in aqueous medium at physiological temperature and pH in the presence of proteins or cells.[199-202]

We synthesized many variants of methacrylated HA as listed in Table 6.1. An excess of methacrylic anhydride with respect to HA was often used because of the limited solubility and potential hydrolysis reaction of methacrylic anhydride in aqueous medium. By varying HA monomer : methacrylic anhydride molar ratio, we consistently obtained low (~ 10%), medium (~ 40 - 50%), and high (100%) degree of modification of HA backbones (~ 47 kDa MW) as determined by ^{1}H NMR (Appendix E).

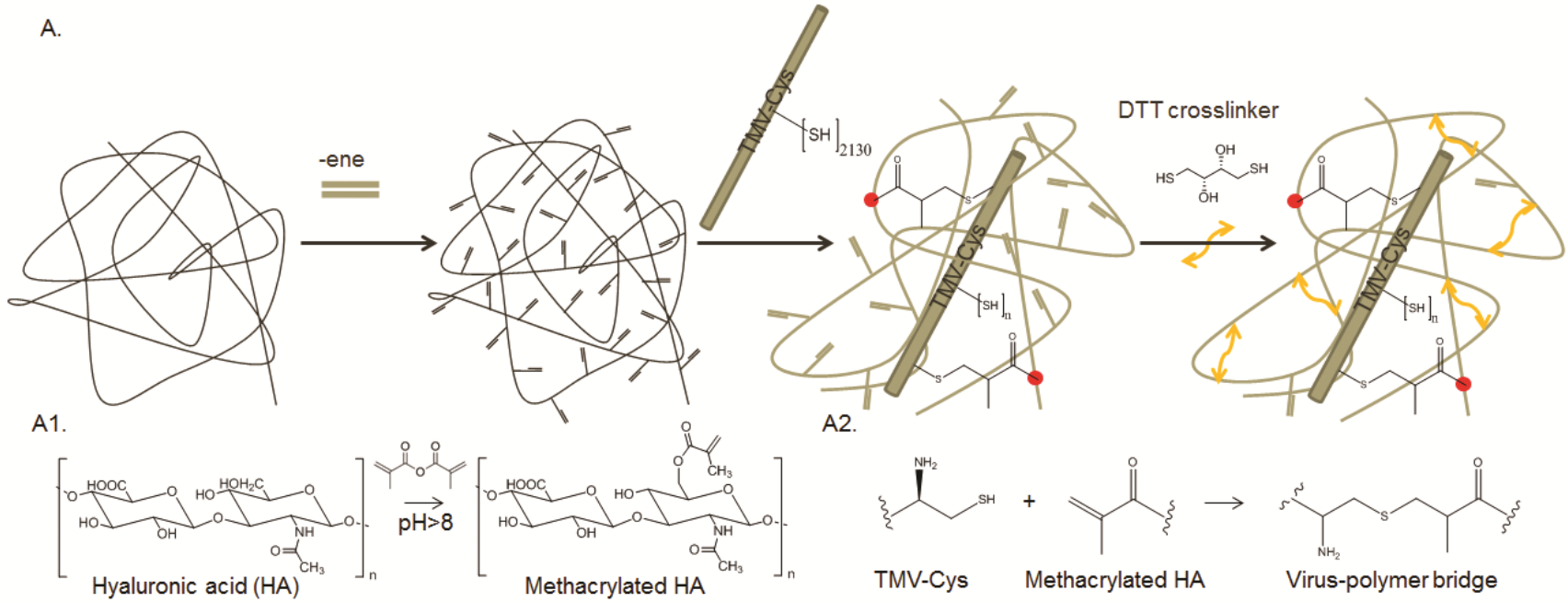

Figure 6.1. Injectable hydrogel from virus-linked biopolymer. The hydrogel synthetic scheme illustrated the incorporation of TMV in the *in situ* crosslinked hydrogel (A). Hyaluronic acid (HA) was reacted with different molar excesses of methacrylic anhydride to yield methacrylated HA in various degrees of modification (A1). TMV-Cys mutant was linked to methcrylated HA backbone via thiol-ene click reaction (A2).

Table 6.1. Percent degree of methacrylation of different macromer size HA when reacting with various molar ratio of methacrylic anhydride.

MW of HA	**HA monomer : Methacrylic anhydride molar ratio**			
	1:3	1:6	1:10	1:12
47 kDa	~ 10%	~ 40-50%	100%	100%
310 kDa	N/A	~ 30%	N/A	~ 75%
1 MDa	N/A	Not detectable	N/A	N/A

N/A data not available

Slightly lower percentage of modification could be obtained from the higher molecular weight HA (310 kDa) using the same reaction condition with 1:6 and 1:12 HA monomer : methacrylic anhydride molar ratio. Nonetheless, the degree of modification could not be detected by ^{1}H NMR when the same reaction condition applied to 1M Da HA, likely due to the high viscosity of the HA solution which reduces the reaction rate. Thus, the modification reaction of high molecular weight HA could be optimized by reducing the concentration of HA polymer. By far, giving optimum viscosity and modularity in a wide range of % methacrylation, 47 kDa HA macromere seemed feasible for our experiment.

The rational supporting the use of relatively small HA macromer (around 50 kDa) was also based on the report by Chung *et al*. They suggested that the hydrogels fabricated from 2 wt% of the 50 kDa HA macromer most resembled the properties of native cartilage and showed the greatest promise for continued development for cartilage regeneration when compared to the hydrogels from the larger HA (tested up to 1100 kDa).[190, 203] For the purpose of future chondrogenic (cartilage) differentiation study of BMSCs, 47 kDa HA was used for the rest of this report. For consistency of the nomenclature for each hydrogel formulation in this report, the terms, "TMV-SH, 0.1% + xx-DMHA, 5%" and "xx-DMHA, 5%," represent for TMV-1Cys modified methacrylated HA hydrogel and non-modified methacrylated HA hydrogel, respectively; with xx-DM indicating degree of methacrylation of HA polymer.

6.2.2 Gelling behavior and mechanical characterization of HA hydrogels

TMV-1Cys (TMV-SH) mutant contained cysteine in addition to the wild-type TMV at *N*-terminus of its hierarchically assembled coat proteins (see Appendix F for TEM image of TMV-1Cys). We covalently conjugated TMV-1Cys to methacrylated HA backbone via Michael addition reaction. The methacrylated HA functionalized with TMV-SH pre-hydrogel solution was then crosslinked to create hydrogel with DDT via the same thiol-ene reaction. Oscillatory rheology was used to study sol-to-gel transition. The DTT molecular crosslinker was added to the pre-hydrogel solution (with and without TMV-SH) right before loading sample onto the rheometer. The gelation time of each hydrogel was determined from crossing-over between storage modulus and loss modulus. Storage modulus G' and loss modulus G" are parameters describing the rheological properties of viscoelastic polymeric materials. Storage modulus G' defined by the ratio of elastic stress to strain, describes the amount of stored (saved) energy during shear, and refers to the elastic properties of the material. Loss modulus G" expressed by the ratio of viscoelastic stress to strain, shows how much energy was dissipated in a cycle of deformation in the form of heat and defines the viscous properties of the material.[204, 205]Here, we observed substantially faster gelation time when TMV-SH was attached and incorporated into the hydrogel (Figure 6.2). Figure 6.2A showed that the modulus cross-over appeared much earlier in the hydrogel formulation with 0.1 wt% TMV-SH. The same study was repeated for 3 times, and the significant difference of average gelation times of the hydrogel with and without TMV-SH was displayed in Figure 6.2B. The gels could be formed *in situ* within averages of 15 min, for the gel with TMV-SH, and 2 h, for the gel without TMV-SH.

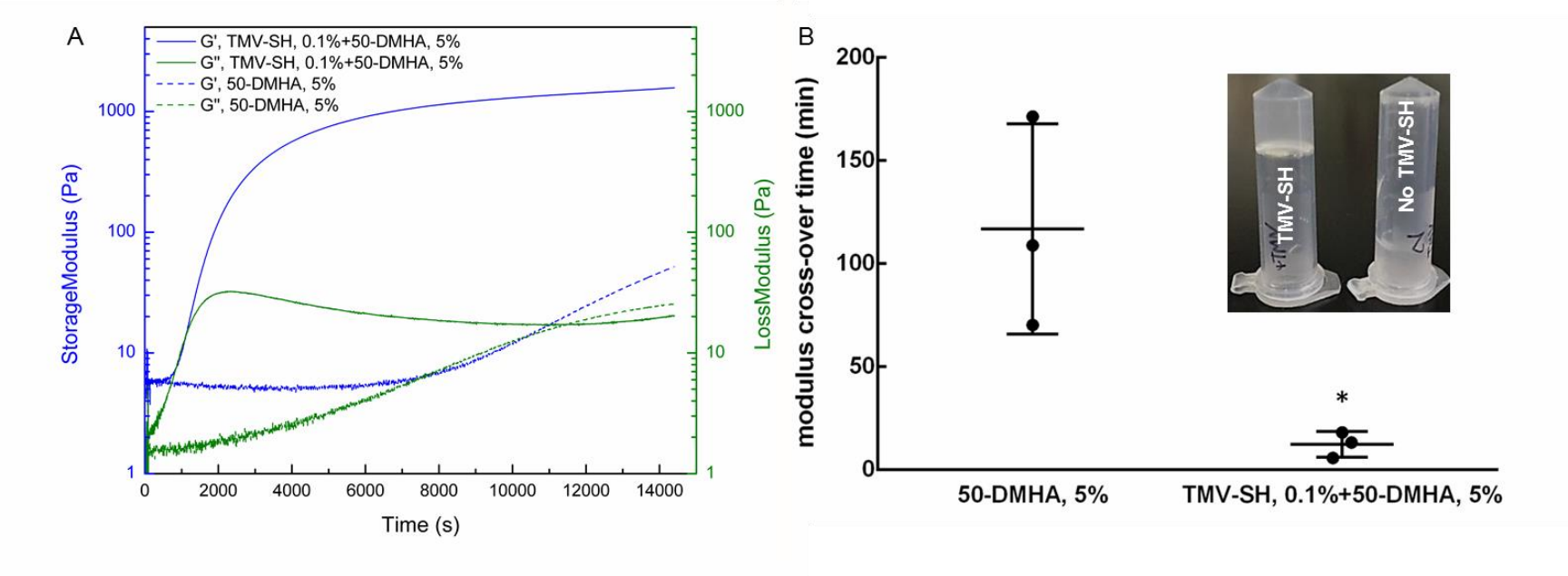

Figure 6.2. Gelation behavior of injectable hydrogels was observed via oscillation time sweep at 25 °C, 2% strain and 10 rad/s frequency. (A) The gel with the crosslinked virus gelled faster and yielded stable solid-like structure hydrogel with higher storage modulus. (B) The average gelation time of TMV-gel was significantly faster than that of the control HA gel. (B inset) The structured hydrogel with virus particles formed when the control hydrogel mixture was still in viscous liquid after fabricated at the same time. The horizontal bars are means ± SD with each data expressed in dot plots (n = 3); *p < 0.05.

The mechanical properties of TMV-SH+HA and control HA hydrogels were assessed through oscillatory rheology. Usually the rheological properties of a viscoelastic material are independent of strain up to a critical strain level γ_c. Beyond this critical strain level, the material's behavior is non-linear and the storage modulus declines. A strain sweep will establish the extent of the material's linearity. Figure 6.3A showed a strain sweep for both types of hydrogel giving higher average G′ of TMV-SH, 0.1% + 30-DMHA (435.60 Pa) than that of 30-DMHA, 5% (304.79 Pa). The critical strain γ_c of TMV-SH, 0.1% + 30-DMHA, 5% was approximately 400%, while 30-DMHA, 5% alone showed γ_c at ~ 200%. Below γ_c, the structure is intact, the material behaves solid-like, and G′ > G″, indicating that the material is highly structured. Increasing the strain above the critical strain disrupts the network structure. This result suggested that the gel with TMV-SH was stiffer than the control HA gel.

In oscillation analysis, frequency sweep is used to characterize materials' structures. It can be used to determine if a material is a three-dimensional network (gel), an entangled solution (paste), or a particle solution (liquid).[206] From Figure 6.3B, the elastic and loss moduli of both gels was essentially frequency-independent ($G' \propto \omega^{0.01\ Hz}$) and very slightly frequency-dependent, respectively; with elastic moduli higher than loss moduli. This viscoelastic behavior defined material's structure as 3D network of a hydrogel consisting of permanent crosslinks. As the test continued within a wide frequency range of 0.01 - 9, the gel maintained its solid-like viscoelasticity (G′ > G″) confirming its high resistance to deformation and subsequent high yield value.[206, 207] Further analysis on this frequency sweep experiment revealed that TMV-SH modified HA gel developed better solid-like behavior by decreasing the loss tangent ($\tan\delta = G''/G'$)

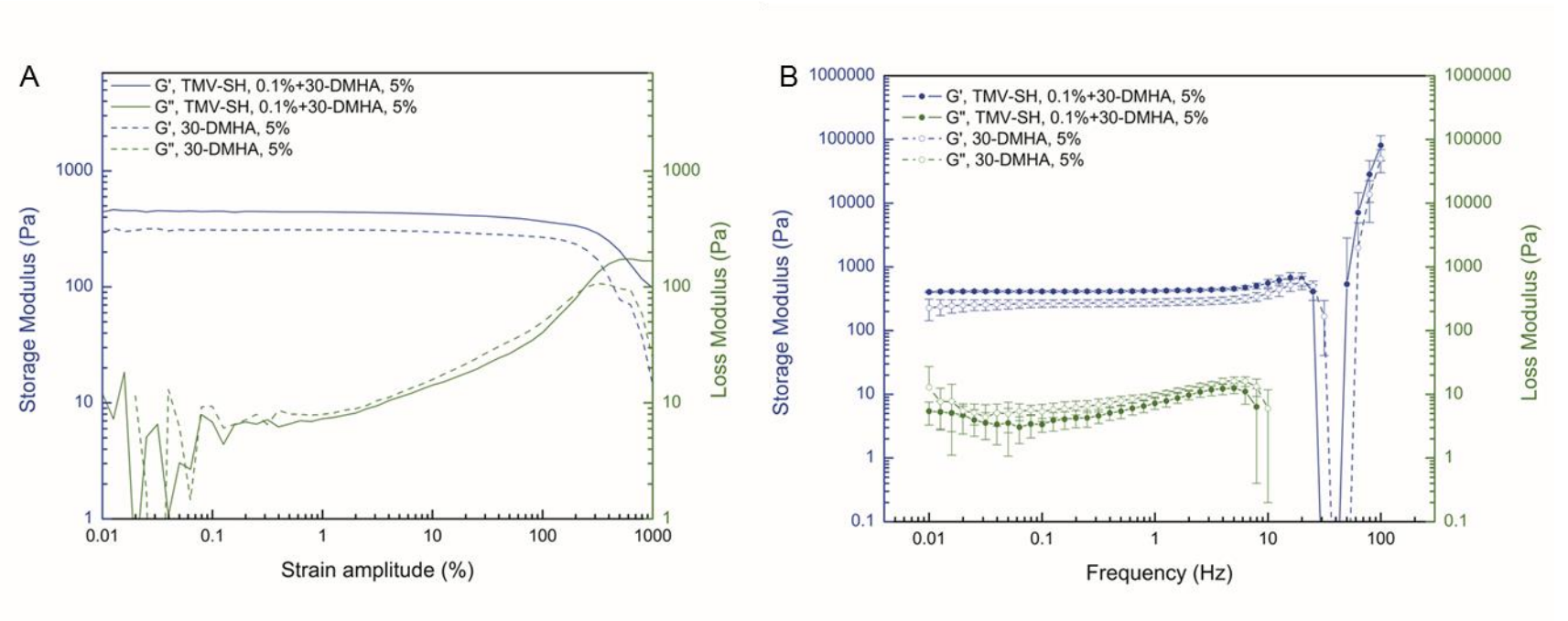

Figure 6.3. Viscoelastic properties of HA hydrogels with and without TMV particle. (A) Amplitude sweeps at 1 Hz frequency showed that TMV-SH modified HA gel increase the critical strain and elastic modulus of the hydrogel. (B) Frequency sweeps at 2% strain amplitude confirmed the increase in gel modulus with TMV-SH modified hydrogel (n = 3). Each plot expressed mean ± SD.

from 0.033 to 0.015. From this test, the average G′ ± SD (taken from the frequency-independent range, n = 3) of TMV-SH, 0.1% + 30-DMHA, 5% and 30-DMHA, 5% gel were calculated 422.89 ± 26.60 Pa and 273.25 ± 23.29 Pa, respectively. This analysis confirmed the result from amplitude sweep that the crosslinked TMV-SH increased the storage modulus of 30-DMHA, 5% gel.

6.2.3 Presentation of TMV-1Cys in HA hydrogels

MALDI-TOF analysis was used to determine the crosslinking between TMV-1Cys and HA backbone after fabrication of hydrogel. The TMV-SH, 0.1% + 50-DMHA, 5% hydrogel was first digested using 1800 units HAase (Hyaluronidase enzyme) for 48 h. The digested-hydrogel solution was then mixed with matrix, dropped on target plate, and subjected to MALDI-TOF analysis. The 2 controls included 1) purified TMV-1Cys in 10 mM potassium phosphate buffer, pH 7; and 2) 50-DMHA, 5% hydrogel digested with 900 units HAase as shown in the last 2 bottom panel of Figure 6.4A. HAase randomly cleaves β-N-acetylhexosamine-[1→4] glycosidic bonds in hyaluronic acid. Figure 6.4A demonstrated that TMV-SH gel obtained pronounced peaks in addition to the peak of original TMV-SH coat protein (around 17630 m/z). One of the additional peaks appeared at 19652 m/z. From this representative peak, the mass difference subtracted from the TMV-1Cys peak was calculated and matched with the molar mass of the possible backbone structure proposed in Figure 6.4B.

To confirm the existence of TMV-1Cys particles in the methacrylated HA hydrogel, spin coating technique following with atomic force microscopy were applied.

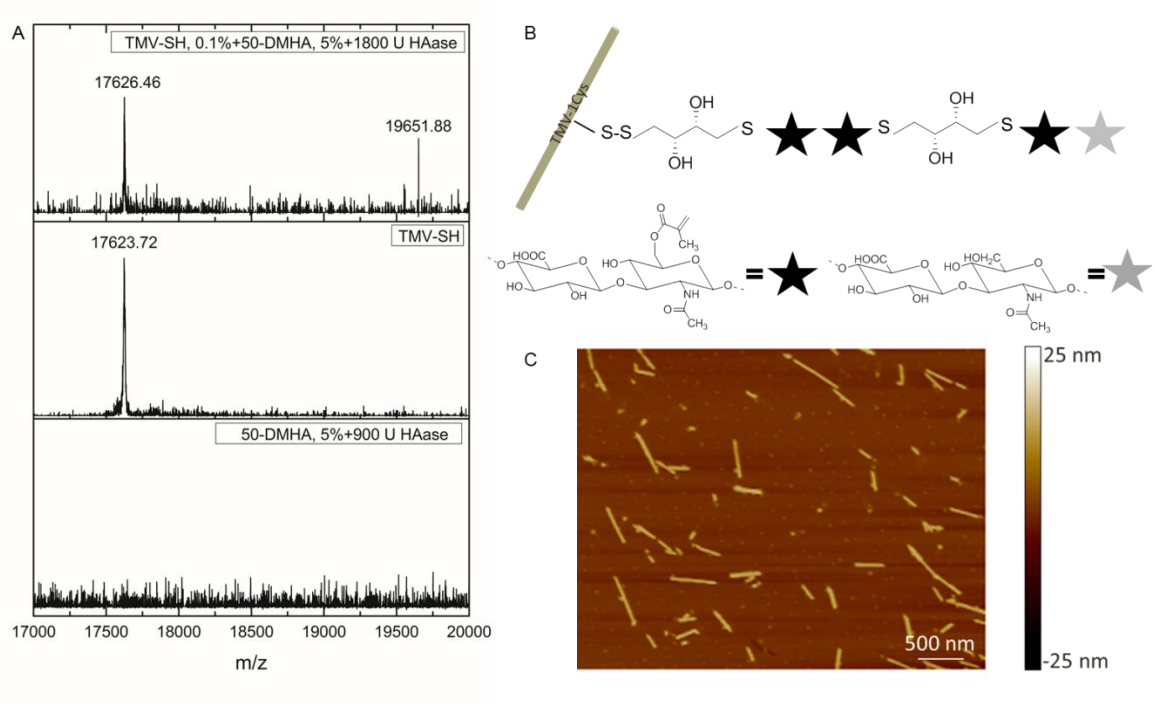

Figure 6.4. Interaction of TMV-1Cys and its structural integrity in modified-HA hydrogel. (A) MALDI-TOF spectra compared the m/z profiles of TMV cys-mutant functionalized hydrogel after enzyme digestion of HA backbone (top panel) with the virus alone (middle panel) and with the control HA hydrogel (last panel). The extra peak marked in the top panel was analyzed to match the structure proposed in (B). (B) From MALDI-TOF analysis, the TMV-1Cys was shown to have a covalent interaction with the polymer backbone. (C) AFM height image (spin coated) showed the presence of TMV-1Cys intact particles in the hydrogel.

The TMV-SH, 0.1% + 50-DMHA, 5% hydrogel, after adding DTT and allowing 10 min gelation, was spin-coated on the silicon wafer. The hydrogel coated wafer was then dried and subjected to AFM imaging. Figure 6.4C showed the height profile of TMV-1Cys particles on the silicon wafer substrate coated with TMV-incorporated hydrogel, which confirmed the existence TMV particles in the hydrogel. TMV-1Cys has the same appearance with wild-type TMV observed by AFM (See appendix G).

6.2.4 Microstructural characterization of hydrogels

As described earlier in chapter 1, the high porosity and interconnectivity of hydrogel are critical for cell survival *in vitro*, when the capillaries are not present, since these properties influence cell migration and diffusion of oxygen, nutrients, waste products and signaling molecules.[148, 208, 209] The extent of ECM secretion also increases by increasing the pore size. It was found that in genipin crosslinked gelatin hydrogels with smaller pores, the tendency was tilted toward cell growth rather than of ECM secretion, resulting in over-confluence during the middle and late stages of differentiation; consequently, the extent of ECM secretion decreased compared to that within gelatin hydrogels with larger pores.[210] The effect of implant pore size on tissue regeneration is emphasized by experiments demonstrating the optimum pore size of 5 μm for neovascularization, 5–15 μm for fibroblast ingrowth, 20 – 125 μm for regeneration of adult mammalian skin, 100 – 350 μm for regeneration of bone, 40 – 100 μm for osteoid ingrowth, and 20 μm for the ingrowth of hepatocytes.[211] In addition, mean pore size has been shown to impact the amount of contraction a graft will undergo after implantation. An average pore diameter

of 20 – 125 μm was required for contraction-inhibiting activity to be observed in collagen–glycosaminoglycan graft copolymers used for dermal repair.[212] To characterize the microstructure of our HA gels, we used scanning electron microscopy (SEM) for imaging hydrogels after freeze-drying (Figure 6.5). The cross-section electron micrograph of TMV-SH, 0.1%+100-DMHA, 3% revealed 20 - 100 μm range of interior pore size with high porosity and interconnectivity. Furthermore, the thin, dense, sheet-like layers of polymer extending along the outer edge of the hydrogel cross-section were observed (Figure 6.5). 100-DMHA, 3% obtained the similar pore architecture except the lesser inter-connectivity with more well-defined pore structure and the thicker layer of dense outer edge (Figure 6.5). Besides, the exterior surfaces of both gels were dense, rough, folded architecture with sub-micron sized pores (< 2 μm). This surface layers were uniform and continuous, which made the surface essentially less porous. This result was consistent with previous studies of HA hydrogels. [213-215]

Apart from the porosity, permeability also has a remarkable effect on proliferation and phenotype of cells.[148, 216] Here, we investigated the permeability of the hydrogels by observing the fluorescent dye diffusion. First, the standard curve of Fluoresceinamine isomer I in PBS was generated from 1 - 10 μg/mL concentration range (See Appendix H). The amount of dye diffused into the pre-saturated hydrogel was calculated from the reduction of fluorescence intensity measured from the medium over time. Figure 6.6 showed that both hydrogels, TMV-SH, 0.1%+50-DMHA, 5% and 50-DMHA, 5%, could absorb the dye in a similar manner. The dye diffusion reached equilibrium within one hour in both hydrogels. The value of dye diffusion presented in Figure 6.6 depicted the dye concentration in the hydrogel percentages of the total dye concentration in the media

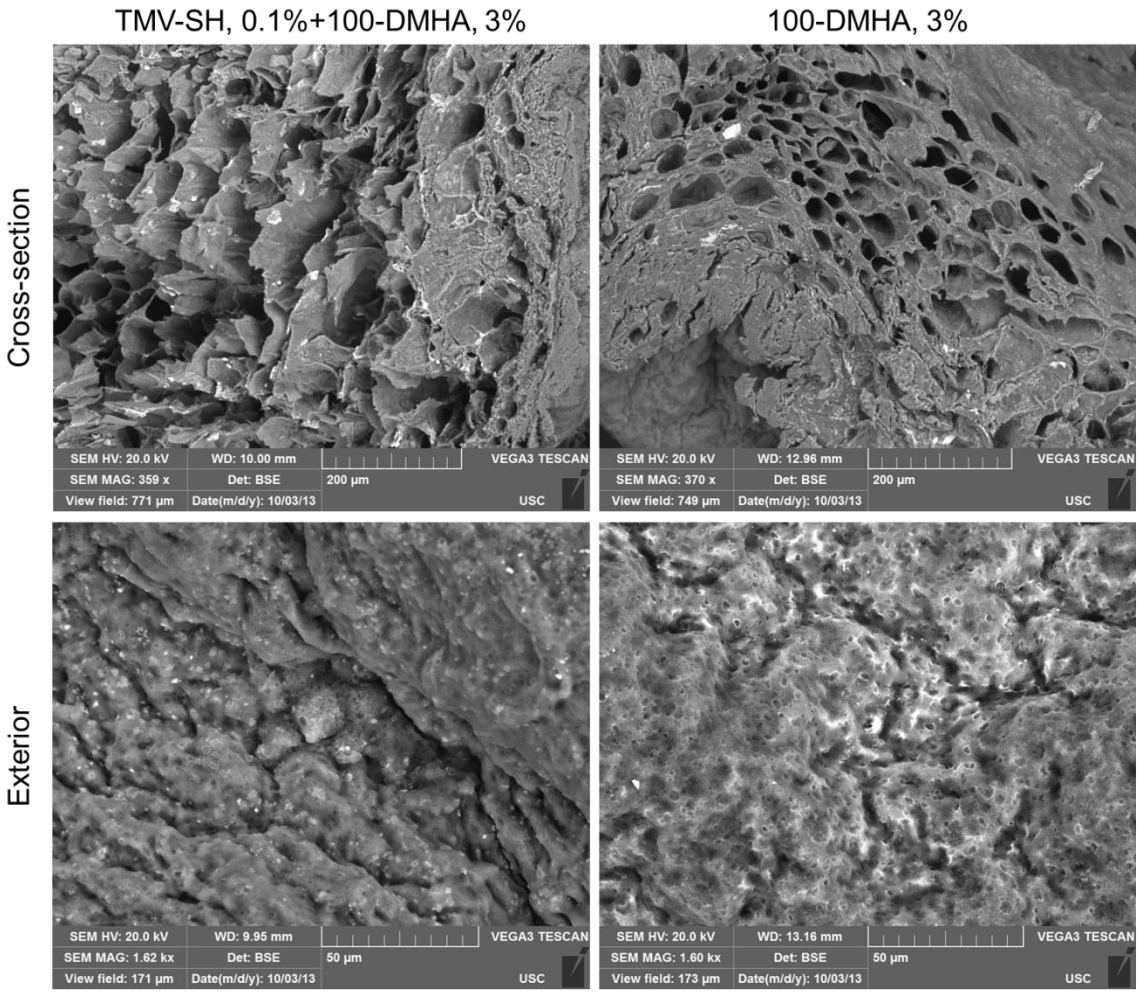

Figure 6.5. Cross-section and surface SEM micrographs of virus-modified injectable hydrogel. The cross-section ESEM images showed the porous interior architecture of both hydrogel after freeze-dried. The virus incorporated hydrogel obtained larger extent of interconnecting channels with thinner dense layers along the outer edge. The exterior surfaces of both hydrogels seemed denser with sub-micron pore architecture.

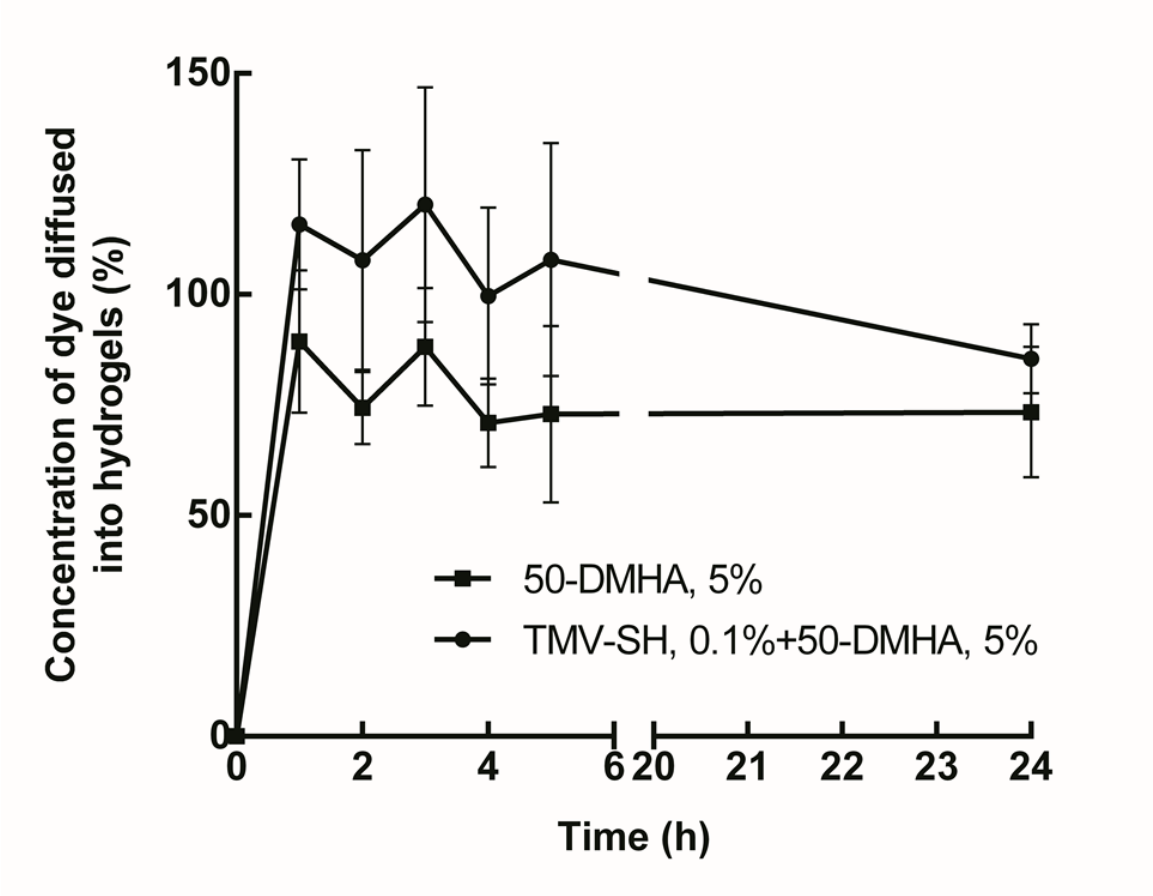

Figure 6.6. Permeability of the hydrogels in term of molecular diffusion was tested using dye diffusion study. The hydrogel functionalized with virus particles allowed faster rate and better diffusion of the fluorescent dye when incubated at 37°C. Each plot represented means ± SD (ANOVA, $p = 0.05$).

with the hydrogel altogether (theoretical). TMV-SH, 0.1%+50-DMHA, 5% gel absorbed slightly more dye at equilibrium around 100% on average comparing to the value calculated for the 50-DMHA, 5% gel, which was around 75% ($p = 0.05$). This might be a consequence from the pore and interconnect structural differences discussed earlier.

6.2.5 Swelling property and stability of hydrogels

To exploit swelling property of each hydrogel, 250 µL of TMV-SH, 0.1%+50-DMHA, 5% and 50-DMHA, 5% hydrogels were fabricated and immersed in 1 mL PBS. The representative of fully structured hydrogel before incubation with PBS was shown in Figure 6.7A inset. Swelling ratio of HA hydrogel with TMV-1Cys was shown to be slightly higher than the control HA gel without the virus nanoparticle in early time points (Figure 6.7A). However, the swelling ratios of both hydrogels became insignificantly different at later time points. This, as well, could be a result of the higher interconnectivity and the thinner wall of TMV-SH, 0.1%+50-DMHA, 5% gel observed from the cross-section scanning electron micrograph. This microstructure of TMV-SH, 0.1%+50-DMHA, 5% gel allowed better water absorption and could entrapped higher volume of aqueous media at faster rate in comparison to 50-DMHA, 5% gel. Slight increases in swelling ratios were observed during the 120 h incubation, which could indicate a possible onset of the degradation of the hydrogel. Stability of both hydrogels was shown in Figure 6.7B. No weight loss was observed within 21 days in PBS.

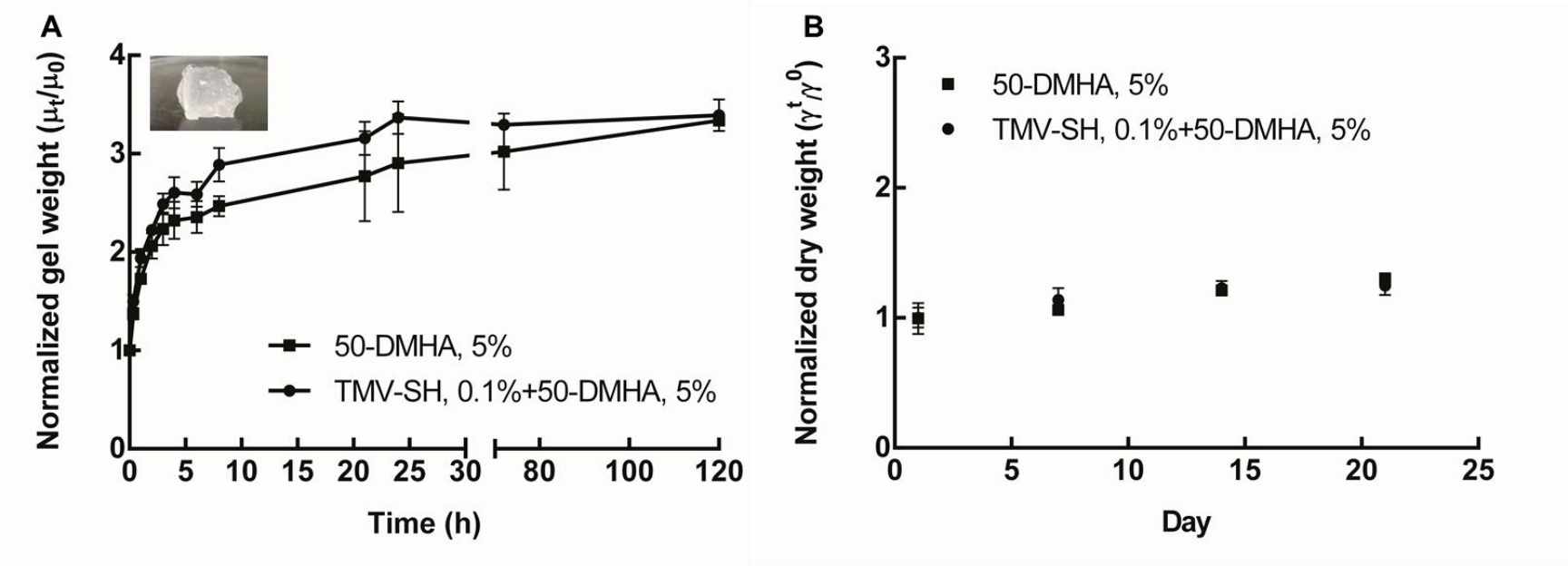

Figure 6.7. Swelling properties and stability of the hydrogels. The hydrogel after gelation (A inset) was immersed into PBS (A) The weight change due to water absorption was monitored over time. Swelling rate appeared faster with the TMV-SH modified hydrogel. (B) No weight decreases were observed from both hydrogels measured after freeze-drying at each time point for up to 3 weeks incubation. The values expressed are means ± SD, n = 3.

6.2.6 In situ encapsulation and culture of bone marrow stromal cells in 3D hydrogel

We next explored the compatibility of TMV-1Cys HA hydrogel for culturing BMSCs. BMSCs were encapsulated *in situ* by mixing the cells (1 million /mL) thoroughly with TMV-SH, 0.1%+50-DMHA, 5% and 50-DMHA, 5% pre-hydrogel solutions in complete DMEM cell culture media before loading into Transwell® inserts. Metabolic rate of BMSCs encapsulated in the hydrogels TMV-SH, 0.1%+50-DMHA, 5% and control hydrogel 50-DMHA, 5% was carried out at different time points using CellTiter-Blue® (CTB) reagent. Metabolite of CTB reagent generated by viable cells is fluorescent. Figure 6.8 showed the preliminary result from each hydrogel, n = 1. The cell metabolic rates in both hydrogels were similar. On day 4, the metabolic rates decreased from the first day of culture, and then increased continuously until the end point on day 15. Cell viability was then confirmed by live-cell staining, Calcein AM (CAM), at different time points. Figure 6.9 illustrated the viable cells in both hydrogels stained green from day 9 and 17.

6.2.7 RNA extraction for future gene study

For application in BMSC differentiations, this cell-encapsulated hydrogel culture was validated for RNA extraction. We were able to purify RNA in the sufficient amount and quality for the future gene expression studies. Figure 6.10 showed an agarose gel with polymerase chain reaction (PCR) products of GAPDH, a house keeping gene, which was synthesized from cDNA of mRNA purified from cells cultured in TMV-SH, 0.1%+50-DMHA, 5% at different time points.

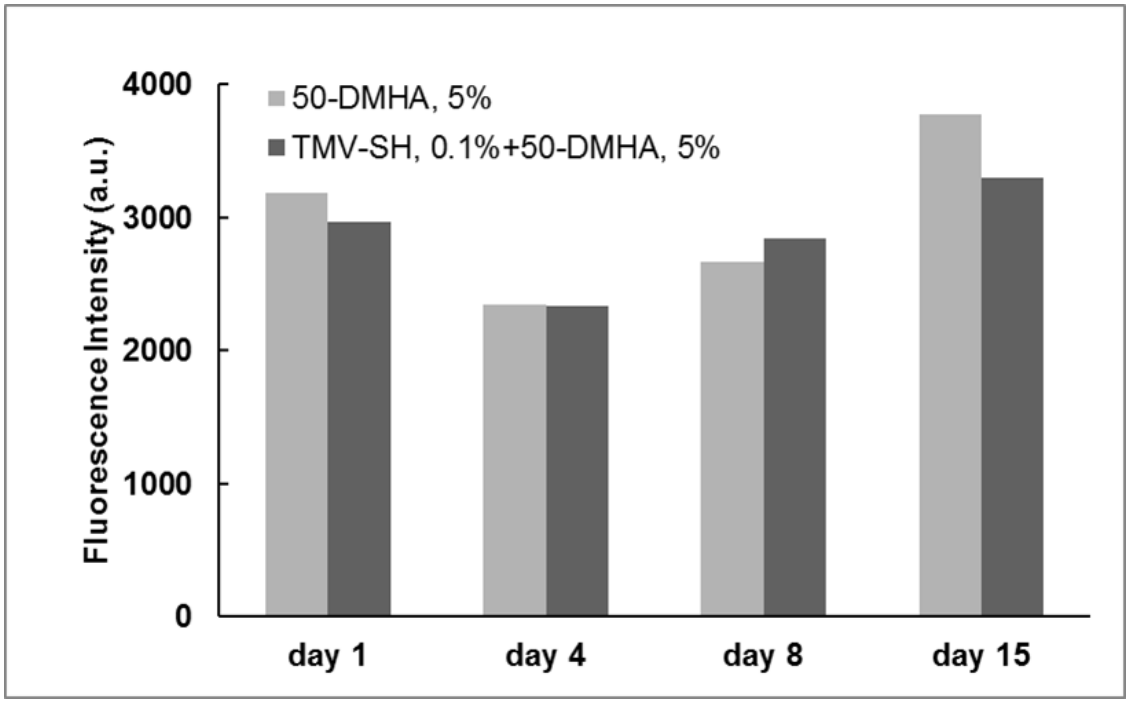

Figure 6.8. Celltiter Blue assay of viable cells encapsulated at a concentration of 1 M/mL in the hydrogels in primary media culture.

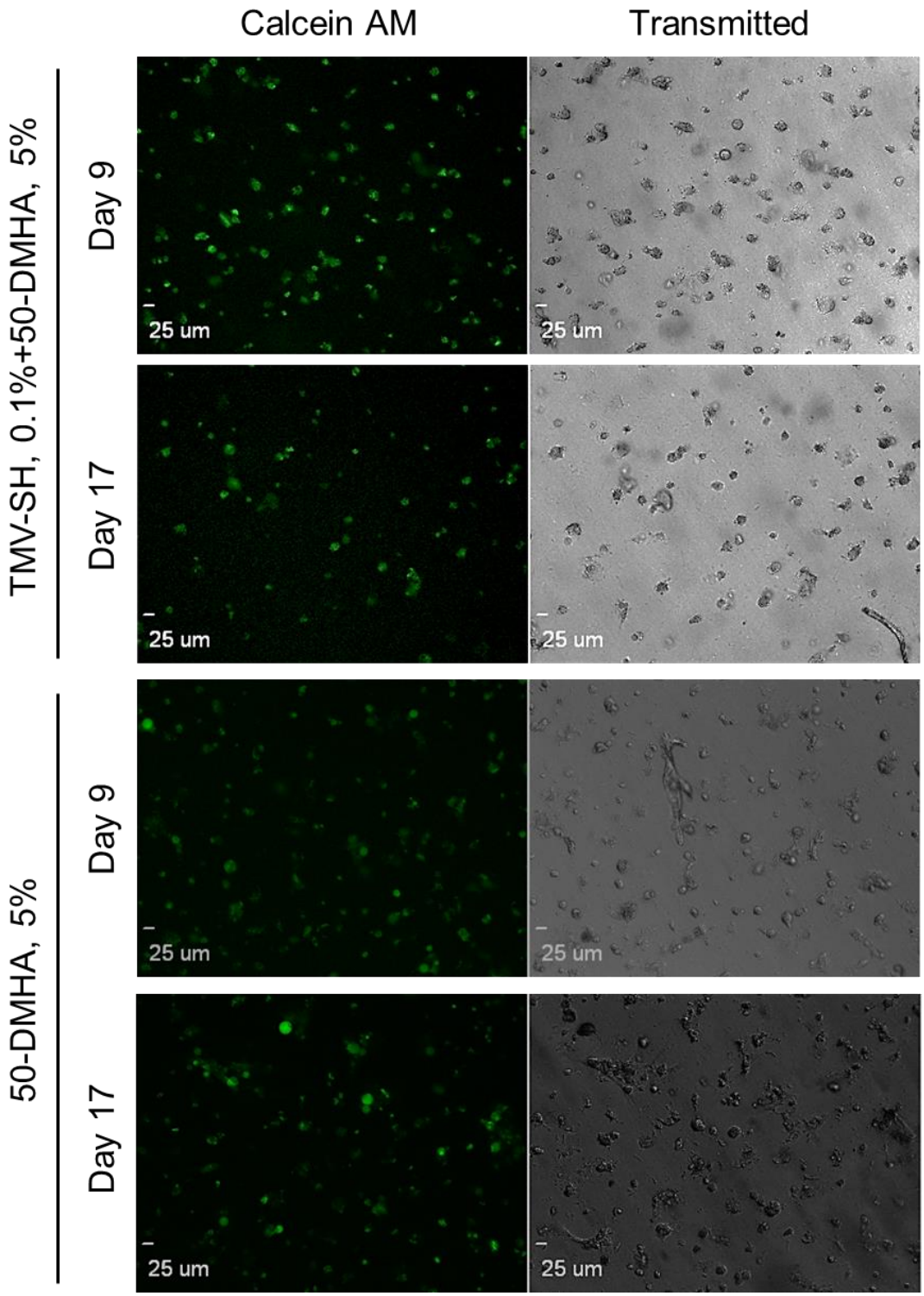

Figure 6.9. Live cell staining of BMSCs cultured in hydrogels. BMSCs were embedded into the 3D hydrogel, *in situ*, at 1 million cells/mL concentration in complete primary media. Day 9 and 17 live cell staining was shown using Calcein AM staining.

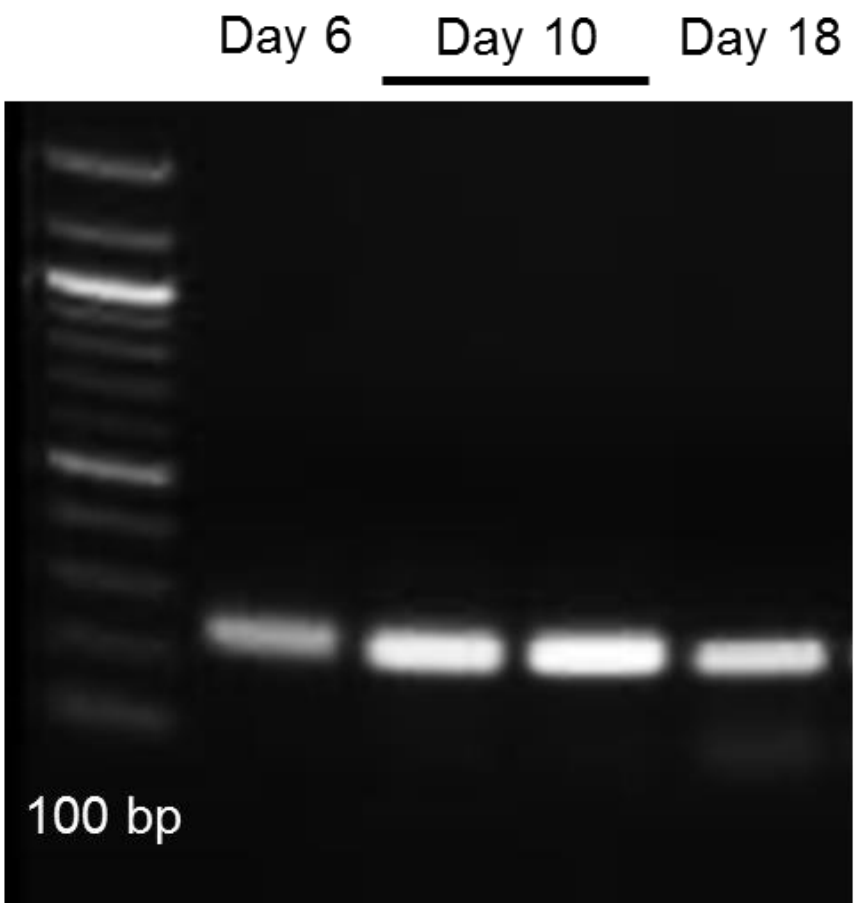

Figure 6.10. Agarose gel image of PCR product derived from mRNA of BMSCs cultured in hydrogels. Sufficient amount of RNA could be isolated from the culture. Gel image shows the PCR product of house-keeping gene from RNA isolated on day 6 (lane 2), 10 (lane 3, 4), and 18 (lane 5).

6.3 Conclusion

HA hydrogel can be engineered to obtain different properties. HA backbone could be modified to have the reactive methacrylic group and the gel can be formed *in situ* after addition of DTT crosslinker via Michael addition reaction under physiological condition. The incorporation of TMV particles could be preceded through the same thiol-ene click reaction between thiol group of TMV-1Cys mutant and the methacrylated HA polymer. The gelation time was improved after addition of TMV-1Cys to 12 minute allowing adequate operation time, yet providing sufficiently rapid rate for clinical efficacy. The resulting gel obtained the micro-and macro-pore structures enabling an exchange of nutrients. The mechanical property of hydrogel could be enhanced by incorporation of TMV-1Cys nanoparticles. The hydrogel was compatible for stem cell culture, and genetic material could be extracted for further gene analysis. This study is considered a foundation of the development of injectable hydrogel with TMV covalently linked to the back-bone polymer that can be further functionalized to direct the encapsulated cell responses in 3D.

6.4 Experimental Section

All chemicals were obtained from commercial suppliers and used as received unless otherwise noted. Wild-type TMV (TMV) and its Cys-mutant (TMV-1Cys) were isolated from infected tobacco leaves following previously established protocols.[26]

6.4.1 HA-methacrylate synthesis

Synthesis of HA-methacrylate was modified from the method originally described by Smeds *et al*.[217] according to the protocol detailed by Marklein *et al*.[218] Briefly, HA of molecular weight 47, 310,or 1000 kDa (Dali) was dissolved at 1 wt% in potassium phosphate buffer, pH 8 and methacrylic anhydride (Alfa Aesar) of different folds molar excess (relative to the HA disaccharide repeat unit) as listed in Table 1 was added dropwise to the solution on ice. The pH of the two-phase reaction mixture was adjusted to 8.0 with 5 M NaOH, and the reaction was allowed to continue for 24 h. at 4 °C with frequent re-adjustment of the pH. The product was dialyzed against milli-Q water for at least 48 h, followed by centrifugation to recover the precipitate, which was then flash frozen in liquid nitrogen, and lyophilized. The powder thus obtained was analyzed by ^{1}H NMR.

6.4.2 HA gelation and rheology

In general, to form crosslinked HA gels, HA-methacrylate polymers with 30-50% degrees of functionalization (hereafter denoted as xx-DMHA; with xx represented % degree of modification) was dissolved in phosphate buffer saline (PBS) at the desired concentration. The crosslinker dl-dithiothreitol (DTT) was added at the ratio of thiol:ene = 1:4. For "TMV-SH, 0.1% + xx-DMHA, 5%", xx-DMHA was dissolved in PBS at 5 wt % concentration, and 10 mg/mL TMV-1Cys was then added before adding DTT to make final concentration of 0.1 wt %. Oscillatory shear rheology was performed using a DHR-3 rheometer (TA instrument) with 12 mm diameter parallel-plate geometry and temperature controlled peltier plate. For the gelation study, the gels were crosslinked in

situ between the rheometer plates in a close chamber protecting hydrogel from dehydration. The measurement in oscillatory time sweep mode (2% strain amplitude, 10 rad/s) immediately started after the freshly prepared pre-hydrogel mixture was loaded on the peltier plate. Typically, 200 μL of the gel solution was used with a gap width of 1 mm between the plates. Amplitude sweeps at constant frequency (1 Hz) were performed to determine the linear viscoelastic range of deformation for each sample, after which frequency sweeps (0.01-100 Hz) were performed at a strain amplitude within the linear range (2%). In amplitude and frequency sweeps measurement, the geometry gaps were conditioned by axial force at 0.5 N for every run.

6.4.3 MALDI-TOF analysis

The 100 μL of pre-formed TMV-SH hydrogel was digested using 1800 U HAase in 1 mL PBS (Type IV-S from bovine testes, Sigma) for 2 days. The control hydrogel without the virus was digested with the 900 U HAase in 200 μL PBS. Each sample was prepared by mixing the virus (0.5 mg/mL, 1 μL) or digested hydrogels solution (1 μL) with 9 μL of matrix solution (saturated sinapic acid in 70% acetonitrile, 0.1% trifluoroacetic acid). One μL of the mixture was spotted on a MALDI plate, air-dried and analyzed by MALDI-TOF mass spectrometry (Bruker Ultraflex MALDI-TOF/TOF).

6.4.4 Atomic force microscopy of TMV-SH hydrogel

Atomic force microscopy (AFM) was performed on the TMV-SH, 0.1% + 50-DMHA, 5% hydrogel. First, 5% methacrylated HA polymer solution in PBA, after adjusting pH to pH 8, was mixed with TMV-1Cys to make 0.1 wt % final concentration. DTT was added

to the mixture. After 10 min gelation, the hydrogel was spin-coated on the silicon wafer. The hydrogel coated wafer was then dried and subjected to AFM imaging. The TMV-1Cys in the hydrogel on the wafers was characterized using tapping-mode AFM images using a NanoScope IIIA MultiMode AFM (Veeco). Si tips with a resonance frequency of approximately 300 kHz, a spring constant of about 40 Nm^{-1} and a scan rate of 1.0 Hz were used.

6.4.5 Environmental scanning electron microscopy

Environmental scanning electron microscopy (ESEM) images were obtained by VEGA3 TESCAN electron microscope. Freeze dried samples were cross-sectioned and mounted on aluminum stubs with carbon tape. Samples were observed under a low vacuum with 20 kV of electron acceleration and a 9.95 -13.16 mm working distance.

6.4.6 Dye diffusion study

After the 150 µL hydrogels were fabricated as mentioned earlier, each gel was soaked into 400 µL of 5 µg/mL fluoresceinamine isomer I (sigma) in PBS. The amount of dye diffused into the hydrogel was calculated from the left-over dye detected from the medium. Dye amounts were transformed from fluorescence intensity measured at 490/520 nm (Ex/Em) by SpectraMax M2 Multi-Mode microplate reader (Molecular Devices). The standard curve was generated from different dye concentrations in the range of 1-10 µg/mL plotted over fluorescence intensities. The amounts of dye diffusion were then calculated into concentrations of dye in the hydrogels and normalized against

the concentrations of dye in total volume (hydrogel volume + medium volume) as shown in the following equation.

Dye concentration diffusion percentage =

$$\frac{\text{amount of dye in hydrogel/hydrogel volume}}{\text{amount of dye in total/(hydrogel volume + dye solution volume)}}$$

6.4.7 Swelling property and stability

Swelling property of each hydrogel was determined by the final weight divided by the initial weight of the hydrogel. The initial weights (~ 250 mg) of hydrogels were recorded (μ_0). Hydrogels were immersed in 1 mL PBS at room temperature, and then the weights after immersion over time were recorded (μ_t). Surrounding water was drained and blotted out with Whatman filter paper from hydrogels before weighing. The swelling ratios were calculated from μ_t/μ_0. For stability test, pre-formed hydrogels (250 µL) were incubated with 1 mL of PBS at room temperature. The hydrogel mass reduction at each time point was monitored. The hydrogel was collected and lyophilized for at least 24 h. before the dry weight was measured. The dry weight at the starting point was measured as γ^0 (~ 16 mg). The dry weight measured at different time point was symbolized γ^t. Normalized hydrogel dry weight was calculated as γ^t/γ^0.

6.4.8 Bone Marrow Stem Cells (BMSCs) isolation and culture

Primary BMSCs were isolated from the bone marrow of young adult 160 - 180 g male Sprague Dawley rats (Charles River Laboratories). The procedures were performed in accordance with the guidelines for animal experimentation by the Institutional Animal Care and Use Committee, School of Medicine, University of South Carolina. Cells were

maintained in complete primary media (Dulbecco's Modified Eagle's Medium (DMEM) supplemented with 10% fetal bovine serum (FBS)), kept at 37 ^{0}C in a CO_2 incubator with 5% CO_2 : 95% air and passaged no more than seven times after isolation.

6.4.9 In situ cell encapsulation with hydrogel matrix

The hydrogels were prepared s previously described, except that the preparation occurred under sterile condition and pre-warmed complete DMEM media was used to dissolve the polymer. TMV-1Cys was filtered to remove all pathogen before mixing. All other components including 5 M NaOH and 0.2 M DTT in PBS were also sterile filtered with 0.2 µm PES membranes. BMSCs were harvested from the tissue culture plate after reaching 80% confluency. The cells were then mixed with the mixture of pre-warmed hydrogel in DMEM media at 1 M/mL concentration right after addition of DTT. One hundred and fifty microliters of the cells-hydrogel mixture was then injected into each Transwell (Corning) that was inserted and anchored in 24 well tissue culture plate, and incubated at 37 ^{0}C in a CO_2 incubator with 5% CO_2 : 95% air. Approximately 6 h after casting the gel into Transwell, 400 µL additional DMEM media was added into each well. The fresh media was exchanged every day for the entire experimental period.

6.4.10 Cell metabolic rate

CellTiter-Blue® (CTB) cell viability assay (Promega) after day 1, 4, 8 and day 15 of culture was performed in a separate sample for each type of hydrogel. The culture media in each well was replaced by 300 mL of pre-warmed media containing 15% CTB and incubated for 20 h at 37 °C and 5% CO_2. The media containing CTB was used without

cells as negative controls. The media containing metabolite of CTB was measured for fluorescence intensity at 560/590 nm (Ex/Em) using SpectraMax M2 Multi-Mode microplate reader (Molecular Devices).

6.4.11 Live cell staining

On day 9 and 17 of cell culture, 10 μg/mL of calcein AM in media was added in each cell-hydrogel culture well and incubated for 30 minutes in 37°C. Then, hydrogels in each well were washed by PBS. After washing, PBS was replaced with fixative solution (4% paraformaldehyde in 1× Dulbecco's Phosphate Buffered Saline; DPBS). Hydrogels were fixed overnight at 4 °C. Fixed hydrogels were then washed with PBS 3 times and stored in PBS. Images of the stained samples were obtained using Olympus IX81 with DSU confocal mode.

6.4.12 RNA isolation

At the cell culture end point, total RNA could be purified from the hydrogel. First, each hydrogel was preserved in RNA later (Qiagen) overnight at 4°C. This step was critical to help protecting RNA from degradation during complex isolation procedures. The preserved hydrogel was then disrupted by high speed homogenization. The tissue homogenizer probe was rinsed with RNase-free water and 10% sodium lauryl sulfate between each sample processing to prevent cross-contamination. Total RNA was subsequently extracted following manufacturers' protocols of either QIAShredder (Qiagen) with E.Z.N.A. Total RNA Kit (Omega) or RNAzol® RT (MRC). The resulting RNA was reverse transcribed by using qScript™ cDNA Supermix (Quanta Biosciences).

RT-PCR was then achieved by the method described as: 45 cycles of PCR (95°C for 20s, 58°C for 15 s, and 72°C for 15 s), after initial denaturation step of 5 minutes at 95°C, by using 0.1 μL of Taq DNA polymerase, 0.5 μL of 10 mM dNTP Mix, 2.5 μL of 10× PCR Buffer, without Mg, 2 pmol/μL of each forward and reverse primers and 30 ng cDNA templates in a final reaction volume of 25 μL. Glyceraldehyde 3-phosphate dehydrogenase (GAPDH) was used as an example gene. Here, we used GAPDH primer sequence from the report by Sitasuwan *et al*.[17] The PCR product was then subjected to standard agarose DNA gel electrophoresis.

REFERENCES

1. Khademhosseini A, Vacanti JP, Langer R. Progress in tissue engineering. Sci Am 2009;300:64-71.

2. Khademhosseini A, Langer R, Borenstein J, Vacanti JP. Microscale technologies for tissue engineering and biology. Proc Natl Acad Sci U S A 2006;103:2480-7.

3. Griffith LG, Naughton G. Tissue Engineering--Current Challenges and Expanding Opportunities. Science 2002;295:1009-14.

4. Khademhosseini A, Langer R. Microengineered hydrogels for tissue engineering. Biomaterials 2007;28:5087-92.

5. Zhu J. Bioactive modification of poly(ethylene glycol) hydrogels for tissue engineering. Biomaterials 2010;31:4639-56.

6. Elisseeff J. Injectable cartilage tissue engineering. Expert Opin Biol Ther 2004;4:1849-59.

7. Bichara DA, Zhao X, Bodugoz-Senturk H, Ballyns FP, Oral E, Randolph MA, Bonassar LJ, Gill TJ, Muratoglu OK. Porous poly(vinyl alcohol)-hydrogel matrix-engineered biosynthetic cartilage. Tissue Eng Part A 2011;17:301-9.

8. Kloxin AM, Kasko AM, Salinas CN, Anseth KS. Photodegradable hydrogels for dynamic tuning of physical and chemical properties. Science 2009;324:59-63.

9. Halberstadt C, Austin C, Rowley J, Culberson C, Loebsack A, Wyatt S, Coleman S, Blacksten L, Burg K, Mooney D, Holder W, Jr. A hydrogel material for plastic and reconstructive applications injected into the subcutaneous space of a sheep. Tissue Eng 2002;8:309-19.

10. Aldaye FA, Senapedis WT, Silver PA, Way JC. A Structurally Tunable DNA-Based Extracellular Matrix. Journal of the American Chemical Society 2010;132:14727-9.

11. Petosa C, Collier RJ, Klimpel KR, Leppla SH, Liddington RC. Crystal structure of the anthrax toxin protective antigen. Nature 1997;385:833-8.

12. Mammen M, Choi S-K, Whitesides GM. Polyvalent Interactions in Biological Systems: Implications for Design and Use of Multivalent Ligands and Inhibitors. Angewandte Chemie International Edition 1998;37:2754-94.

13. Kiessling LL, Gestwicki JE, Strong LE. Synthetic Multivalent Ligands as Probes of Signal Transduction. Angewandte Chemie International Edition 2006;45:2348-68.

14. Petrie TA, Raynor JE, Dumbauld DW, Lee TT, Jagtap S, Templeman KL, Collard DM, Garcia AJ. Multivalent integrin-specific ligands enhance tissue healing and biomaterial integration. Sci Transl Med 2010;2:45ra60.

15. Lee LA, Wang Q. Dynamic 3D Patterning of Biochemical Cues by using Photoinduced Bioorthogonal Reactions. Angewandte Chemie International Edition 2012;51:4004-5.

16. Kaur G, Valarmathi MT, Potts JD, Jabbari E, Sabo-Attwood T, Wang Q. Regulation of osteogenic differentiation of rat bone marrow stromal cells on 2D nanorod substrates. Biomaterials 2010;31:1732-41.

17. Sitasuwan P, Lee LA, Bo P, Davis EN, Lin Y, Wang Q. A plant virus substrate induces early upregulation of BMP2 for rapid bone formation. Integr Biol (Camb) 2012;4:651-60.

18. Stubbs G. Tobacco mosaic virus particle structure and the initiation of disassembly. Philos Trans R Soc Lond B Biol Sci 1999;354:551-7.

19. Butler PJ. Self-assembly of tobacco mosaic virus: the role of an intermediate aggregate in generating both specificity and speed. Philos Trans R Soc Lond B Biol Sci 1999;354:537-50.

20. Schlick TL, Ding Z, Kovacs EW, Francis MB. Dual-Surface Modification of the Tobacco Mosaic Virus. Journal of the American Chemical Society 2005;127:3718-3723.

21. Lee LA, Wang Q. Adaptations of nanoscale viruses and other protein cages for medical applications. Nanomedicine: Nanotechnology, Biology and Medicine 2006;2:137-49.

22. Gerasopoulos K, McCarthy M, Banerjee P, Fan X, Culver JN, Ghodssi R. Biofabrication methods for the patterned assembly and synthesis of viral nanotemplates. Nanotechnology 2010;21:055304.

23. Bruckman MA, Kaur G, Lee LA, Xie F, Sepulveda J, Breitenkamp R, Zhang X, Joralemon M, Russell TP, Emrick T, Wang Q. Surface modification of tobacco mosaic virus with "click" chemistry. ChemBioChem 2008;9:519-23.

24. Lee LA, Nguyen QL, Wu L, Horvath G, Nelson RS, Wang Q. Mutant plant viruses with cell binding motifs provide differential adhesion strengths and morphologies. Biomacromolecules 2012;13:422-31.

25. Kaur G, Wang C, Sun J, Wang Q. The synergistic effects of multivalent ligand display and nanotopography on osteogenic differentiation of rat bone marrow stem cells. Biomaterials 2010;31:5813-24.

26. Hsiong SX, Boontheekul T, Huebsch N, Mooney DJ. Cyclic arginine-glycine-aspartate peptides enhance three-dimensional stem cell osteogenic differentiation. Tissue Eng Part A 2009;15:263-72.

27. Eiselt P, Yeh J, Latvala RK, Shea LD, Mooney DJ. Porous carriers for biomedical applications based on alginate hydrogels. Biomaterials 2000;21:1921-7.

28. Barbetta A, Barigelli E, Dentini M. Porous Alginate Hydrogels: Synthetic Methods for Tailoring the Porous Texture. Biomacromolecules 2009;10:2328-37.

29. Drury JL, Mooney DJ. Hydrogels for tissue engineering: scaffold design variables and applications. Biomaterials 2003;24:4337-51.

30. Rokstad AM, Donati I, Borgogna M, Oberholzer J, Strand BL, Espevik T, Skjak-Braek G. Cell-compatible covalently reinforced beads obtained from a chemoenzymatically engineered alginate. Biomaterials 2006;27:4726-37.

31. Owen TA, Aronow M, Shalhoub V, Barone LM, Wilming L, Tassinari MS, Kennedy MB, Pockwinse S, Lian JB, Stein GS. Progressive development of the rat osteoblast phenotype in vitro: reciprocal relationships in expression of genes associated with osteoblast proliferation and differentiation during formation of the bone extracellular matrix. J Cell Physiol 1990;143:420-30.

32. Kaur G, Valarmathi MT, Potts JD, Wang Q. The promotion of osteoblastic differentiation of rat bone marrow stromal cells by a polyvalent plant mosaic virus. Biomaterials 2008;29:4074-81.

33. Langer R. Perspectives and Challenges in Tissue Engineering and Regenerative Medicine. Advanced Materials 2009;21:3235-6.

34. He L, Liu B, Xipeng G, Xie G, Liao S, Quan D, Cai D, Lu J, Ramakrishna S. Microstructure and properties of nano-fibrous PCL-b-PLLA scaffolds for cartilage tissue engineering. Eur Cell Mater 2009;18:63-74.

35. Klompmaker J, Jansen HW, Veth RP, Nielsen HK, de Groot JH, Pennings AJ. Porous polymer implants for repair of full-thickness defects of articular cartilage: an experimental study in rabbit and dog. Biomaterials 1992;13:625-34.

36. Lee LA, Muhammad SM, Nguyen QL, Sitasuwan P, Horvath G, Wang Q. Multivalent ligand displayed on plant virus induces rapid onset of bone differentiation. Mol Pharm 2012;9:2121-5.

37. Luckanagul J, Lee LA, Nguyen QL, Sitasuwan P, Yang X, Shazly T, Wang Q. Porous alginate hydrogel functionalized with virus as three-dimensional scaffolds for bone differentiation. Biomacromolecules 2012;13:3949-58.

38. Lee LA, Nguyen HG, Wang Q. Altering the landscape of viruses and bionanoparticles. Org Biomol Chem 2011;9:6189-95.

39. Simons K, Helenius A, Leonard K, Sarvas M, Gething MJ. Formation of protein micelles from amphiphilic membrane proteins. Proc Natl Acad Sci U S A 1978;75:5306-10.

40. Reilly GC, Engler AJ. Intrinsic extracellular matrix properties regulate stem cell differentiation. Journal of biomechanics 2010;43:55-62.

41. Xiao C, Weng L, Zhang L. Improvement of physical properties of crosslinked alginate and carboxymethyl konjac glucomannan blend films. Journal of Applied Polymer Science 2002;84:2554-60.

42. Destito G, Yeh R, Rae CS, Finn MG, Manchester M. Folic acid-mediated targeting of cowpea mosaic virus particles to tumor cells. Chem Biol 2007;14:1152-62.

43. Moioli EK, Hong L, Mao JJ. Inhibition of osteogenic differentiation of human mesenchymal stem cells. Wound Repair Regen 2007;15:413-21.

44. Healy KE, Guldberg RE. Bone tissue engineering. J Musculoskelet Neuronal Interact 2007;7:328-30.

45. Stein GS, Lian JB, Owen TA. Relationship of cell growth to the regulation of tissue-specific gene expression during osteoblast differentiation. FASEB J 1990;4:3111-23.

46. Pockwinse SM, Wilming LG, Conlon DM, Stein GS, Lian JB. Expression of cell growth and bone specific genes at single cell resolution during development of bone tissue-like organization in primary osteoblast cultures. J Cell Biochem 1992;49:310-23.

47. Gallagher WH, Lauffer MA. Calcium ion binding by tobacco mosaic virus. J Mol Biol 1983;170:905-19.

48. Gallagher WH, Lauffer MA. Calcium ion binding by isolated tobacco mosaic virus coat protein. J Mol Biol 1983;170:921-9.

49. Venugopal J, Prabhakaran MP, Zhang Y, Low S, Choon AT, Ramakrishna S. Biomimetic hydroxyapatite-containing composite nanofibrous substrates for bone tissue engineering. Philos Transact A Math Phys Eng Sci 2010;368:2065-81.

50. Evangelista MB, Hsiong SX, Fernandes R, Sampaio P, Kong HJ, Barrias CC, Salema R, Barbosa MA, Mooney DJ, Granja PL. Upregulation of bone cell differentiation through immobilization within a synthetic extracellular matrix. Biomaterials 2007;28:3644-55.

51. Yang F, Williams CG, Wang DA, Lee H, Manson PN, Elisseeff J. The effect of incorporating RGD adhesive peptide in polyethylene glycol diacrylate hydrogel on osteogenesis of bone marrow stromal cells. Biomaterials 2005;26:5991-8.

52. Huang C, Das A, Barker D, Tholpady S, Wang T, Cui Q, Ogle R, Botchwey E. Local delivery of FTY720 accelerates cranial allograft incorporation and bone formation. Cell Tissue Res 2012;347:553-66.

53. Zhang H, Migneco F, Lin CY, Hollister SJ. Chemically-conjugated bone morphogenetic protein-2 on three-dimensional polycaprolactone scaffolds stimulates osteogenic activity in bone marrow stromal cells. Tissue Eng Part A 2010;16:3441-8.

54. Liu Z, Qiao J, Niu Z, Wang Q. Natural supramolecular building blocks: from virus coat proteins to viral nanoparticles. Chem Soc Rev 2012;41:6178-94.

55. Pokorski JK, Steinmetz NF. The art of engineering viral nanoparticles. Mol Pharm 2011;8:29-43.

56. Chung WJ, Merzlyak A, Yoo SY, Lee SW. Genetically engineered liquid-crystalline viral films for directing neural cell growth. Langmuir 2010;26:9885-90.

57. Merzlyak A, Indrakanti S, Lee SW. Genetically engineered nanofiber-like viruses for tissue regenerating materials. Nano Lett 2009;9:846-52.

58. Mills CA, Martinez E, Errachid A, Engel E, Funes M, Moormann C, Wahlbrink T, Gomila G, Planell J, Samitier J. Nanoembossed polymer substrates for biomedical surface interaction studies. J Nanosci Nanotechnol 2007;7:4588-94.

59. Steinmetz NF. Viral nanoparticles as platforms for next-generation therapeutics and imaging devices. Nanomedicine 2010;6:634-41.

60. Steinmetz NF. Viral nanoparticles in drug delivery and imaging. Mol Pharm 2013;10:1-2.

61. Wen AM, Rambhia PH, French RH, Steinmetz NF. Design rules for nanomedical engineering: from physical virology to the applications of virus-based materials in medicine. J Biol Phys 2013;39:301-25.

62. Bruckman MA, Randolph LN, VanMeter A, Hern S, Shoffstall AJ, Taurog RE, Steinmetz NF. Biodistribution, pharmacokinetics, and blood compatibility of native and PEGylated tobacco mosaic virus nano-rods and -spheres in mice. Virology 2014;449:163-73.

63. Kaiser CR, Flenniken ML, Gillitzer E, Harmsen AL, Harmsen AG, Jutila MA, Douglas T, Young MJ. Biodistribution studies of protein cage nanoparticles demonstrate broad tissue distribution and rapid clearance in vivo. Int J Nanomedicine 2007;2:715-33.

64. Lewis JD, Destito G, Zijlstra A, Gonzalez MJ, Quigley JP, Manchester M, Stuhlmann H. Viral nanoparticles as tools for intravital vascular imaging. Nat Med 2006;12:354-60.

65. Molenaar TJ, Michon I, de Haas SA, van Berkel TJ, Kuiper J, Biessen EA. Uptake and processing of modified bacteriophage M13 in mice: implications for phage display. Virology 2002;293:182-91.

66. Singh P, Prasuhn D, Yeh RM, Destito G, Rae CS, Osborn K, Finn MG, Manchester M. Bio-distribution, toxicity and pathology of cowpea mosaic virus nanoparticles in vivo. J Control Release 2007;120:41-50.

67. Wu M, Shi J, Fan D, Zhou Q, Wang F, Niu Z, Huang Y. Biobehavior in normal and tumor-bearing mice of tobacco mosaic virus. Biomacromolecules 2013;14:4032-7.

68. Manchester M, Singh P. Virus-based nanoparticles (VNPs): platform technologies for diagnostic imaging. Adv Drug Deliv Rev 2006;58:1505-22.

69. Wen AM, Lee KL, Yildiz I, Bruckman MA, Shukla S, Steinmetz NF. Viral nanoparticles for in vivo tumor imaging. J Vis Exp 2012:e4352.

70. Rappaport I. The antigenic structure of tobacco mosaic virus. Adv Virus Res 1965;11:223-75.

71. Van Regenmortel MH, Altschuh D, Zeder-Lutz G. Tobacco mosaic virus: a model antigen to study virus-antibody interactions. Biochimie 1993;75:731-9.

72. Hinrichs J, Berger S, Shaw JG. Induction of antibodies to plant viral proteins by DNA-based immunization. J Virol Methods 1997;66:195-202.

73. Smith ML, Corbo T, Bernales J, Lindbo JA, Pogue GP, Palmer KE, McCormick AA. Assembly of trans-encapsidated recombinant viral vectors engineered from Tobacco mosaic virus and Semliki Forest virus and their evaluation as immunogens. Virology 2007;358:321-33.

74. Van Regenmortel MH. The antigenicity of tobacco mosaic virus. Philos Trans R Soc Lond B Biol Sci 1999;354:559-68.

75. Heinz FX, Allison SL, Stiasny K, Schalich J, Holzmann H, Mandl CW, Kunz C. Recombinant and virion-derived soluble and particulate immunogens for vaccination against tick-borne encephalitis. Vaccine 1995;13:1636-42.

76. Smith ML, Lindbo JA, Dillard-Telm S, Brosio PM, Lasnik AB, McCormick AA, Nguyen LV, Palmer KE. Modified tobacco mosaic virus particles as scaffolds for display of protein antigens for vaccine applications. Virology 2006;348:475-88.

77. Staczek J, Bendahmane M, Gilleland LB, Beachy RN, Gilleland HE, Jr. Immunization with a chimeric tobacco mosaic virus containing an epitope of outer membrane protein F of Pseudomonas aeruginosa provides protection against challenge with P. aeruginosa. Vaccine 2000;18:2266-74.

78. Zan X, Sitasuwan P, Powell J, Dreher TW, Wang Q. Polyvalent display of RGD motifs on turnip yellow mosaic virus for enhanced stem cell adhesion and spreading. Acta Biomater 2012;8:2978-85.

79. McCormick AA, Palmer KE. Genetically engineered Tobacco mosaic virus as nanoparticle vaccines. Expert Rev Vaccines 2008;7:33-41.

80. Modelska A, Dietzschold B, Sleysh N, Fu ZF, Steplewski K, Hooper DC, Koprowski H, Yusibov V. Immunization against rabies with plant-derived antigen. Proc Natl Acad Sci U S A 1998;95:2481-5.

81. Pinchuk LM, Filipov NM. Differential effects of age on circulating and splenic leukocyte populations in C57BL/6 and BALB/c male mice. Immun Ageing 2008;5:1.

82. Veriter S, Mergen J, Goebbels RM, Aouassar N, Gregoire C, Jordan B, Leveque P, Gallez B, Gianello P, Dufrane D. In vivo selection of biocompatible alginates for islet encapsulation and subcutaneous transplantation. Tissue Eng Part A 2010;16:1503-13.

83. Nunamaker EA, Purcell EK, Kipke DR. In vivo stability and biocompatibility of implanted calcium alginate disks. J Biomed Mater Res A 2007;83:1128-37.

84. Lee KY, Mooney DJ. Hydrogels for tissue engineering. Chem Rev 2001;101:1869-79.

85. Nicodemus GD, Bryant SJ. Cell encapsulation in biodegradable hydrogels for tissue engineering applications. Tissue Eng Part B Rev 2008;14:149-65.

86. Andersen T, Melvik JE, Gaserod O, Alsberg E, Christensen BE. Ionically gelled alginate foams: physical properties controlled by operational and macromolecular parameters. Biomacromolecules 2012;13:3703-10.

87. Augst AD, Kong HJ, Mooney DJ. Alginate hydrogels as biomaterials. Macromol Biosci 2006;6:623-33.

88. Holme HK, Lindmo K, Kristiansen A, Smidsrod O. Thermal depolymerization of alginate in the solid state. Carbohydrate Polymers 2003;54:431-8.

89. Nsereko S, Amiji M. Localized delivery of paclitaxel in solid tumors from biodegradable chitin microparticle formulations. Biomaterials 2002;23:2723-31.

90. Pittenger MF, Mackay AM, Beck SC, Jaiswal RK, Douglas R, Mosca JD, Moorman MA, Simonetti DW, Craig S, Marshak DR. Multilineage potential of adult human mesenchymal stem cells. Science 1999;284:143-7.

91. Prockop DJ. Marrow stromal cells as stem cells for nonhematopoietic tissues. Science 1997;276:71-4.

92. Caplan AI. Adult mesenchymal stem cells for tissue engineering versus regenerative medicine. J Cell Physiol 2007;213:341-7.

93. Satija NK, Singh VK, Verma YK, Gupta P, Sharma S, Afrin F, Sharma M, Sharma P, Tripathi RP, Gurudutta GU. Mesenchymal stem cell-based therapy: a new paradigm in regenerative medicine. J Cell Mol Med 2009;13:4385-402.

94. Eliopoulos N, Lejeune L, Martineau D, Galipeau J. Human-compatible collagen matrix for prolonged and reversible systemic delivery of erythropoietin in mice from gene-modified marrow stromal cells. Mol Ther 2004;10:741-8.

95. Schu S, Nosov M, O'Flynn L, Shaw G, Treacy O, Barry F, Murphy M, O'Brien T, Ritter T. Immunogenicity of allogeneic mesenchymal stem cells. J Cell Mol Med 2012;16:2094-103.

96. Prigozhina TB, Khitrin S, Elkin G, Eizik O, Morecki S, Slavin S. Mesenchymal stromal cells lose their immunosuppressive potential after allotransplantation. Exp Hematol 2008;36:1370-6.

97. Nauta AJ, Westerhuis G, Kruisselbrink AB, Lurvink EG, Willemze R, Fibbe WE. Donor-derived mesenchymal stem cells are immunogenic in an allogeneic host and stimulate donor graft rejection in a nonmyeloablative setting. Blood 2006;108:2114-20.

98. Mukonoweshuro B, Brown CJ, Fisher J, Ingham E. Immunogenicity of undifferentiated and differentiated allogeneic mouse mesenchymal stem cells. Journal of Tissue Engineering 2014;5.

99. Tse WT, Pendleton JD, Beyer WM, Egalka MC, Guinan EC. Suppression of allogeneic T-cell proliferation by human marrow stromal cells: implications in transplantation. Transplantation 2003;75:389-97.

100. Le Blanc K, Tammik L, Sundberg B, Haynesworth SE, Ringden O. Mesenchymal stem cells inhibit and stimulate mixed lymphocyte cultures and mitogenic responses independently of the major histocompatibility complex. Scand J Immunol 2003;57:11-20.

101. Aggarwal S, Pittenger MF. Human mesenchymal stem cells modulate allogeneic immune cell responses. Blood 2005;105:1815-22.

102. Rasmusson I, Ringden O, Sundberg B, Le Blanc K. Mesenchymal stem cells inhibit lymphocyte proliferation by mitogens and alloantigens by different mechanisms. Exp Cell Res 2005;305:33-41.

103. Ryan JM, Barry FP, Murphy JM, Mahon BP. Mesenchymal stem cells avoid allogeneic rejection. J Inflamm (Lond) 2005;2:8.

104. Augello A, Tasso R, Negrini SM, Amateis A, Indiveri F, Cancedda R, Pennesi G. Bone marrow mesenchymal progenitor cells inhibit lymphocyte proliferation by activation of the programmed death 1 pathway. Eur J Immunol 2005;35:1482-90.

105. Rafei M, Hsieh J, Fortier S, Li M, Yuan S, Birman E, Forner K, Boivin MN, Doody K, Tremblay M, Annabi B, Galipeau J. Mesenchymal stromal cell-derived CCL2 suppresses plasma cell immunoglobulin production via STAT3 inactivation and PAX5 induction. Blood 2008;112:4991-8.

106. Comoli P, Ginevri F, Maccario R, Avanzini MA, Marconi M, Groff A, Cometa A, Cioni M, Porretti L, Barberi W, Frassoni F, Locatelli F. Human mesenchymal stem cells inhibit antibody production induced in vitro by allostimulation. Nephrol Dial Transplant 2008;23:1196-202.

107. Corcione A, Benvenuto F, Ferretti E, Giunti D, Cappiello V, Cazzanti F, Risso M, Gualandi F, Mancardi GL, Pistoia V, Uccelli A. Human mesenchymal stem cells modulate B-cell functions. Blood 2006;107:367-72.

108. Martin PK, Stilhano RS, Samoto VY, Takiya CM, Peres GB, da Silva Michelacci YM, da Silva FH, Pereira VG, D'Almeida V, Marques FL, Otake AH, Chammas R, Han SW. Mesenchymal stem cells do not prevent antibody responses against human alpha-L-iduronidase when used to treat mucopolysaccharidosis type I. PLoS One 2014;9:e92420.

109. Fumimoto Y, Matsuyama A, Komoda H, Okura H, Lee CM, Nagao A, Nishida T, Ito T, Sawa Y. Creation of a rich subcutaneous vascular network with implanted adipose tissue-derived stromal cells and adipose tissue enhances subcutaneous grafting of islets in diabetic mice. Tissue Eng Part C Methods 2009;15:437-44.

110. Moodley Y, Atienza D, Manuelpillai U, Samuel CS, Tchongue J, Ilancheran S, Boyd R, Trounson A. Human umbilical cord mesenchymal stem cells reduce fibrosis of bleomycin-induced lung injury. Am J Pathol 2009;175:303-13.

111. Leung VY, Aladin DM, Lv F, Tam V, Sun Y, Lau RY, Hung SC, Ngan AH, Tang B, Lim CT, Wu EX, Luk KD, Lu WW, Masuda K, Chan D, Cheung KM. Mesenchymal stem cells reduce intervertebral disc fibrosis and facilitate repair. Stem Cells 2014.

112. Chong PP, Selvaratnam L, Abbas AA, Kamarul T. Human peripheral blood derived mesenchymal stem cells demonstrate similar characteristics and chondrogenic differentiation potential to bone marrow derived mesenchymal stem cells. J Orthop Res 2012;30:634-42.

113. Perry CR. Bone repair techniques, bone graft, and bone graft substitutes. Clin Orthop Relat Res 1999:71-86.

114. Rimondini L, Nicoli-Aldini N, Fini M, Guzzardella G, Tschon M, Giardino R. In vivo experimental study on bone regeneration in critical bone defects using an injectable biodegradable PLA/PGA copolymer. Oral Surg Oral Med Oral Pathol Oral Radiol Endod 2005;99:148-54.

115. Fini M, Nicoli Aldini N, Gandolfi MG, Mattioli Belmonte M, Giavaresi G, Zucchini C, De Benedittis A, Amati S, Ravaglioli A, Krayewski A, Rocca M, Guzzardella GA, Biagini G, Giardino R. Biomaterials for orthopedic surgery in osteoporotic bone: a comparative study in osteopenic rats. Int J Artif Organs 1997;20:291-7.

116. Goldberg VM, Stevenson S. Natural history of autografts and allografts. Clin Orthop Relat Res 1987:7-16.

117. Fini M, Motta A, Torricelli P, Giavaresi G, Nicoli Aldini N, Tschon M, Giardino R, Migliaresi C. The healing of confined critical size cancellous defects in the presence of silk fibroin hydrogel. Biomaterials 2005;26:3527-36.

118. Schmitz JP, Hollinger JO. The critical size defect as an experimental model for craniomandibulofacial nonunions. Clin Orthop Relat Res 1986:299-308.

119. Cancedda R, Giannoni P, Mastrogiacomo M. A tissue engineering approach to bone repair in large animal models and in clinical practice. Biomaterials 2007;28:4240-50.

120. Bodde EW, Spauwen PH, Mikos AG, Jansen JA. Closing capacity of segmental radius defects in rabbits. J Biomed Mater Res A 2008;85:206-17.

121. Pearce AI, Richards RG, Milz S, Schneider E, Pearce SG. Animal models for implant biomaterial research in bone: a review. Eur Cell Mater 2007;13:1-10.

122. Freeman E, Turnbull RS. The value of osseous coagulum as a graft material. J Periodontal Res 1973;8:229-36.

123. Takagi K, Urist MR. The reaction of the dura to bone morphogenetic protein (BMP) in repair of skull defects. Ann Surg 1982;196:100-9.

124. Ferland CE, Laverty S, Beaudry F, Vachon P. Gait analysis and pain response of two rodent models of osteoarthritis. Pharmacol Biochem Behav 2011;97:603-10.

125. Spicer PP, Kretlow JD, Young S, Jansen JA, Kasper FK, Mikos AG. Evaluation of bone regeneration using the rat critical size calvarial defect. Nat Protoc 2012;7:1918-29.

126. Yin Z, Nguyen HG, Chowdhury S, Bentley P, Bruckman MA, Miermont A, Gildersleeve JC, Wang Q, Huang X. Tobacco mosaic virus as a new carrier for tumor associated carbohydrate antigens. Bioconjug Chem 2012;23:1694-703.

127. Karpova OV, Ivanov KI, Rodionova NP, Dorokhov Yu L, Atabekov JG. Nontranslatability and dissimilar behavior in plants and protoplasts of viral RNA and movement protein complexes formed in vitro. Virology 1997;230:11-21.

128. Mallajosyula JK, Hiatt E, Hume S, Johnson A, Jeevan T, Chikwamba R, Pogue GP, Bratcher B, Haydon H, Webby RJ, McCormick AA. Single-dose monomeric HA subunit vaccine generates full protection from influenza challenge. Hum Vaccin Immunother 2013;10.

129. Sengupta P. The Laboratory Rat: Relating Its Age With Human's. Int J Prev Med 2013;4:624-30.

130. Piao Y, Liu Y, Xie X. Change trends of organ weight background data in sprague dawley rats at different ages. J Toxicol Pathol 2013;26:29-34.

131. De Jong WH, Hagens WI, Krystek P, Burger MC, Sips AJ, Geertsma RE. Particle size-dependent organ distribution of gold nanoparticles after intravenous administration. Biomaterials 2008;29:1912-9.

132. De Jong WH, Van Der Ven LT, Sleijffers A, Park MV, Jansen EH, Van Loveren H, Vandebriel RJ. Systemic and immunotoxicity of silver nanoparticles in an intravenous 28 days repeated dose toxicity study in rats. Biomaterials 2013;34:8333-43.

133. Lankveld DP, Oomen AG, Krystek P, Neigh A, Troost-de Jong A, Noorlander CW, Van Eijkeren JC, Geertsma RE, De Jong WH. The kinetics of the tissue distribution of silver nanoparticles of different sizes. Biomaterials 2010;31:8350-61.

134. Schoeffner DJ, Warren DA, Muralidara S, Bruckner JV, Simmons JE. Organ weights and fat volume in rats as a function of strain and age. J Toxicol Environ Health A 1999;56:449-62.

135. Mirfazaelian A, Fisher JW. Organ growth functions in maturing male Sprague-Dawley rats based on a collective database. J Toxicol Environ Health A 2007;70:1052-63.

136. Mirfazaelian A, Kim KB, Lee S, Kim HJ, Bruckner JV, Fisher JW. Organ growth functions in maturing male Sprague-Dawley rats. J Toxicol Environ Health A 2007;70:429-38.

137. Kim YS, Min KS, Jeong DH, Jang JH, Kim HW, Kim EC. Effects of fibroblast growth factor-2 on the expression and regulation of chemokines in human dental pulp cells. J Endod 2010;36:1824-30.

138. Xia Z, Triffitt JT. A review on macrophage responses to biomaterials. Biomed Mater 2006;1:R1-9.

139. Schutte RJ, Xie L, Klitzman B, Reichert WM. In vivo cytokine-associated responses to biomaterials. Biomaterials 2009;30:160-8.

140. Bellis SL. Advantages of RGD peptides for directing cell association with biomaterials. Biomaterials 2011;32:4205-10.

141. Shu XZ, Ghosh K, Liu Y, Palumbo FS, Luo Y, Clark RA, Prestwich GD. Attachment and spreading of fibroblasts on an RGD peptide-modified injectable hyaluronan hydrogel. J Biomed Mater Res A 2004;68:365-75.

142. Kallai I, Mizrahi O, Tawackoli W, Gazit Z, Pelled G, Gazit D. Microcomputed tomography-based structural analysis of various bone tissue regeneration models. Nat Protoc 2011;6:105-10.

143. Holdsworth DW, Thornton MM. Micro-CT in small animal and specimen imaging. Trends in Biotechnology 2002;20:S34-S39.

144. Chen J, Bly RA, Saad MM, AlKhodary MA, El-Backly RM, Cohen DJ, Kattamis N, Fatta MM, Moore WA, Arnold CB, Marei MK, Soboyejo WO. In-vivo study of adhesion and bone growth around implanted laser groove/RGD-functionalized Ti-6Al-4V pins in rabbit femurs. Materials Science and Engineering: C 2011;31:826-832.

145. Ferris DM, Moodie GD, Dimond PM, Gioranni CW, Ehrlich MG, Valentini RF. RGD-coated titanium implants stimulate increased bone formation in vivo. Biomaterials 1999;20:2323-31.

146. Kroese-Deutman HC, van den Dolder J, Spauwen PH, Jansen JA. Influence of RGD-loaded titanium implants on bone formation in vivo. Tissue Eng 2005;11:1867-75.

147. Liu SQ, Tian Q, Hedrick JL, Po Hui JH, Ee PL, Yang YY. Biomimetic hydrogels for chondrogenic differentiation of human mesenchymal stem cells to neocartilage. Biomaterials 2010;31:7298-307.

148. Kock L, van Donkelaar CC, Ito K. Tissue engineering of functional articular cartilage: the current status. Cell Tissue Res 2012;347:613-27.

149. Ahmed TA, Hincke MT. Strategies for articular cartilage lesion repair and functional restoration. Tissue Eng Part B Rev 2010;16:305-29.

150. Toh WS, Spector M, Lee EH, Cao T. Biomaterial-mediated delivery of microenvironmental cues for repair and regeneration of articular cartilage. Mol Pharm 2011;8:994-1001.

151. Hoffman AS. Hydrogels for biomedical applications. Adv Drug Deliv Rev 2002;54:3-12.

152. Toh WS, Lee EH, Guo XM, Chan JK, Yeow CH, Choo AB, Cao T. Cartilage repair using hyaluronan hydrogel-encapsulated human embryonic stem cell-derived chondrogenic cells. Biomaterials 2010;31:6968-80.

153. Caplan AI. Mesenchymal stem cells. J Orthop Res 1991;9:641-50.

154. Rogers JJ, Young HE, Adkison LR, Lucas PA, Black AC, Jr. Differentiation factors induce expression of muscle, fat, cartilage, and bone in a clone of mouse pluripotent mesenchymal stem cells. Am Surg 1995;61:231-6.

155. Huang AH, Farrell MJ, Mauck RL. Mechanics and mechanobiology of mesenchymal stem cell-based engineered cartilage. J Biomech 2010;43:128-36.

156. Connelly JT, Garcia AJ, Levenston ME. Inhibition of in vitro chondrogenesis in RGD-modified three-dimensional alginate gels. Biomaterials 2007;28:1071-83.

157. Lee HJ, Yu C, Chansakul T, Hwang NS, Varghese S, Yu SM, Elisseeff JH. Enhanced chondrogenesis of mesenchymal stem cells in collagen mimetic peptide-mediated microenvironment. Tissue Eng Part A 2008;14:1843-51.

158. Kim IL, Khetan S, Baker BM, Chen CS, Burdick JA. Fibrous hyaluronic acid hydrogels that direct MSC chondrogenesis through mechanical and adhesive cues. Biomaterials 2013;34:5571-80.

159. Comisar WA, Kazmers NH, Mooney DJ, Linderman JJ. Engineering RGD nanopatterned hydrogels to control preosteoblast behavior: a combined computational and experimental approach. Biomaterials 2007;28:4409-17.

160. Cukierman E, Pankov R, Stevens DR, Yamada KM. Taking cell-matrix adhesions to the third dimension. Science 2001;294:1708-12.

161. Huebsch N, Arany PR, Mao AS, Shvartsman D, Ali OA, Bencherif SA, Rivera-Feliciano J, Mooney DJ. Harnessing traction-mediated manipulation of the cell/matrix interface to control stem-cell fate. Nat Mater 2010;9:518-26.

162. Wang X, Yan C, Ye K, He Y, Li Z, Ding J. Effect of RGD nanospacing on differentiation of stem cells. Biomaterials 2013;34:2865-74.

163. Wang X, Ye K, Li Z, Yan C, Ding J. Adhesion, proliferation, and differentiation of mesenchymal stem cells on RGD nanopatterns of varied nanospacings. Organogenesis 2013;9:280-6.

164. Kiani C, Chen L, Wu YJ, Yee AJ, Yang BB. Structure and function of aggrecan. Cell Res 2002;12:19-32.

165. Posey KL, Hecht JT. The role of cartilage oligomeric matrix protein (COMP) in skeletal disease. Curr Drug Targets 2008;9:869-77.

166. Kosher RA, Kulyk WM, Gay SW. Collagen gene expression during limb cartilage differentiation. J Cell Biol 1986;102:1151-6.

167. Akiyama H, Chaboissier MC, Martin JF, Schedl A, de Crombrugghe B. The transcription factor Sox9 has essential roles in successive steps of the chondrocyte differentiation pathway and is required for expression of Sox5 and Sox6. Genes Dev 2002;16:2813-28.

168. Grassel S, Ahmed N, Gottl C, Grifka J. Gene and protein expression profile of naive and osteo-chondrogenically differentiated rat bone marrow-derived mesenchymal progenitor cells. Int J Mol Med 2009;23:745-55.

169. Hwang NS, Varghese S, Theprungsirikul P, Canver A, Elisseeff J. Enhanced chondrogenic differentiation of murine embryonic stem cells in hydrogels with glucosamine. Biomaterials 2006;27:6015-23.

170. Wang C, Hao J, Zhang F, Su K, Wang DA. RNA extraction from polysaccharide-based cell-laden hydrogel scaffolds. Anal Biochem 2008;380:333-4.

171. Wang C, Li X, Yao Y, Wang DA. Concurrent extraction of proteins and RNA from cell-laden hydrogel scaffold free of polysaccharide interference. J Chromatogr B Analyt Technol Biomed Life Sci 2009;877:3762-6.

172. Wang L, Stegemann JP. Extraction of high quality RNA from polysaccharide matrices using cetyltrimethylammonium bromide. Biomaterials 2010;31:1612-8.

173. DeLise AM, Fischer L, Tuan RS. Cellular interactions and signaling in cartilage development. Osteoarthritis Cartilage 2000;8:309-34.

174. Fischer L, Boland G, Tuan RS. Wnt signaling during BMP-2 stimulation of mesenchymal chondrogenesis. J Cell Biochem 2002;84:816-31.

175. Yoon BS, Lyons KM. Multiple functions of BMPs in chondrogenesis. J Cell Biochem 2004;93:93-103.

176. Bhardwaj N, Kundu SC. Chondrogenic differentiation of rat MSCs on porous scaffolds of silk fibroin/chitosan blends. Biomaterials 2012;33:2848-57.

177. Salinas CN, Anseth KS. The enhancement of chondrogenic differentiation of human mesenchymal stem cells by enzymatically regulated RGD functionalities. Biomaterials 2008;29:2370-7.

178. Lee KL, Uhde-Holzem K, Fischer R, Commandeur U, Steinmetz NF. Genetic engineering and chemical conjugation of potato virus X. Methods Mol Biol 2014;1108:3-21.

179. Yi H, Rubloff GW, Culver JN. TMV microarrays: hybridization-based assembly of DNA-programmed viral nanotemplates. Langmuir 2007;23:2663-7.

180. Yi H, Nisar S, Lee SY, Powers MA, Bentley WE, Payne GF, Ghodssi R, Rubloff GW, Harris MT, Culver JN. Patterned assembly of genetically modified viral nanotemplates via nucleic acid hybridization. Nano Lett 2005;5:1931-6.

181. Royston E, Ghosh A, Kofinas P, Harris MT, Culver JN. Self-assembly of virus-structured high surface area nanomaterials and their application as battery electrodes. Langmuir 2008;24:906-12.

182. Laurent TC, Fraser JR. Hyaluronan. FASEB J 1992;6:2397-404.

183. Sahoo S, Chung C, Khetan S, Burdick JA. Hydrolytically degradable hyaluronic acid hydrogels with controlled temporal structures. Biomacromolecules 2008;9:1088-92.

184. Chen WY, Abatangelo G. Functions of hyaluronan in wound repair. Wound Repair Regen 1999;7:79-89.

185. Balazs EA, Laurent TC, Jeanloz RW. Nomenclature of hyaluronic acid. Biochem J 1986;235:903.

186. Turley EA, Noble PW, Bourguignon LY. Signaling properties of hyaluronan receptors. J Biol Chem 2002;277:4589-92.

187. Hascall VC, Majors AK, De La Motte CA, Evanko SP, Wang A, Drazba JA, Strong SA, Wight TN. Intracellular hyaluronan: a new frontier for inflammation? Biochim Biophys Acta 2004;1673:3-12.

188. Ghatak S, Misra S, Toole BP. Hyaluronan oligosaccharides inhibit anchorage-independent growth of tumor cells by suppressing the phosphoinositide 3-kinase/Akt cell survival pathway. J Biol Chem 2002;277:38013-20.

189. Toole BP, Wight TN, Tammi MI. Hyaluronan-cell interactions in cancer and vascular disease. J Biol Chem 2002;277:4593-6.

190. Burdick JA, Prestwich GD. Hyaluronic acid hydrogels for biomedical applications. Adv Mater 2011;23:H41-56.

191. Marklein RA, Burdick JA. Spatially controlled hydrogel mechanics to modulate stem cell interactions. Soft Matter 2010;6:136-43.

192. Chung C, Burdick JA. Influence of three-dimensional hyaluronic acid microenvironments on mesenchymal stem cell chondrogenesis. Tissue Eng Part A 2009;15:243-54.

193. Serban MA, Prestwich GD. Modular extracellular matrices: solutions for the puzzle. Methods 2008;45:93-8.

194. Fedorovich NE, Oudshoorn MH, van Geemen D, Hennink WE, Alblas J, Dhert WJ. The effect of photopolymerization on stem cells embedded in hydrogels. Biomaterials 2009;30:344-53.

195. Ananthanarayanan B, Kim Y, Kumar S. Elucidating the mechanobiology of malignant brain tumors using a brain matrix-mimetic hyaluronic acid hydrogel platform. Biomaterials 2011;32:7913-23.

196. Amini AA, Nair LS. Injectable hydrogels for bone and cartilage repair. Biomed Mater 2012;7:024105.

197. Liu X, Jin X, Ma PX. Nanofibrous hollow microspheres self-assembled from star-shaped polymers as injectable cell carriers for knee repair. Nat Mater 2011;10:398-406.

198. Nicodemus GD, Bryant SJ. The role of hydrogel structure and dynamic loading on chondrocyte gene expression and matrix formation. J Biomech 2008;41:1528-36.

199. Elbert DL, Pratt AB, Lutolf MP, Halstenberg S, Hubbell JA. Protein delivery from materials formed by self-selective conjugate addition reactions. J Control Release 2001;76:11-25.

200. Khetan S, Burdick J. Cellular encapsulation in 3D hydrogels for tissue engineering. J Vis Exp 2009.

201. Lutolf MP, Hubbell JA. Synthesis and physicochemical characterization of end-linked poly(ethylene glycol)-co-peptide hydrogels formed by Michael-type addition. Biomacromolecules 2003;4:713-22.

202. Nair DP, Podgórski M, Chatani S, Gong T, Xi W, Fenoli CR, Bowman CN. The Thiol-Michael Addition Click Reaction: A Powerful and Widely Used Tool in Materials Chemistry. Chemistry of Materials 2013;26:724-44.

203. Chung C, Mesa J, Randolph MA, Yaremchuk M, Burdick JA. Influence of gel properties on neocartilage formation by auricular chondrocytes photoencapsulated in hyaluronic acid networks. J Biomed Mater Res A 2006;77:518-25.

204. Weng L, Chen X, Chen W. Rheological characterization of in situ crosslinkable hydrogels formulated from oxidized dextran and N-carboxyethyl chitosan. Biomacromolecules 2007;8:1109-15.

205. Li T, Ci T, Chen L, Yu L, Ding J. Salt-induced reentrant hydrogel of poly(ethylene glycol)-poly(lactide-co-glycolide) block copolymers. Polym Chem 2014;5:979-91.

206. Ngwuluka N, Choonara Y, Kumar P, Modi G, Toit L, Pillay V. A Hybrid Methacrylate-Sodium Carboxymethylcellulose Interpolyelectrolyte Complex: Rheometry and in Silico Disposition for Controlled Drug Release. Materials 2013;6:4284-308.

207. Yucel T, Cebe P, Kaplan DL. Vortex-Induced Injectable Silk Fibroin Hydrogels. Biophys J 2009;97:2044-50.

208. Nuernberger S, Cyran N, Albrecht C, Redl H, Vecsei V, Marlovits S. The influence of scaffold architecture on chondrocyte distribution and behavior in matrix-associated chondrocyte transplantation grafts. Biomaterials 2011;32:1032-40.

209. Annabi N, Nichol JW, Zhong X, Ji C, Koshy S, Khademhosseini A, Dehghani F. Controlling the porosity and microarchitecture of hydrogels for tissue engineering. Tissue Eng Part B Rev 2010;16:371-83.

210. Lien SM, Ko LY, Huang TJ. Effect of pore size on ECM secretion and cell growth in gelatin scaffold for articular cartilage tissue engineering. Acta Biomater 2009;5:670-9.

211. Whang K, Healy KE, Elenz DR, Nam EK, Tsai DC, Thomas CH, Nuber GW, Glorieux FH, Travers R, Sprague SM. Engineering bone regeneration with bioabsorbable scaffolds with novel microarchitecture. Tissue Eng 1999;5:35-51.

212. Yannas IV, Lee E, Orgill DP, Skrabut EM, Murphy GF. Synthesis and characterization of a model extracellular matrix that induces partial regeneration of adult mammalian skin. Proc Natl Acad Sci U S A 1989;86:933-7.

213. Segura T, Anderson BC, Chung PH, Webber RE, Shull KR, Shea LD. Crosslinked hyaluronic acid hydrogels: a strategy to functionalize and pattern. Biomaterials 2005;26:359-71.

214. Brigham MD, Bick A, Lo E, Bendali A, Burdick JA, Khademhosseini A. Mechanically robust and bioadhesive collagen and photocrosslinkable hyaluronic acid semi-interpenetrating networks. Tissue Eng Part A 2009;15:1645-53.

215. Eng D, Caplan M, Preul M, Panitch A. Hyaluronan scaffolds: a balance between backbone functionalization and bioactivity. Acta Biomater 2010;6:2407-14.

216. Jeong CG, Hollister SJ. Mechanical and biochemical assessments of three-dimensional poly(1,8-octanediol-co-citrate) scaffold pore shape and permeability effects on in vitro chondrogenesis using primary chondrocytes. Tissue Eng Part A 2010;16:3759-68.

217. Smeds KA, Pfister-Serres A, Miki D, Dastgheib K, Inoue M, Hatchell DL, Grinstaff MW. Photocrosslinkable polysaccharides for in situ hydrogel formation. J Biomed Mater Res 2001;54:115-21.

218. Marklein RA, Burdick JA. Controlling stem cell fate with material design. Adv Mater 2010;22:175-89.

APPENDIX A – COPYRIGHT CLEARANCE FOR CHAPTER 1

Home | Create Account | Help

ACS Publications
High quality. High impact.

Title: Porous Alginate Hydrogel Functionalized with Virus as Three-Dimensional Scaffolds for Bone Differentiation

Author: Jittima Luckanagul, L. Andrew Lee, Quyen L. Nguyen, Pongkwan Sitasuwan, Xiaoming Yang, Tarek Shazly, and Qian Wang

Publication: Biomacromolecules

Publisher: American Chemical Society

Date: Dec 1, 2012

User ID

Password

Enable Auto Login

LOGIN

Forgot Password/User ID?

If you're a copyright.com user, you can login to RightsLink using your copyright.com credentials. Already a **RightsLink user** or want to learn more?

PERMISSION/LICENSE IS GRANTED FOR YOUR ORDER AT NO CHARGE

This type of permission/license, instead of the standard Terms & Conditions, is sent to you because no fee is being charged for your order. Please note the following:

- Permission is granted for your request in both print and electronic formats, and translations.
- If figures and/or tables were requested, they may be adapted or used in part.
- Please print this page for your records and send a copy of it to your publisher/graduate school.
- Appropriate credit for the requested material should be given as follows: "Reprinted (adapted) with permission from (COMPLETE REFERENCE CITATION). Copyright (YEAR) American Chemical Society." Insert appropriate information in place of the capitalized words.
- One-time permission is granted only for the use specified in your request. No additional uses are granted (such as derivative works or other editions). For any other uses, please submit a new request.

BACK | CLOSE WINDOW

APPENDIX B – ALIZARIN RED STAINING ON SCAFFOLDS

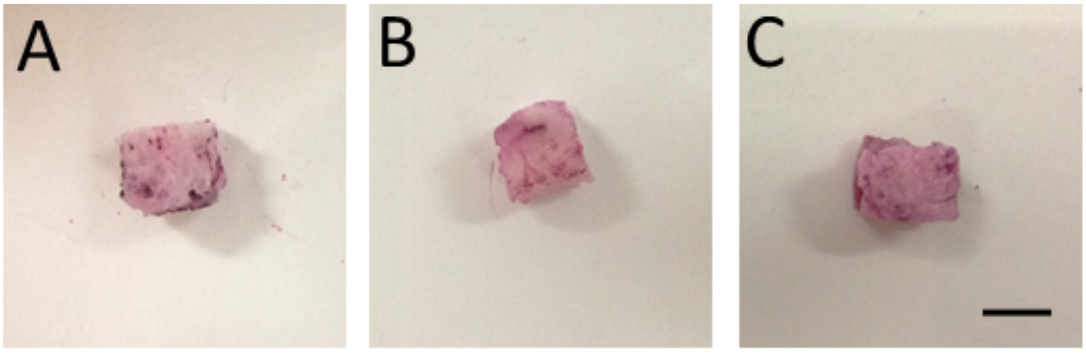

Figure B.1. Alizarin Red staining on controls (A) PAH, (B) TMV-PAH, and (C) RGD-PAH without BMSCs showed lighter color (pink) compared to the cultured hydrogels. Scale bar = 2 mm.

APPENDIX C – TMV-FLUORESCEIN

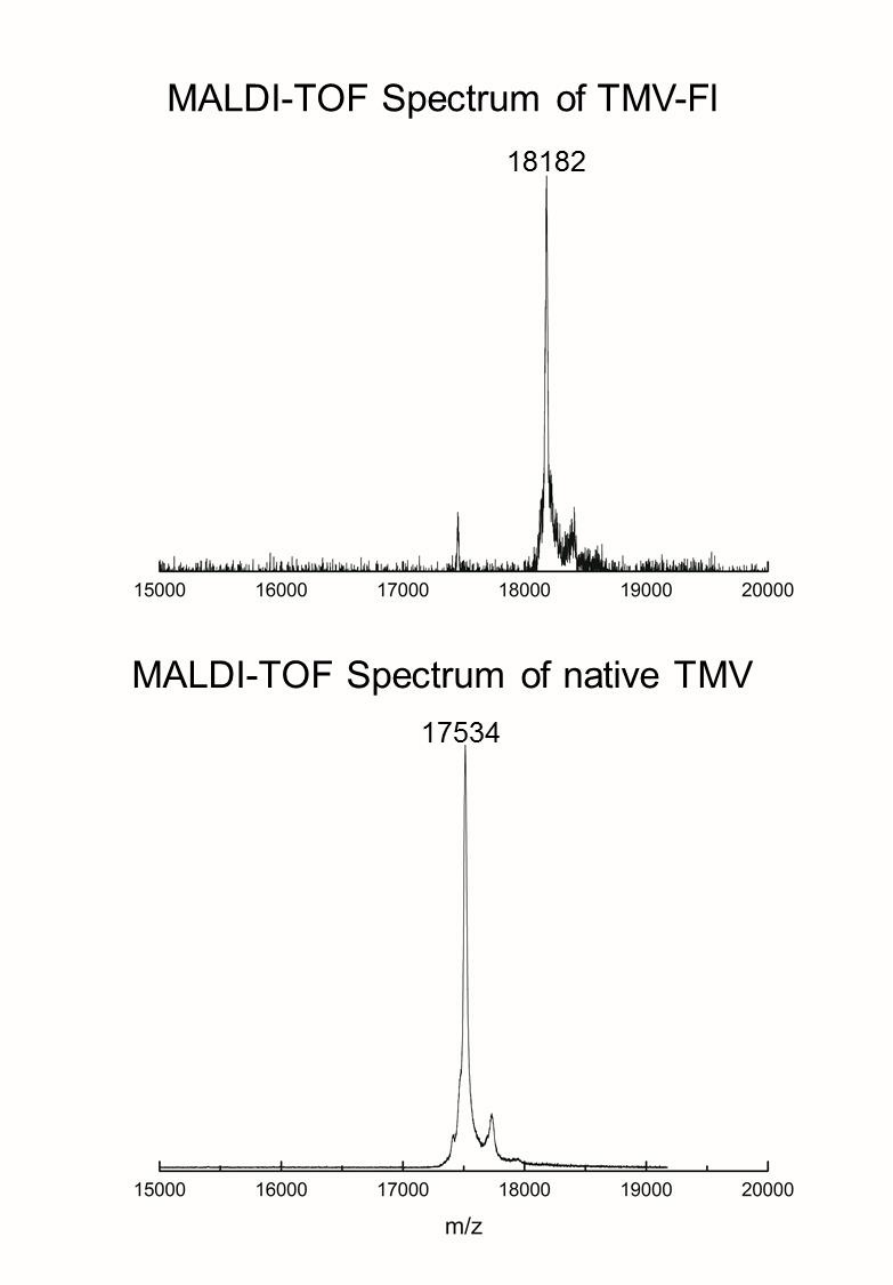

Figure C.1. MALDI-TOF characterization of fluorescein-modified wild-type TMV.

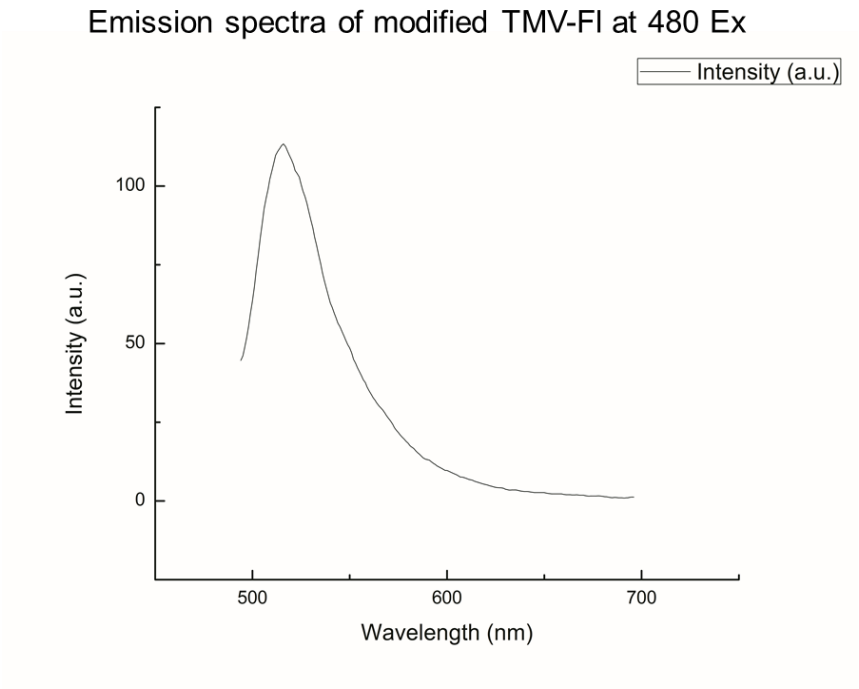

Figure C.2. Fluorescence spectrum of fluorescein-modified wild-type TMV.

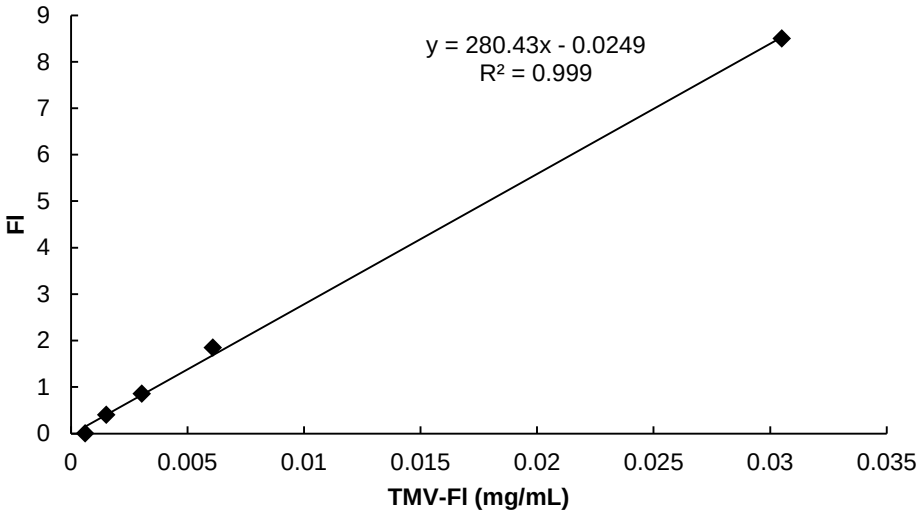

Figure C.3. Fluorescence spectroscopy calibration with linear fitting curve and equation for quantification of fluorescein-modified wild-type TMV.

APPENDIX D – TWO DIMENSIONAL CONSTRUCTS OF BONE EXCISES

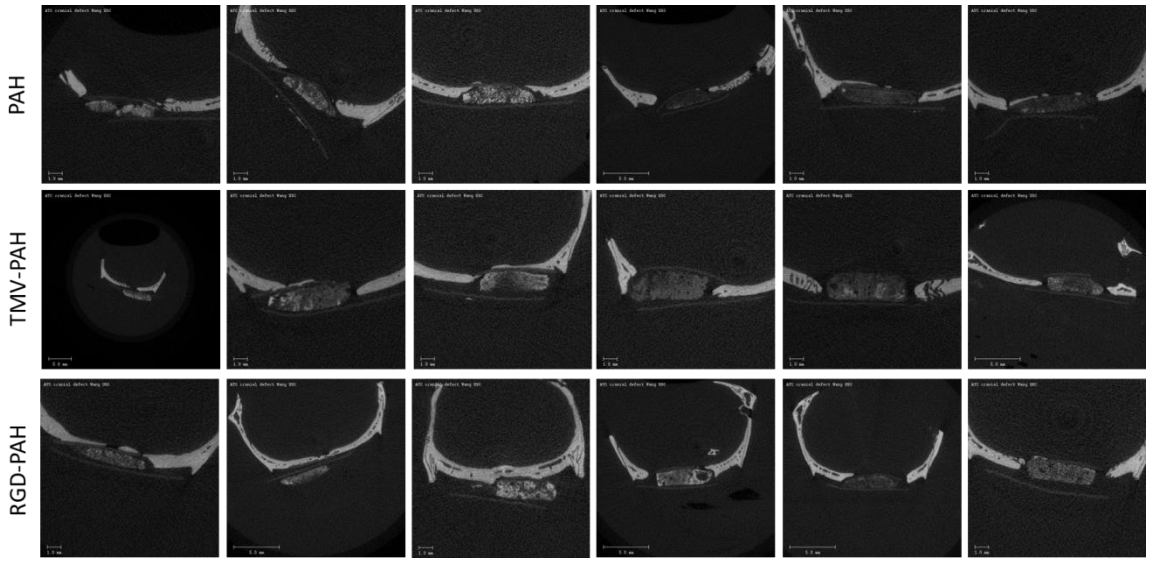

Figure D.1. Two dimensional constructs of bone excises from rats with PAH, TMV-PAH, and RGD-PAH implanted.

APPENDIX E – REPRESENTATIVE ^{1}H NMR SPECTRA OF METHACRYLATED HA

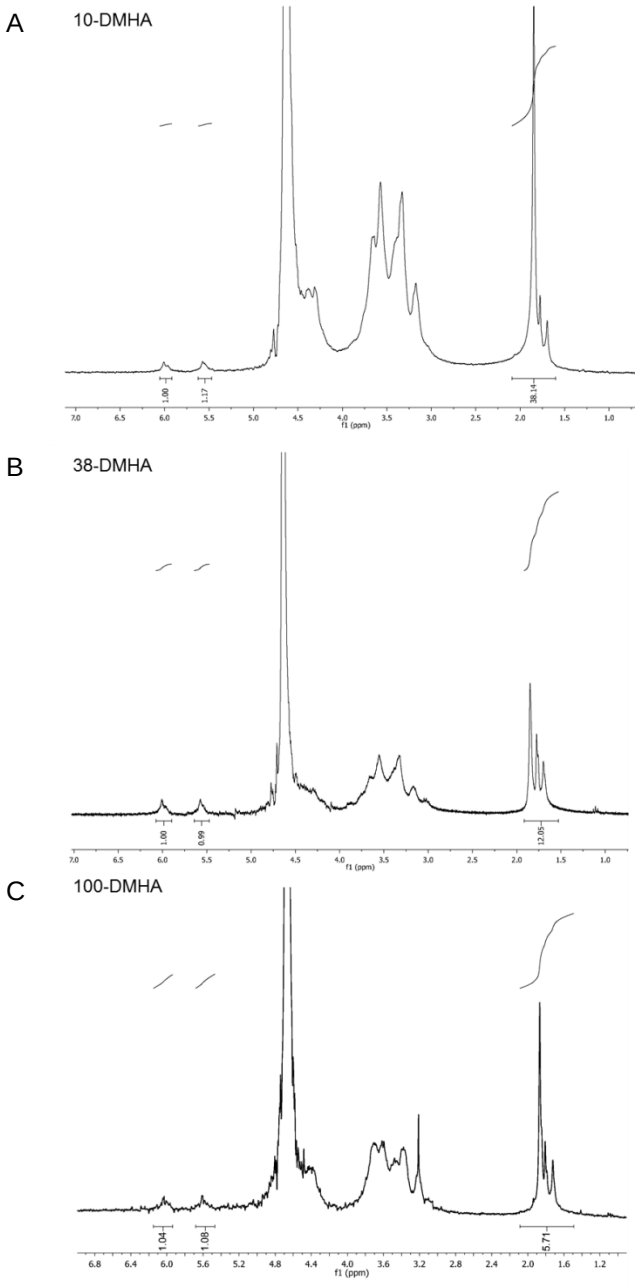

Figure E.1. ^{1}H NMR spectra of methacrylated HA with 10% (A), 38% (B), and 100% (C) degree of modification.

APPENDIX F – TEM ELECTRON MICROGRAPH OF TMV-1CYS

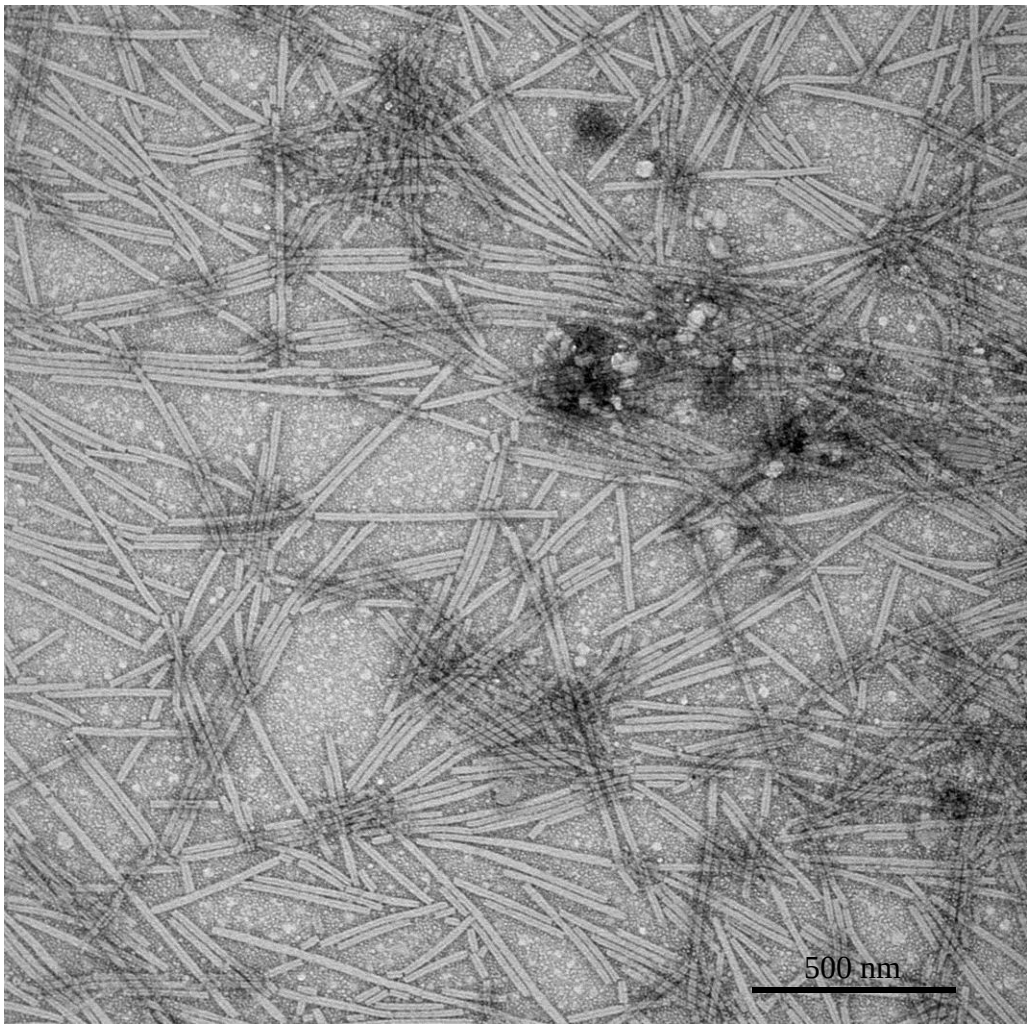

Figure F.1. Transmission electronmicrograph of TMV-1Cys.

APPENDIX G – AFM IMAGE OF WILD-TYPE TMV

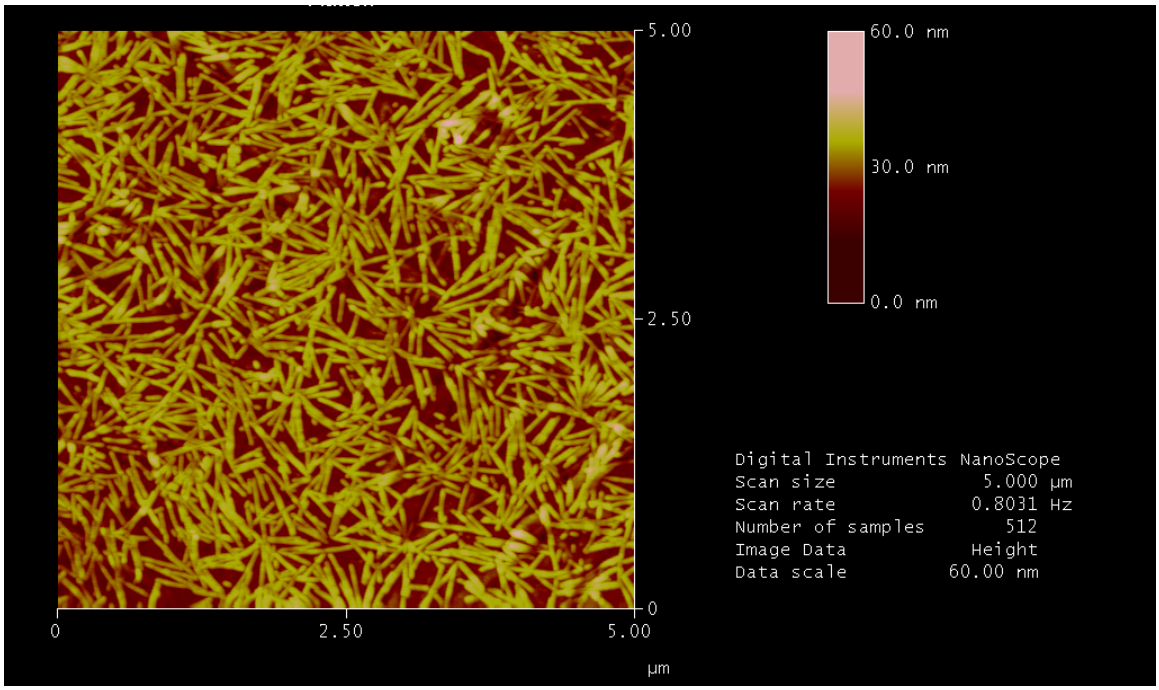

Figure G.1. Atomic force microscopy of wild-type TMV.

APPENDIX H – STANDARD CURVE FOR DYE DIFFUSION STUDY

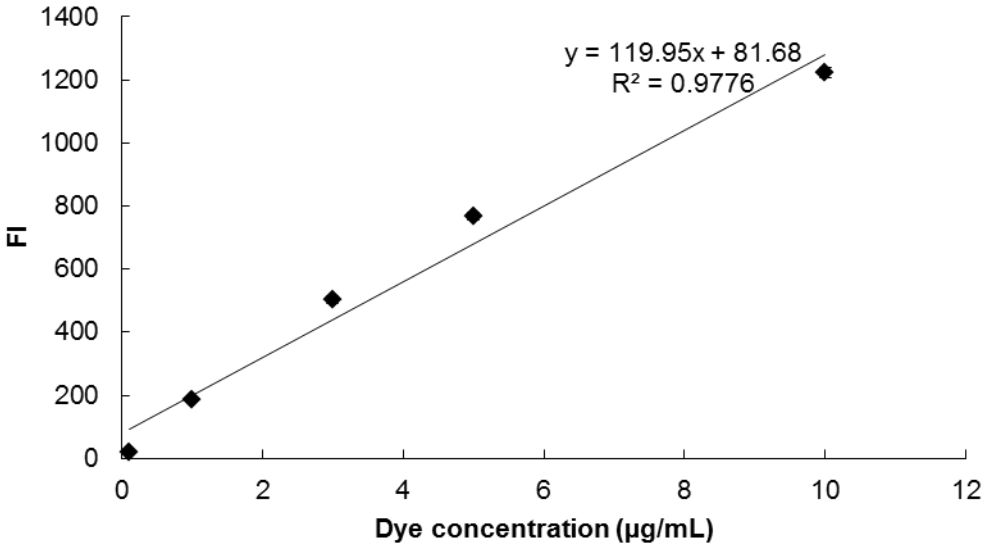

Figure H.1. Fluorescence spectroscopy calibration with linear fitting curve and equation for quantification of fluorescein amine isomer I.